NISTIR 5278R

Semiconductor Reference Waveform Pulse Generator: Interim Progress Report

William L. Gans

U.S. DEPARTMENT OF COMMERCE
Technology Administration
National Institute of Standards
and Technology
Electricity Division
Electronics and Electrical Engineering Laboratory
Gaithersburg, MD 20899

NIST

NISTIR 5278R

Semiconductor Reference Waveform Pulse Generator: Interim Progress Report

William L. Gans

U.S. DEPARTMENT OF COMMERCE
Technology Administration
National Institute of Standards
and Technology
Electricity Division
Electronics and Electrical Engineering Laboratory
Gaithersburg, MD 20899

December 1993

U.S. DEPARTMENT OF COMMERCE
Ronald H. Brown, Secretary

TECHNOLOGY ADMINISTRATION
Mary L. Good, Under Secretary for Technology

NATIONAL INSTITUTE OF STANDARDS AND TECHNOLOGY
Arati Prabhakar, Director

Table of Contents

I. Introduction 1

II. Filter Fabrication Work - 1987-1991 2

III. Conclusions and Recommendations 12

References 13

Appendix A: A Solid-State Reference Waveform Standard 55

Appendix B: Two-Layer Dielectric Microstrip Line Structure: SiO_2 on Si and GaAs on Si: Modeling and Measurement 61

List of Tables

Table 1 Estimated values of the electrical and physical parameters of the 2.5, 3.75, and 5.0 cm filters 3

Table 2 Model predictions for the values of the electrical and physical parameters of the 100, 200, 500, and 1000 ps filters 5

Table 3 First revision of the model predictions for the values of the electrical and physical parameters of the 100 ps filter 7

Table 4 Second revision of the model predictions for the values of the electrical and physical parameters of the 100 ps filter 8

Table 5 "As-built" estimates for the values of the electrical and physical parameters of the 100 ps filter 9

Table 6 "As-built" estimates for the values of the equivalent-circuit parameters of the 100 ps filter 11

List of Figures

Figure 1 Tunnel diode reference pulse waveform for step-response testing of the 2.5, 3.75, and 5.0 cm silicon filters. Time scale is 200 ps/div and voltage scale is 50 mV/div. The three "X"s on the waveform plot in this and similar figures represent the 10%-, 50%-, and 90%-points of the transitions. A plot of the amplitude histogram is also shown 14

Figure 2 Pulse response waveform for the 2.5 cm silicon filter. Time scale is 200 ps/div and voltage scale is 50 mV/div. A plot of the amplitude histogram is also shown 15

Figure 3 Pulse response waveform for the 3.75 cm silicon filter. Time scale is 200 ps/div and voltage scale is 50 mV/div. A plot of the amplitude histogram is also shown 16

Figure 4 Pulse response waveform for the 5.0 cm silicon filter. Time scale is 200 ps/div and voltage scale is 50 mV/div. A plot of the amplitude histogram is also shown 17

Figure 5 Model-predicted step response waveform for the 2.5 cm silicon filter. Time scale is 300 ps/div and voltage scale is 100 mV/div 18

Figure 6 Model-predicted step response waveform for the 3.75 cm silicon filter. Time scale is 300 ps/div and voltage scale is 100 mV/div 19

Figure 7 Model-predicted step response waveform for the 5.0 cm silicon filter. Time scale is 300 ps/div and voltage scale is 100 mV/div 20

Figure 8 Log-log plot of model-predicted filter attenuation versus frequency for the 2.5 cm silicon filter. Frequency range is from 10 MHz to 1 THz and attenuation range is from 0.01 dB to 1000 dB. 21

Figure 9 Log-log plot of model-predicted filter attenuation versus frequency for the 3.75 cm silicon filter. Frequency range is from 10 MHz to 1 THz and attenuation range is from 0.01 dB to 1000 dB 22

Figure 10 Log-log plot of model-predicted filter attenuation versus frequency for the 5.0 cm silicon filter. Frequency range is from 10 MHz to 1 THz and attenuation range is from 0.01 dB to 1000 dB 23

Figure 11 Plot of model-predicted characteristic impedance magnitude versus log frequency for the 5.0 cm silicon filter. Frequency range is 10 MHz to 1 THz and vertical scale is 5 Ω/div 24

Figure 12 Photographs of the TDR signatures of the 5.0 cm silicon filter 25

Figure 13 Model-predicted step response waveform for a 100 ps silicon filter based on the parameters shown in table 2. Time scale is 300 ps/div and voltage scale is 100 mV/div 26

Figure 14 Model-predicted step response waveform for a 200 ps silicon filter based on the parameters shown in table 2. Time scale is 300 ps/div and voltage scale is 100 mV/div 27

Figure 15 Model-predicted step response waveform for a 500 ps silicon filter based on the parameters shown in table 2. Time scale is 300 ps/div and voltage scale is 100 mV/div 28

Figure 16 Model-predicted step response waveform for a 1000 ps silicon filter based on the parameters shown in table 2. Time scale is 500 ps/div and voltage scale is 100 mV/div 29

Figure 17 Log-log plot of model-predicted filter attenuation versus frequency for a 100 ps silicon filter based on the parameters shown in table 2. Frequency range is from 10 MHz to 1 THz and attenuation range is from 0.1 dB to 10000 dB 30

Figure 18 Log-log plot of model-predicted filter attenuation versus frequency for a 200 ps silicon filter based on the parameters shown in table 2. Frequency range is from 10 MHz to 1 THz and attenuation range is from 0.1 dB to 10000 dB 31

Figure 19 Log-log plot of model-predicted filter attenuation versus frequency for a 500 ps silicon filter based on the parameters shown in table 2. Frequency range is from 10 MHz to 1 THz and attenuation range is from 0.1 dB to 1000 dB 32

Figure 20 Log-log plot of model-predicted filter attenuation versus frequency for a 1000 ps silicon filter based on the parameters shown in table 2. Frequency range is from 10 MHz to 1 THz and attenuation range is from 0.1 dB to 1000 dB 33

Figure 21 Plot of model-predicted characteristic impedance magnitude versus log frequency for a 100 ps silicon filter based on the parameters shown in table 2. Frequency range is 10 MHz to 1 THz and vertical scale is 2 Ω/div 34

Figure 22 Plot of model-predicted characteristic impedance magnitude versus log frequency for a 200 ps silicon filter based on the parameters shown in table 2. Frequency range is 10 MHz to 1 THz and vertical scale is 5 Ω/div 35

Figure 23 Plot of model-predicted characteristic impedance magnitude versus log frequency for a 500 ps silicon filter based on the parameters shown in table 2. Frequency range is 10 MHz to 1 THz and vertical scale is 5 Ω/div 36

Figure 24 Plot of model-predicted characteristic impedance magnitude versus log frequency for a 1000 ps silicon filter based on the parameters shown in table 2. Frequency range is 10 MHz to 1 THz and vertical scale is 10 Ω/div 37

Figure 25 Model-predicted step response waveform for a 100 ps silicon filter based on the parameters shown in table 4. Time scale is 200 ps/div and voltage scale is 100 mV/div 38

Figure 26 Model-predicted impulse response waveform for a 100 ps silicon filter based on the parameters shown in table 4. Time scale is 200 ps/div and vertical scale is 1/time (ns) 39

Figure 27 Log-log plot of model-predicted filter attenuation versus frequency for a 100 ps silicon filter based on the parameters shown in table 4. Frequency range is from 10 MHz to 1 THz and attenuation range is from 0.1 dB to 10000 dB 40

Figure 28 Plot of model-predicted characteristic impedance magnitude versus log frequency for a 100 ps silicon filter based on the parameters shown in table 4. Frequency range is 10 MHz to 1 THz and vertical scale is 2 Ω/div 41

Figure 29 Engineering sketch of the 3-inch silicon wafer layout for five 100 ps silicon filter microstrip circuits 42

Figure 30 Plot of the short-circuit-reflection waveform used as a reference in the TDR tests of the prototype silicon filter microstrip circuits 43

Figure 31 Plot of TDR reflected waveform from prototype silicon filter circuit #2. Time scale is 500 ps/div and vertical scale is 20 mV/div 44

Figure 32 Plot of TDR reflected waveform from prototype silicon filter circuit #3. Time scale is 500 ps/div and vertical scale is 20 mV/div 45

Figure 33 Plot of TDR reflected waveform from prototype silicon filter circuit #4. Time scale is 500 ps/div and vertical scale is 20 mV/div 46

Figure 34 Plot of TDR reflected waveform from prototype silicon filter circuit #6. Time scale is 500 ps/div and vertical scale is 20 mV/div 47

Figure 35 Plot of TDR reflected waveform from prototype silicon filter circuit #7. Time scale is 500 ps/div and vertical scale is 20 mV/div 48

Figure 36 Plot of step-like transmission waveform used as a reference for the transmission tests of the prototype silicon filter microstrip circuits 49

Figure 37 Plot of transmission response waveform for prototype silicon filter circuit #2. Time scale is 2 ns/div and vertical scale is 20 mV/div 50

Figure 38 Plot of transmission response waveform for prototype silicon filter circuit #3. Time scale is 2 ns/div and vertical scale is 20 mV/div 51

Figure 39 Plot of transmission response waveform for prototype silicon filter circuit #4. Time scale is 2 ns/div and vertical scale is 20 mV/div 52

Figure 40 Plot of transmission response waveform for prototype silicon filter circuit #6. Time scale is 2 ns/div and vertical scale is 20 mV/div 53

Figure 41 Plot of transmission response waveform for prototype silicon filter circuit #7. Time scale is 2 ns/div and vertical scale is 20 mV/div 54

SEMICONDUCTOR REFERENCE WAVEFORM PULSE GENERATOR: INTERIM PROGRESS REPORT

William L. Gans
National Institute of Standards and Technology
Gaithersburg, Maryland 20899

This is an interim progress report to sponsor on work performed by National Institute of Standards and Technology (NIST) personnel from January 1, 1989 to September 30, 1991. A brief history of the project from 1980 to 1989 is presented, followed by a detailed, chronological description of all work performed during the reporting period. Essentially, this work consisted of modeling, design, construction, and prototype testing of a 100 ps semiconductor reference waveform pulse generator. Although the results reported here do not indicate close agreement between model and actual device, we recommend continuation of this work as time and funds permit.

Key words: Debye dielectric, distributed-element filter, Maxwell-Wagner capacitor, microstrip circuit, pulse generator, reference pulse generator, time domain.

I. Introduction

In the fall of 1980, NIST began work on the design of a solid-state microstrip reference waveform generator for fast electrical pulses. The motivation for this work was to make a solid-state, distributed-element microstrip filter which, when driven by a suitably fast step-like electrical pulse (transition duration ≈ 20 ps), would serve as a reference pulse standard for the calibration of fast oscilloscopes and other fast pulse generators [1,2]. This "solid-state filter" was intended to replace an earlier NIST filter design that utilized a liquid-dielectric-filled 7 mm coaxial transmission line of about 30 cm in length. The expected advantages of the solid-state filter, as compared to the liquid-dielectric filter, were small size, ease of fabrication, reduced cost, and wider range of electrical step responses. With respect to the latter, the realistic range of step responses for the liquid-dielectric filters is from about 50 ps to perhaps 500 ps, whereas the possible range using solid-state filters is from about 5 ps to perhaps 1 ns.

The DoD Calibration Coordination Group (CCG) provided partial funding support for this work, first during fiscal years 83, 84, and 85 as CCG Project #170, and then during fiscal years 87 and 89 as CCG Project #210. During these CCG-funded years, quarterly progress reports were delivered to CCG personnel as required. The total amount of CCG funding received by NIST for this work was $458k, $279k from 1983 to 1985 and $179k from 1987 to 1989.

Two NIST staff members initiated this work, Dr. Norris S. Nahman, who developed the basic theory and design criteria in 1980-81, and Dr. Robert A. Lawton, who worked on building the first filter prototype from 1981 through 1986. Two journal publications were written during the 1981-86 time period; they are included in this report as Appendices A and B. At the end of 1986, the status of the project was that the mathematical model shown in Appendix A had been programmed into a computer and four prototype filters had been built. The first of the four prototypes was built and tested in 1983-4; these results were discussed in the Appendix A paper. The other three prototypes were fabricated in 1986 with the assistance of NIST personnel in the Semiconductor Electronics Division in Gaithersburg, MD, but were still in wafer form, undiced and unmounted. Also in 1986, the model software was tested and verified by comparison with frequency-domain measurements as described in the Appendix B paper. The project work then was assumed by Mr. William L. Gans in January of 1987 and continued until the end of 1991.

Along with this introduction, this report consists of two additional sections. Section 2 deals with the work performed from 1987 through 1991, and Section 3 contains NIST's conclusions and recommendations.

II. Filter Fabrication Work - 1987-1991

In early 1987, two improvements to the microstrip filter mounts were implemented. First, the mounts were redesigned to be adjustable in order to accommodate filters with differing physical dimensions. The earlier mounts required semiconductor microstrips of some exact length and thickness; if a different length or thickness were required, it was necessary to machine new mounts. By making the newly designed mounts with adjustments for microstrip length and/or thickness, it became possible to accommodate practically any realistic circuit length or wafer thickness. Second, male "K" connectors were ordered in addition to the female "K" connectors that were already being used. These connectors form the transition from the planar transmission line geometry of the microstrip circuit to a 3 mm coaxial geometry required for connecting the filters to other instrumentation. By changing from female "K" connectors at both ends of the filter to opposite-sex connectors, it became possible to perform direct insertion measurements on the filter circuits with no need for male-to-male connector adapters.

By the spring of 1987, the filter mathematical model had been transferred from a personal computer (PC) to a super minicomputer. With this larger, faster computer, it became possible to use parameter variational techniques to optimize the filter design in a reasonable amount of time. Also, with greater computational speed it became possible to perform forward and inverse discrete Fourier transforms (DFTs) with arrays of 32k points. (The PC was not programmed to perform DFTs so no time-domain information was available during the earlier filter design and analysis process.) With this improved software, it became possible to obtain both numerical and graphical data for both the filter frequency domain parameters (complex propagation function, $\gamma(j\omega)$, and complex impedance, $Z_o(j\omega)$), and the filter time domain parameters (impulse response, h(t), and step response, s(t)). (Note: The

filter mathematical theory will not be repeated here; see Appendices A and B for discussion of this theory and definition of symbols used for filter mathematical parameters.)

Also in the spring of 1987, it was determined that NIST personnel in Gaithersburg could no longer provide assistance. This assistance had been to deposit thick layers (from 5 to 20 μm) of silicon dioxide (SiO_2) on the silicon wafers, one of the most critical steps in the filter fabrication process. Finding another semiconductor facility capable of performing this processing step, or finding a suitable alternative process, became the largest single technical obstacle for the project.

In the summer of 1987 fabrication was of the three prototype filters that had been left in wafer form in 1986 was completed. For these filters it was decided to switch from using aluminum for the circuit metallization to using gold. This change allowed installing the microstrip circuits into the newly designed mounts without soldering; the gold-to-gold contact between the "K" connector's center pin and the microstrip circuit metallization requires only a pressure contact. The filter circuits were all cut from the same wafer and had lengths of 2.50 cm, 3.75 cm, and 5.0 cm. The estimates for the other circuit parameters are listed in the following table:

Table 1

Estimated values of the electrical and physical parameters of the 2.5, 3.75, and 5.0 cm filters.

SYMBOL	PARAMETER	VALUE
σ_{Au}	Conductivity of gold metallization	4.6×10^{7} S/m
σ_{Si}	Conductivity of doped-silicon substrate	37.4 S/m
σ_{SiO2}	Conductivity of silicon dioxide layer	1.0×10^{-18} S/m
$\epsilon_{r(Si)}$	Relative dielectric constant of silicon	11.7
$\epsilon_{r(SiO2)}$	Relative dielectric constant of silicon dioxide	3.6
d_1	Thickness of silicon dioxide layer	2.0×10^{-5} m
d_2	Thickness of doped-silicon substrate	3.0×10^{-4} m
w	Width of the gold metallization line	1.3×10^{-4} m
T	Thickness of the gold metallization line	1.0×10^{-5} m

The attached figures show the responses of these three circuits and indicate very encouraging results. Figure 1 is a plot of the tunnel diode drive pulse directly into the Automatic Pulse Measurement System (APMS) sampler; the observed first transition

duration of this pulse is 32.16 ps. Figure 2 shows the response of the 2.50 cm filter to the drive pulse and exhibits a first transition duration of 123.70 ps. Figure 3 is the response of the 3.75 cm filter with a first transition duration of 153.46 ps, and figure 4 shows the response of the 5.00 cm filter with a first transition duration of 172.44 ps. Using root-sum-of-squares to correct for the 32.16 ps first transition duration of the drive pulse, estimates for the step responses of the three filters become 119.4 ps, 150.1 ps, and 169.4 ps.

Figure 5 is a plot of the model-predicted step response of the 2.50 cm filter, figure 6, the step response of the 3.75 cm filter, and figure 7, the 5.00 cm filter. The three model step responses are 117.2 ps, 136.8 ps, and 166.1 ps, respectively. Comparing the modeled and measured step responses for the three lines indicates very good agreement; the percent deviations were +1.9%, +9.7%, and +2.0%, respectively.

The model also predicts that the step responses of the lines should exhibit a circuit-length dependence that varies approximately as the square root of the length. This step response-versus-(length)^{½} dependence was verified by simply plotting the three measured-data points on a time-versus-(length)^{½} graph and verifying approximate linearity.

The fact that there were three filters of varying lengths also allowed verification of the model itself. Figure 8 is a plot of the modeled $|S_{21}(j\omega)|$, the attenuation of the filter in dB versus frequency, for the 2.50 cm line. Figure 9 is a similar plot for the 3.75 cm line, and figure 10, that for the 5.00 cm line. Two things can be deduced from these curves. First, the frequency-squared dependence on circuit attenuation that the model predicts can be verified. Looking at figure 8, for example, it can be observed that the attenuation at 1 GHz is about 0.4 dB while the attenuation at 10 GHz is about 30 dB. Thus, in this linear region of the curve, there is about a two decade increase in attenuation for a one decade increase in frequency; the attenuation, indeed, varies quite closely as a function of f^2. Second, in this linear region of the curves, the model predicts that the circuit attenuation should vary linearly with circuit length. From figures 8, 9, and 10, one can observe that at 3 GHz, for example, the circuit attenuations are about 3 dB, 4.5 dB, and 6 dB, respectively. Thus, the attenuation does vary linearly with length.

Along with step response, the other parameter that is most important for a reference waveform standard is characteristic impedance. Figure 11 is a plot of the modeled $|Z_o(j\omega)|$, the magnitude of the filter characteristic impedance versus frequency for the 5.00 cm line. It is observed from this curve that Z_o is about 46 Ω up to a frequency of about 2 GHz. Figure 12 shows photographs of the Time Domain Reflectometry (TDR) signatures of the 5.00 cm line, one looking in one end of the line and the other looking in the other end. Both photographs indicate that the filter characteristic impedance is about 46 Ω. (The slight upward slopes of the TDR signatures shown in figure 12 are due to the distributed ohmic losses in the lines.) As with step response, the agreement between the model and the as-built filters for characteristic impedance appeared to be good. The fact that the characteristic impedance shown in figure 11 increases rapidly above 2 GHz is not the problem that it might appear to be. From figure 10, it can be observed that the filter

attenuation at 2 GHz is about 3 dB and is rising rapidly with frequency above 2 GHz. Thus, although the characteristic impedance of these filters deviates significantly from 50 Ω above some frequency, the relative amount of energy passing through these filters is negligible above that frequency.

With the encouraging results from the three prototype lines, it was decided to attempt the design and fabrication of a complete set of filters, first with target step responses of 200, 400, 600, 800, and 1000 ps, and later, a set of four filters with step responses of 100, 200, 500, and 1000 ps. By experimenting with the more powerful computer model, a set of physical parameters was developed for each of the four filters that appeared to be realizable. These parameters are shown in table 2.

Table 2

Model predictions for the values of the electrical and physical parameters of the 100, 200, 500, and 1000 ps filters.

Parameter	100 ps filter	200 ps filter	500 ps filter	1000 ps filter
σ_{Au} (S/m)	4.6×10^{7}	4.6×10^{7}	4.6×10^{7}	4.6×10^{7}
σ_{Si} (S/m)	100	100	9	9
σ_{SiO2} (S/m)	1.0×10^{-18}	1.0×10^{-18}	1.0×10^{-18}	1.0×10^{-18}
$\epsilon_{r(Si)}$	11.7	11.7	11.7	11.7
$\epsilon_{r(SiO2)}$	4.0	4.0	4.0	4.0
Si thickness (m)	2.45×10^{-4}	1.33×10^{-3}	6.35×10^{-4}	1.45×10^{-3}
SiO_2 thickness (m)	1.82×10^{-5}	1.10×10^{-5}	1.33×10^{-5}	1.07×10^{-5}
Au thickness (m)	1.0×10^{-5}	1.0×10^{-5}	1.0×10^{-5}	1.0×10^{-5}
Au line width (m)	1.0×10^{-4}	1.0×10^{-4}	1.0×10^{-4}	1.0×10^{-4}
Au line length (m)	6.2×10^{-2}	6.2×10^{-2}	6.2×10^{-2}	6.2×10^{-2}
Au line resistance (Ω)	1.35	1.35	1.35	1.35

The modeled step response transition durations for these lines are 97.7, 198.4, 500.5, and 999.5 ps, respectively, and their mid-frequency characteristic impedances are all very close to 50.0 Ω. Figures 13 through 16 show plots of the modeled step responses for these four filters. $|S_{21}(j\omega)|$ plots for the four filters are shown in figures 17 through 20, and $|Z_o(j\omega)|$ plots are shown in figures 21 through 24. The overall shape of all of these plots very closely matches the corresponding plots for the three previously built prototypes, so it was

concluded that the computer model was behaving properly for the above-listed filter parameters.

At the end of 1987, with the four sets of filter design parameters established, we were ready to begin filter fabrication. No vendors were found that could supply us with ready-made doped-silicon wafers at the required conductivities and thicknesses. As a result, two n-type phosphorus-doped silicon ingots were procured from Wacker-Siltronic Corporation, Portland, OR, one with a conductivity of 100 S/m and the other with a conductivity of 9 S/m.[†]

Concurrently, a search was conducted for a semiconductor facility that could deposit the required thick (10-20 μm) coatings of SiO_2 (or some other similar material such as silicon nitride) on the silicon wafers. From this search it became evident that, although many semiconductor processing laboratories routinely coated silicon wafers with 1 or 2 μm-thick layers of SiO_2, virtually none were found that would agree to attempt the much thicker coatings that are required. Finally, one vendor expressed interest, Silica Source Technologies, Tempe, AZ. The result of detailed negotiations with this vendor was that they required $45k to attempt a few test wafer coatings. Since this was too costly, it was decided to investigate the possibility of coating the wafers with polyimides.

With no CCG funding provided for FY-88, efforts continued with the filter development as time and NIST internal funding permitted. In February, 1988, Semiconductor Processing Company, Boston, MA, was contracted to slice our two doped-silicon ingots into the four required sets of polished wafers. In April, at least 30 good wafers for each of the four filters were received.

In the spring of 1988, a small quantity of Pyralin PD polyimide solution was ordered from E. I. DuPont de Nemours Company, Wilmington, DE, in order to test the possibility of using a polyimide dielectric coating for the wafers instead of a SiO_2 coating. It was quickly determined that neither NIST nor the University of Colorado had the capabilities and/or facilities to perform the wafer processes necessary to deposit thick layers of polyimide. Contacts were then made with personnel at Ball Brothers Research, Boulder, who had both the facilities and experience with working with these materials. By late summer, 1988, after some discussion and negotiations with Ball Brothers, it was decided to drop the idea of using polyimides for several reasons. First, too much money ($35k) was requested by Ball Brothers to experiment with the process. Second, they were not especially confident that the technique would work, and third, they did not have an oven that could reach the high

---

[†] Certain commercial equipment, instruments, or materials are identified in this paper in order to specify adequately the experimental procedure. Such identification does not imply recommendation or endorsement by the National Institute of Standards and Technology, nor does it imply that the materials or equipment identified are necessarily the best available for the purpose.

temperature necessary for the final cure step (450°C). Also, polyimide coatings are known to absorb water, which could impart a humidity dependence on the filters.

In the fall of 1988 (FY-89) some additional funding from CCG ($50k) was received to continue this work. With the amount of money and time available, our attempts were limited to trying to build only the 100 ps filter. Also, the filter computer model was used to redesign the filter slightly, inserting a better value for $\epsilon_{r(SiO2)}$, and reducing the thickness of the SiO_2 coating. The revised filter parameters are listed in table 3.

Table 3

First revision of the model predictions for the values of the electrical and physical parameters of the 100 ps filter.

Parameter	100 ps Filter Values
σ_{Au} (S/m)	4.6×10^{7}
σ_{Si} (S/m)	100
σ_{SiO2} (S/m)	1.0×10^{-18}
$\epsilon_{r(Si)}$	11.7
$\epsilon_{r(SiO2)}$	3.6
Si thickness (m)	2.45×10^{-4}
SiO_2 thickness (m)	1.62×10^{-5}
Au line thickness (m)	1.0×10^{-5}
Au line width (m)	1.0×10^{-4}
Au line length (m)	6.2×10^{-2}
Au line resistance (Ω)	1.35

At the suggestion of NIST personnel in Gaithersburg, contacts were made with Vapor Technologies, Inc., Mount Vernon, NY, who advertised a recently developed process for the deposition of thick layers of dielectric on a semiconductor substrate. They referred to this process as Low Temperature Arc Vapor Deposition (LTAVD), and it appeared to be very promising.

In the spring of 1989, the 100 ps filter was once again redesigned in order to use yet a better value for $\epsilon_{r(SiO2)}$ and to reduce slightly the length of the filter gold line. These changes yielded our final design for the filter and are listed in table 4.

Table 4

Second revision of the model predictions for the values of the electrical and physical parameters of the 100 ps filter.

Parameter	100 ps Filter Values
σ_{Au} (S/m)	4.6×10^{7}
σ_{Si} (S/m)	100
σ_{SiO2} (S/m)	1.0×10^{-18}
$\epsilon_{r(Si)}$	11.7
$\epsilon_{r(SiO2)}$	3.78
Si thickness (m)	2.45×10^{-4}
SiO_2 thickness (m)	1.71×10^{-5}
Au line thickness (m)	1.0×10^{-5}
Au line width (m)	1.0×10^{-4}
Au line length (m)	6.0×10^{-2}
Au line resistance (Ω)	1.30

Figure 25 shows the time domain step response of the filter predicted from the table 4 data. The corresponding time domain impulse response is shown in figure 26. A plot of the frequency-domain parameter $|S_{21}(j\omega)|$ is shown in figure 27, and a plot of $|Z_o(j\omega)|$ is shown in figure 28. As shown in figure 25, the step response of this filter design is 97.656 ps and the characteristic impedance is very close to 50.0 Ω in the mid-frequency region, as seen in figure 28.

After further discussions with Vapor Technologies, it was learned that they were not equipped to use their technique for our thick-coating purposes. It was decided then to recontact Silica Source Technology, Tempe, AZ, to try and renegotiate using their Low Pressure Chemical Vapor Deposition (LPCVD) process to provide a 17.1 μm SiO_2 coating. After some preliminary discussions the contract specifications were written, and the NIST-Boulder purchasing department advertised a Request for Quotation (RFQ). Two responses were received, one from Silica Source Technology and one from Thin-Film Research, Inc., Westford, MA. While Silica Source Technology could provide only the SiO_2 coating, further discussions with Thin-Film Research indicated that they could do all of the required wafer processing steps. Therefore, it was decided to rewrite the contract specifications and to re-bid the contract, including specifications for all of the wafer processing steps. After a great

deal of negotiation and comparative analysis, Thin-Film Research was contracted ($25k) in August, 1989, to carry out a 9-step statement-of-work.

The contract specified that NIST would supply the doped-silicon wafers, masks for defining the SiO_2 and gold deposition patterns, and the gold. Thin-Film Research would measure the thickness and conductivity of each wafer, coat each with 17.1 μm of SiO_2 using their Ion Assisted, Electron Beam Physical Vapor Deposition technique, measure the coating thicknesses, deposit the necessary gold (1 μm coating on the unpolished side of each wafer and 10 μm gold lines on the polished side), dice the wafers to the required circuit sizes, and send the circuits and all measured data back to NIST. Figure 29 is a sketch of the 3-inch silicon wafer layout for five microstrip circuits.

Almost exactly one year later (August, 1990) NIST received all of the measured data for twenty good wafers from Thin-Film Research. They had finally completed the SiO_2 coating of the wafers after much delay and difficulty. All of the "as-built" data were analyzed, and the model was recomputed with mean values from these data. The final, as-built model parameters are listed in table 5.

Table 5

"As-built" estimates for the values of the electrical and physical parameters of the 100 ps filter.

Parameter	100 ps Filter Values
σ_{Au} (S/m)	4.6×10^{7}
σ_{Si} (S/m)	86.28
σ_{SiO2} (S/m)	1.0×10^{-18}
$\epsilon_{r(Si)}$	11.7
$\epsilon_{r(SiO2)}$	3.78
Si thickness (m)	2.5235×10^{-4}
SiO_2 thickness (m)	1.705×10^{-5}
Au line thickness (m)	1.0×10^{-5}
Au line width (m)	1.005×10^{-4}
Au line length (m)	5.2×10^{-2}
Au line resistance (Ω)	1.08

Notice that the doped-silicon conductivity, the silicon thickness, and the predicted gold line length all differ noticeably from the model data in table 4. Notice also that with the SiO_2 deposited, the only two parameters that still could be varied easily were the gold line width and the gold line length. The failure to obtain the target values was discussed with Thin-Films Research personnel and they agreed to perform the gold deposition on a single wafer. The intent was to fabricate five filter circuits on a single wafer, each with a different gold line width, in order to determine which line width yielded a circuit characteristic impedance closest to 50.0 Ω. Accordingly, in the fall of 1990, NIST made the gold-deposition mask necessary for the process and sent it, along with 100 g of pure gold, to Thin-Films Research. This mask was designed to yield gold line widths of 90, 95, 100, 105, and 110 μm. Thin-Films Research agreed to perform the gold deposition, dice the five circuits, and return the circuits and all measurement results. The circuits were received in May, 1991. According to the Thin-Films Research measurement data, the gold line thicknesses were all about 10.5 μm, and the line widths were about 98 μm (line #7), 102 μm (line #6), 108 μm (line #4), 115 μm (line #3), and 120 μm (line #2). (The line number notation is that of Thin-Films Research.)

The five circuits were then mounted in the NIST adjustable microstrip filter mounts and their time-domain transmission and reflection characteristics measured with a 20 GHz-bandwidth sampling oscilloscope. Figure 30 is a plot of the internal, 200 mV, positive-transition, step-like pulse generated by the sampling oscilloscope (channel 1), as reflected from a short circuit. The time window of this plot has been chosen so that the earlier, positive pulse transition occurs off the left edge of the plot. All that is shown in this time window is the (later) negative transition, representing only the reflection from the short circuit. This plotted signal switches from about 200 mV to about 0 V, which is the amplitude of the internally generated step-like pulse. Figures 31 through 35 are plots of the reflections from lines 2, 3, 4, 6, and 7, respectively, for the step-like internal pulse stimulus. An approximation for both the characteristic impedance and the pulse velocity of propagation can be determined for the five lines from these reflection plots.

For an ideal, lossless, 50.0 Ω filter, one would expect to see almost no reflections, and the plot would be essentially a flat, horizontal line at about the 200 mV level. If some loss in the ideal filter is allowed, then the plot would have a slight positive slope (i.e., a ramp) for a time duration equal to 2τ, where τ is the length of time required for the pulse to propagate through the filter. From the mathematical model for the microstrip filter (see Appendix A), this time interval can be approximated as,

$$\tau = l\sqrt{LC_1}, \tag{1}$$

where l is the length of the line, and the per-unit-length equivalent-circuit parameters derived from the mathematical model are listed in table 6.

Table 6

"As-built" estimates for the values of the equivalent-circuit parameters of the 100 ps filter.

SYMBOL	PARAMETER	VALUE
L	Series inductance per meter (H/m)	6.14×10^{-7}
R	Series resistance per meter (Ω/m)	21.63
C_1	SiO_2 shunt capacitance per meter (F/m)	2.45×10^{-10}
C_2	Si substrate shunt capacitance per meter (F/m)	1.37×10^{-10}
G_1	SiO_2 shunt conductance per meter (S/m)	≈ 0
G_2	Si substrate shunt conductance per meter (S/m)	107.85

Substituting values into equation 1 for l (from table 5), L, and C_1, the model-predicted value for 2τ is 1.23 ns. Looking at figures 31 through 35, it can be seen that 2τ varies from about 1.9 ns for line #7 to about 2.4 ns for line #2. (This time is measured from the beginning of the negative transition, located at about the first time division, to the time of the first secondary reflection, which occurs at about the fifth time division.) Clearly, this time is too large, implying that the velocity of propagation along the lines is much too slow compared to the model prediction.

For the characteristic impedance, the model predicts (mid-frequency approximation) an estimate of,

$$Z_o \sim \sqrt{\frac{L}{C_1}} \qquad (2)$$

which, when the values of L and C_1 from table 6 are substituted, yields a model-predicted characteristic impedance of 50.0 Ω. The approximate characteristic impedance from the reflection plots can be determined by means of the following equation:

$$Z_{filter} = Z_o \frac{V_2}{2V_1 - V_2} \qquad (3)$$

where, for any time point, Z_o is 50.0 Ω, V_1 is the original pulse amplitude (assumed to start at 0 V), and V_2 is the voltage at the time point of interest. Thus, in figure 35, for example, (line #7) the average voltage, V_2, in the second time division is about 125 mV while the original pulse amplitude is about 200 mV. Substituting these values into equation 3 yields

a characteristic impedance of about 23 Ω. Looking at the reflection plots for all five lines, it can be seen that they all possess impedances that are about half or less of the target 50 Ω impedance. In addition, only the plots for lines #3 and #7 exhibit the slightly positive linear ramp that would be expected (in time divisions 2 through 5); the other three lines exhibit reflection plots in these time divisions that are very puzzling indeed.

Figure 36 is a plot of the transmission reference waveform generated from channel 1 of the 20 GHz-bandwidth sampling oscilloscope and measured on channel 4 of this scope. This pulse has a first transition duration of about 35 ps. Figures 37 through 41 are plots of the filter transmission responses to this pulse, with figure 37 corresponding to line #2, 38 to line #3, 39 to line #4, 40 to line #6, and 41 to line #7. Since the characteristic impedances of these lines are so far from 50 Ω, and because they are fairly short in length, it is impossible to read estimates for the first transition durations (10%-90%) from these figures. Secondary reflections from the gross impedance mismatches interfere with the transmission waveform well before the response signal level has had time to reach its 90% value. However, one can read the (10%-50%) transition durations. Using the automated estimating features of the sampling oscilloscope, these (10%-50%) transition durations were found to be about 557 ps (line #2), 382 ps (line #3), 395 ps (line #4), 365 ps (line #6), and 286 ps (line #7). The model predicts that the (10%-90%) transition durations are symmetrical about the 50%-points. Therefore The (10%-90%) transition durations should be twice these values, or, 1114, 764, 790, 730, and 572 ps. These values far exceed the target, model-predicted value of 97.66 ps. At this point (September, 1991) it was concluded that something was very wrong with the five prototype filters that had been fabricated by Thin-Films Research, and with no remaining funds, all work on this project was stopped.

III. Conclusions and Recommendations

The fact that the five prototype filter circuits missed the target by such a large amount is due to one of two possibilities. Either the mathematical model contains some gross error or else the five circuits were not fabricated to the specifications. Since the model predicted the behavior of the first three circuits quite well (see table 1 and figures 1 through 12), the likelihood of its complete failure is not likely. On the other hand, all of the as-built measurement data accompanying the five prototype circuits from Thin-Films Research appears to be quite good (see table 5). It is clear that more work must be done in order to identify the real problem(s) and provide a solution.

It is the recommendation of NIST personnel that work continue on the filter project as funding and time permit. Thin-Films Research has been instructed to return to NIST the 19 SiO_2-coated wafers still in their possession along with the circuit mask. The next step, then, will be to attempt an "autopsy" on one of the five circuits and on one of the 19 wafers to determine, independently, the physical parameters of each. If it is found that the wafers and circuits fabricated by Thin-Films Research are indeed as specified, then the mathematical model will be investigated. Once the problem has been identified with a high degree of probability, the fabrication of new circuits will be undertaken.

References

[1] W. D. McCaa, Jr. and N. S. Nahman, "Generation of reference waveforms by uniform lossy transmission lines," IEEE Trans. Instrum. Meas., vol. IM-19, no. 4, pp. 382-390, Nov. 1970.

[2] N. S. Nahman, R. M. Jickling, and D. R. Holt, "Reference waveform generation using Debye dielectric dispersion," Nat. Bur. Stand. (U.S.) NBSIR 73-304, Dec. 1972.

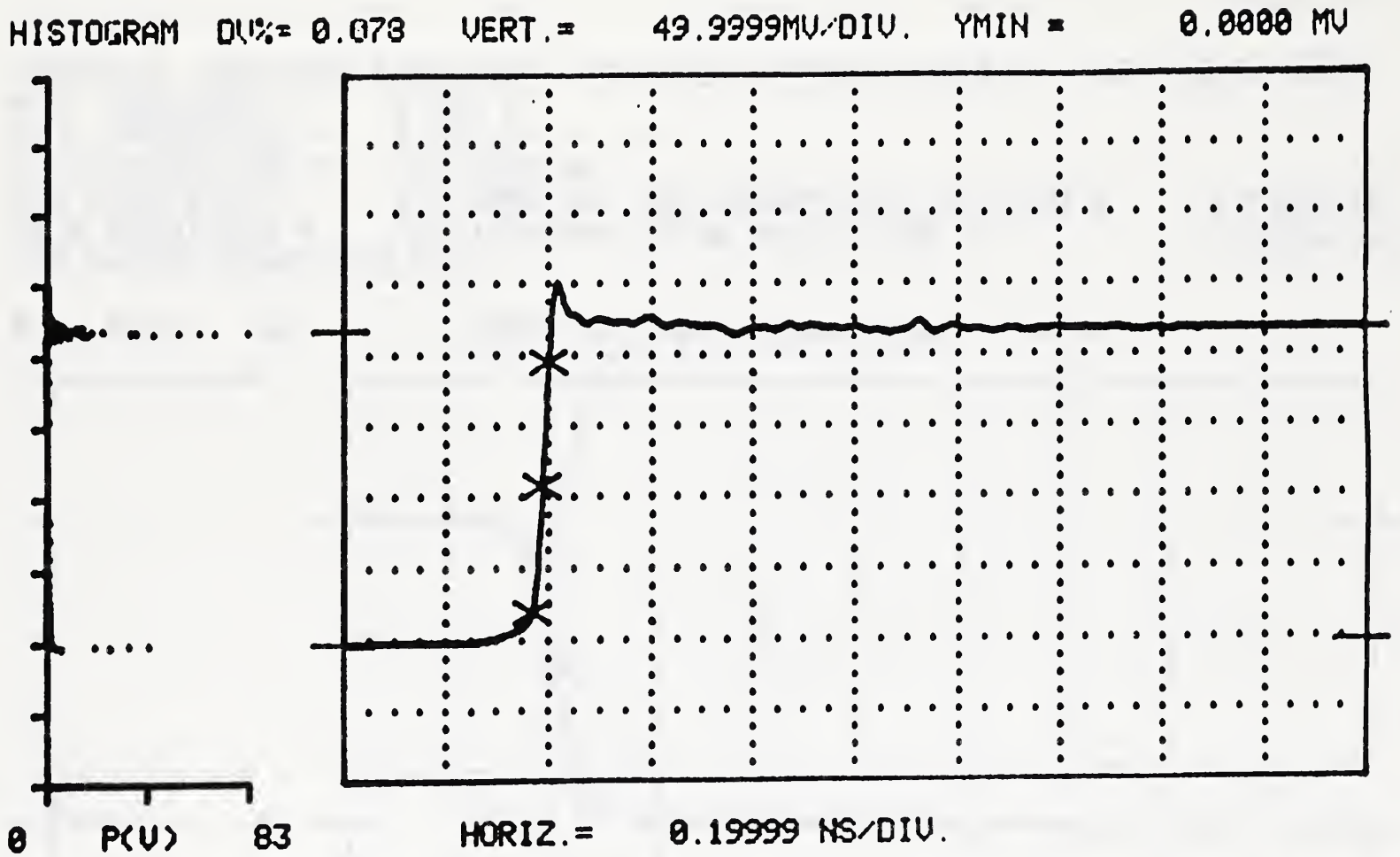

FIGURE 1

THE PULSE PARAMETERS ARE:

BASE MAGNITUDE =	97.7533 MV	PULSE START TIME =	0.39171 NS
TOP MAGNITUDE =	318.0830 MV	1ST TRANSITION DURATION =	0.03216 NS
PULSE AMPLITUDE =	220.3300 MV		
MAX. UNDERSHOOT =	0.313 %		
MAX. OVERSHOOT =	14.484 %		

COMMENTS: REFERENCE WAVEFORM---HP-1106A--#732-00869--------9/4/87----WLG

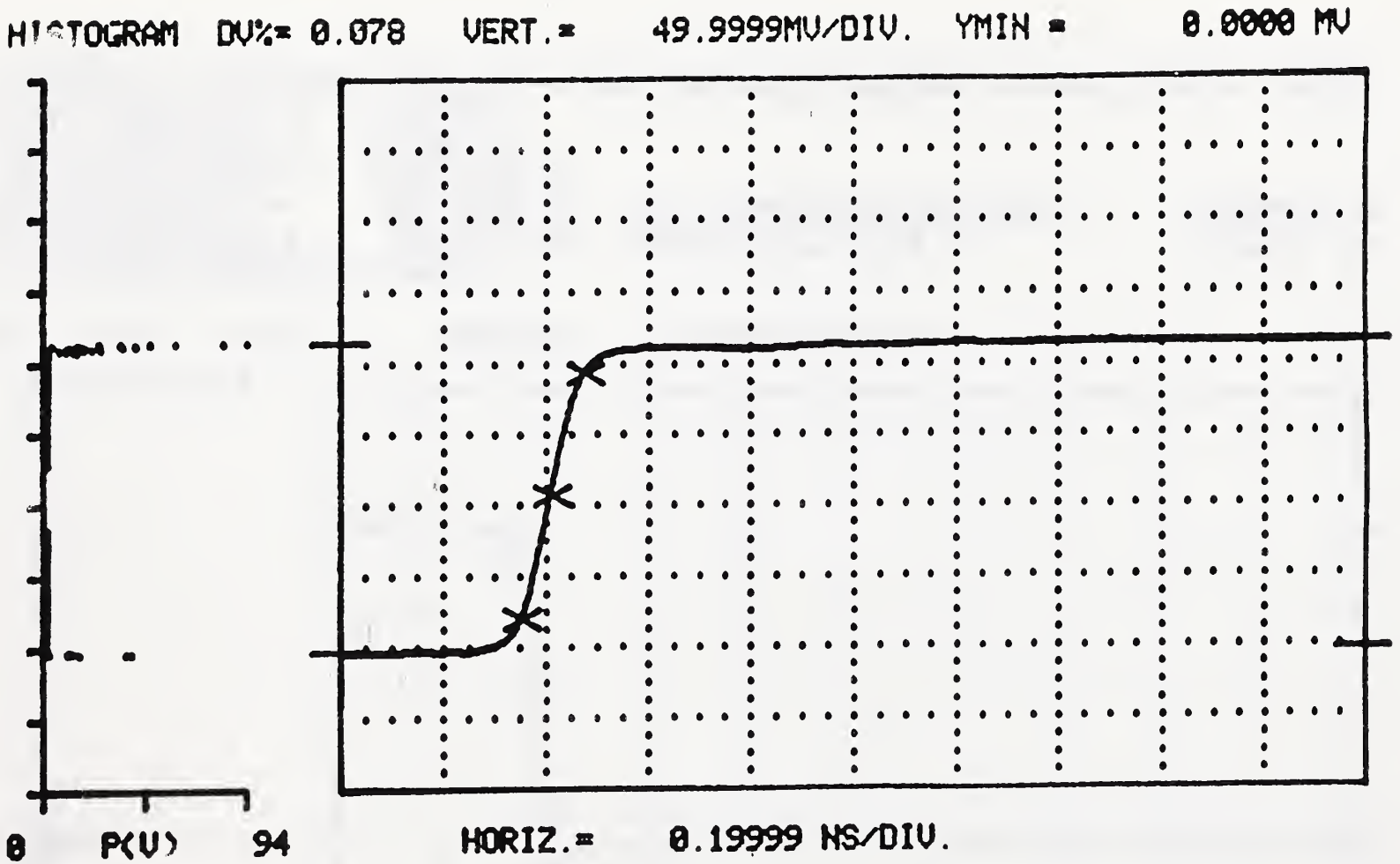

THE PULSE PARAMETERS ARE:

BASE MAGNITUDE =	96.1918 MV	PULSE START TIME =	0.40879 NS
TOP MAGNITUDE =	313.8320 MV	1ST TRANSITION DURATION =	0.12370 NS
PULSE AMPLITUDE =	217.6400 MV		
MAX. UNDERSHOOT =	0.117 %		
MAX. OVERSHOOT =	0.117 %		

COMMENTS: RESPONSE WAVEFORM---1.0 INCH SILICON FILTER------9/4/87----HLG

FIGURE 2

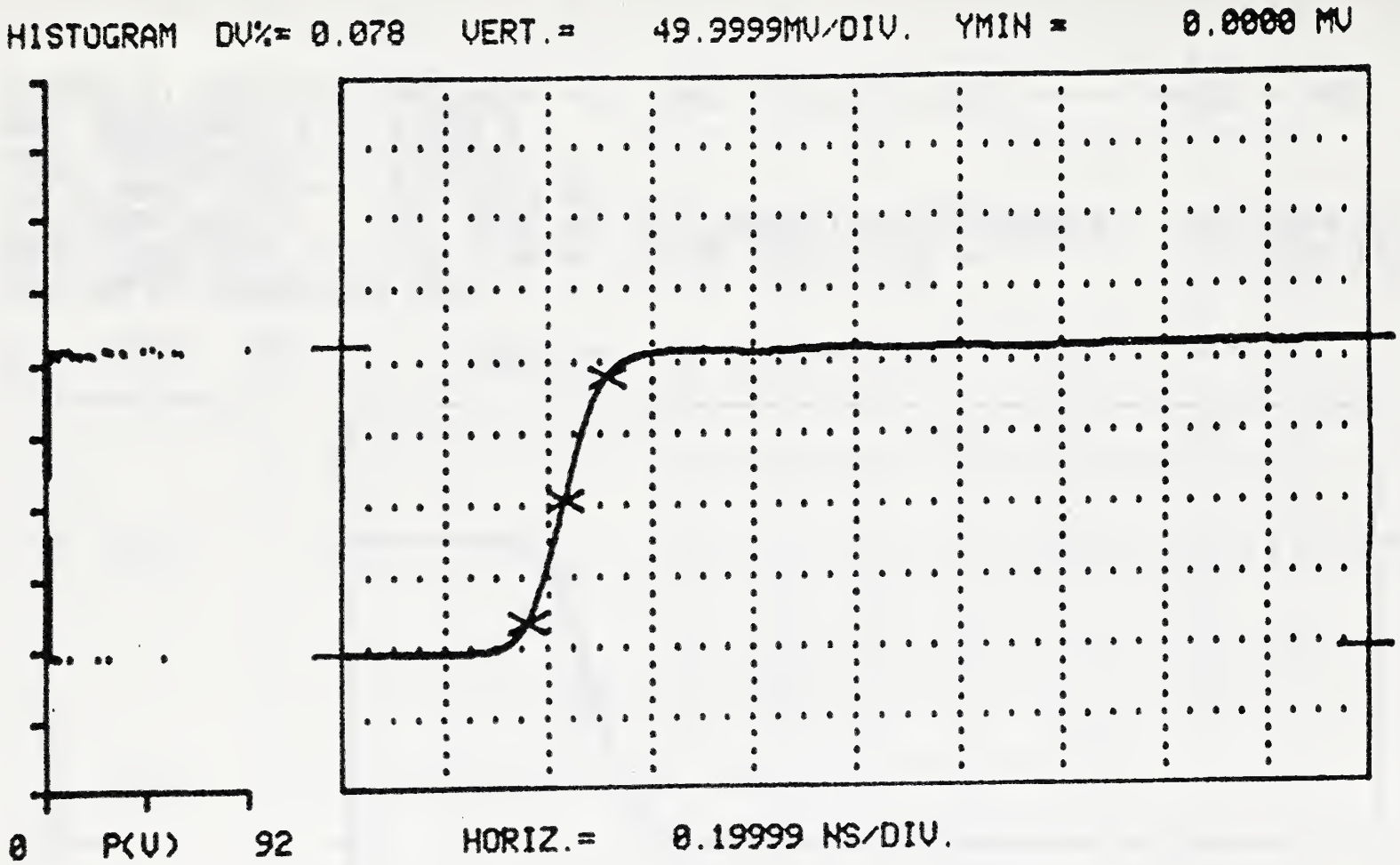

THE PULSE PARAMETERS ARE:

BASE MAGNITUDE =	95.7505 MV	PULSE START TIME =	0.43259 NS
TOP MAGNITUDE =	310.9710 MV	1ST TRANSITION DURATION =	0.15346 NS
PULSE AMPLITUDE =	215.2200 MV		
MAX. UNDERSHOOT =	0.195 %		
MAX. OVERSHOOT =	0.117 %		

COMMENTS: RESPONSE WAVEFORM---1.5 INCH SILICON FILTER------9/4/87----WLG

FIGURE 3

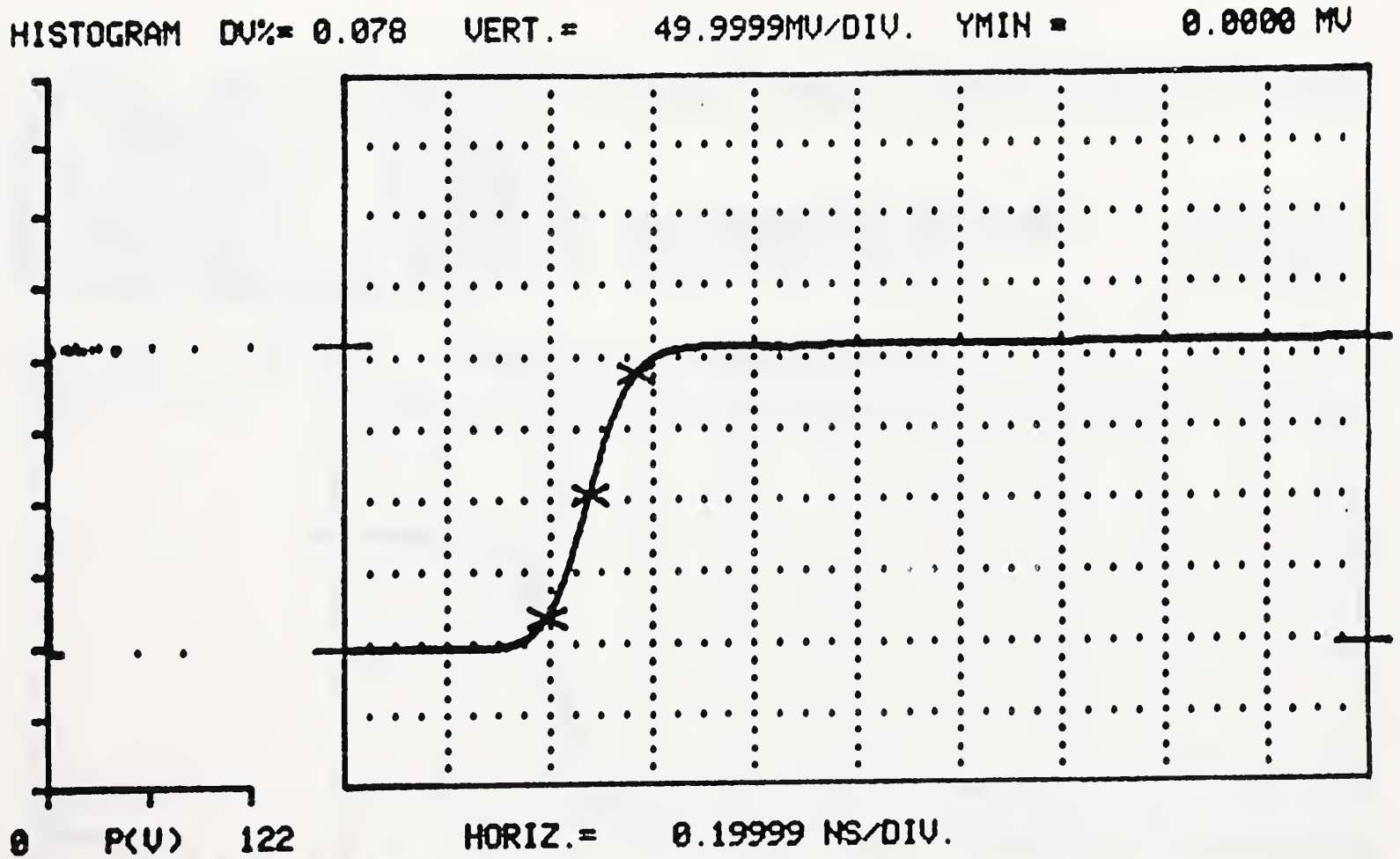

FIGURE 4

THE PULSE PARAMETERS ARE:

BASE MAGNITUDE =	96.4888 MV	PULSE START TIME =	0.47749 NS
TOP MAGNITUDE =	309.5810 MV	1ST TRANSITION DURATION =	0.17244 NS
PULSE AMPLITUDE =	213.0920 MV		
MAX. UNDERSHOOT =	0.039 %		
MAX. OVERSHOOT =	0.352 %		

COMMENTS: RESPONSE WAVEFORM---2.0 INCH SILICON FILTER------9/4/87----WLG

FIGURE 5

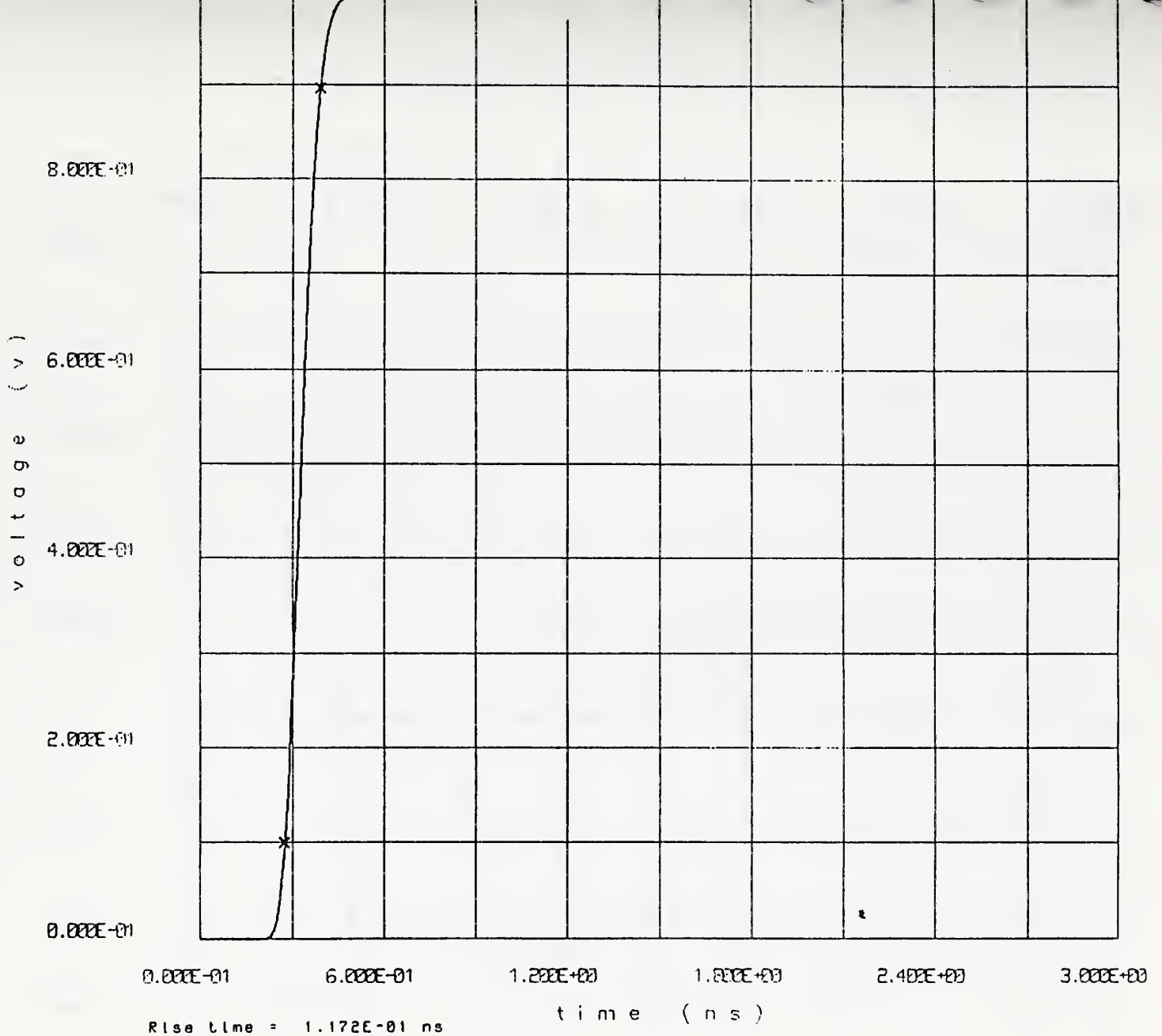

step371n2.50

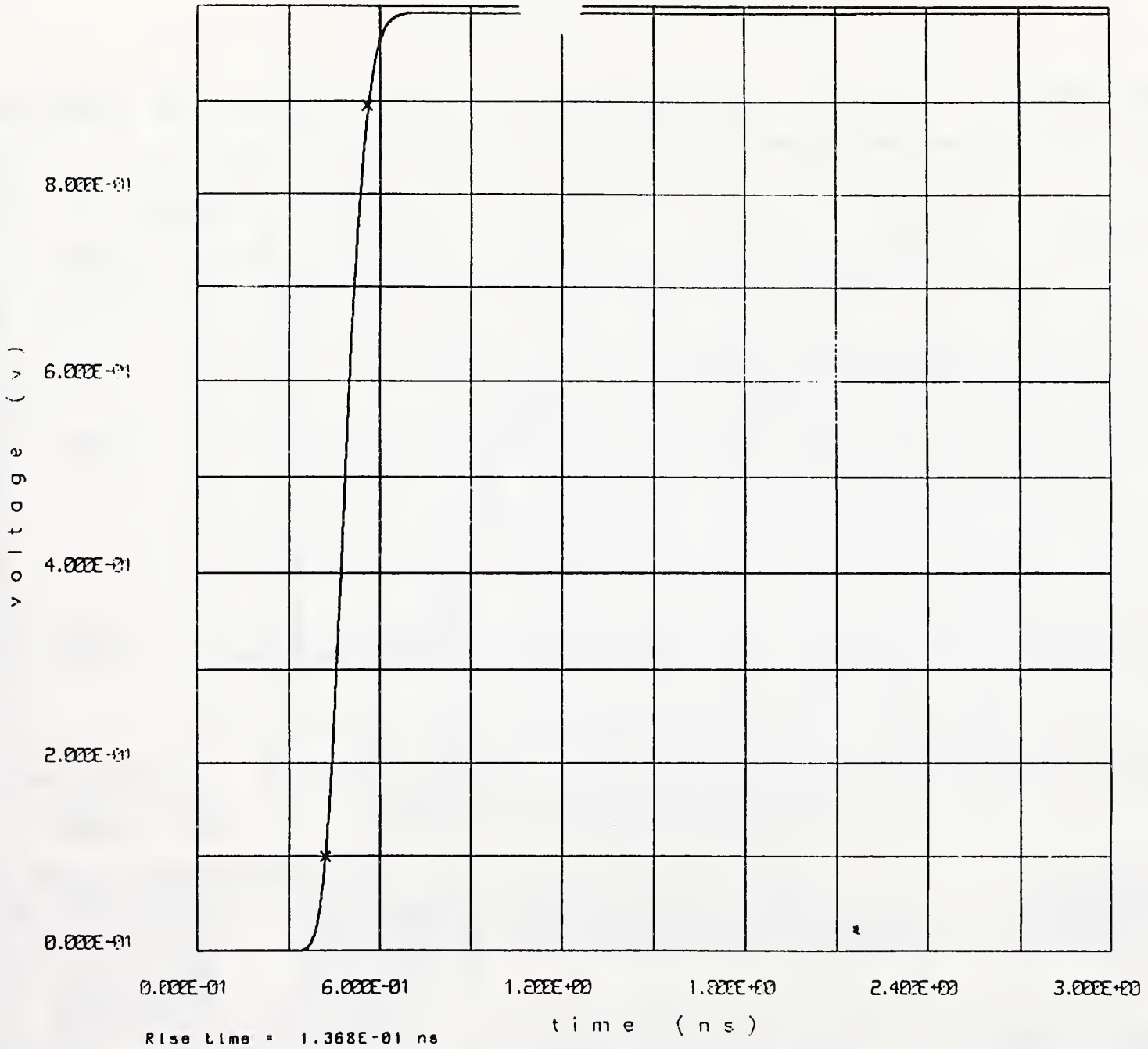

step37ln3.75

FIGURE 6

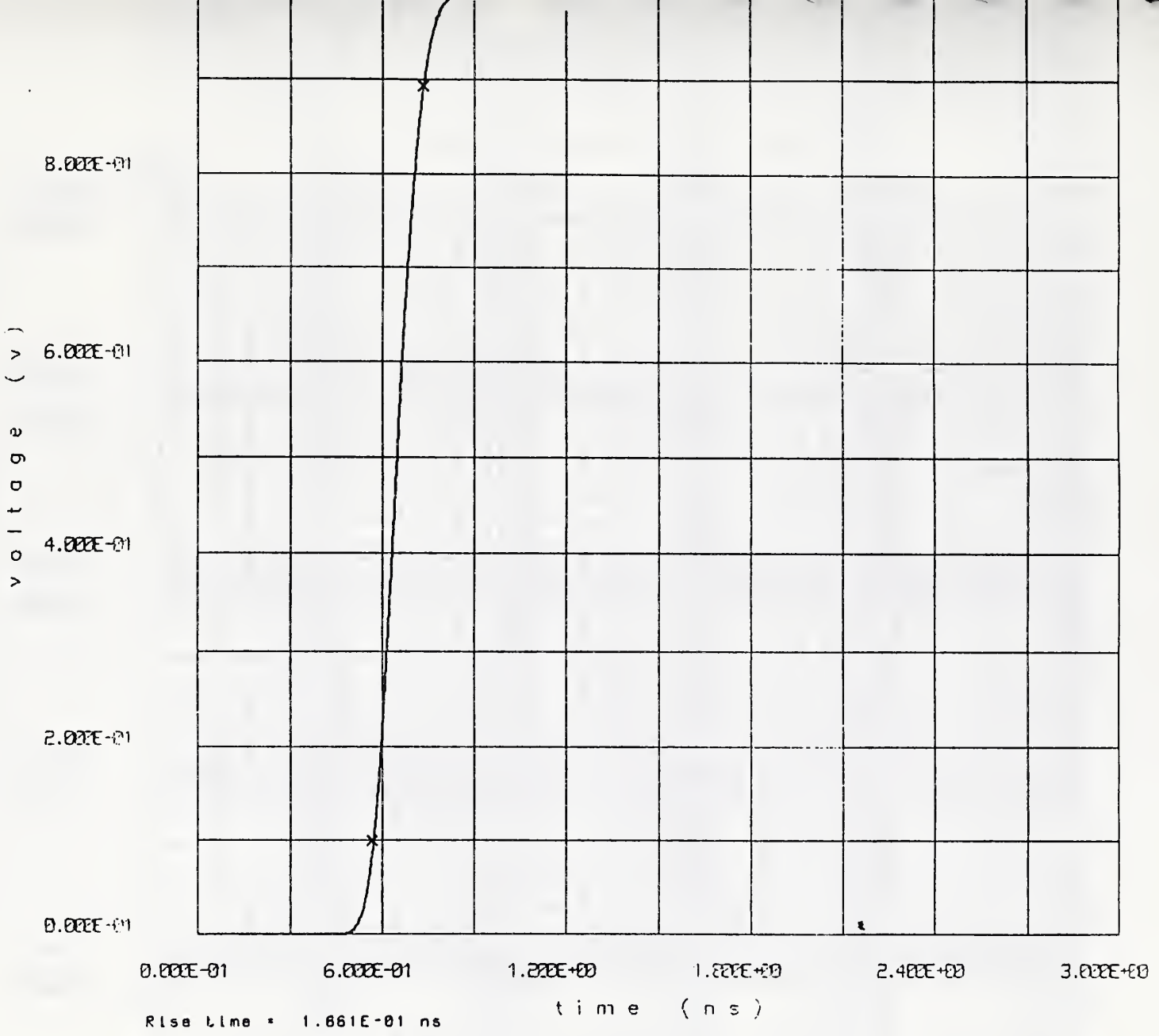
8.000E-01
6.000E-01
4.000E-01
2.000E-01
0.000E-01
voltage (v)
0.000E-01
6.000E-01
1.200E+00
1.800E+00
2.400E+00
3.000E+00
time (ns)
Rise time = 1.861E-01 ns
step37in5.00

FIGURE 7

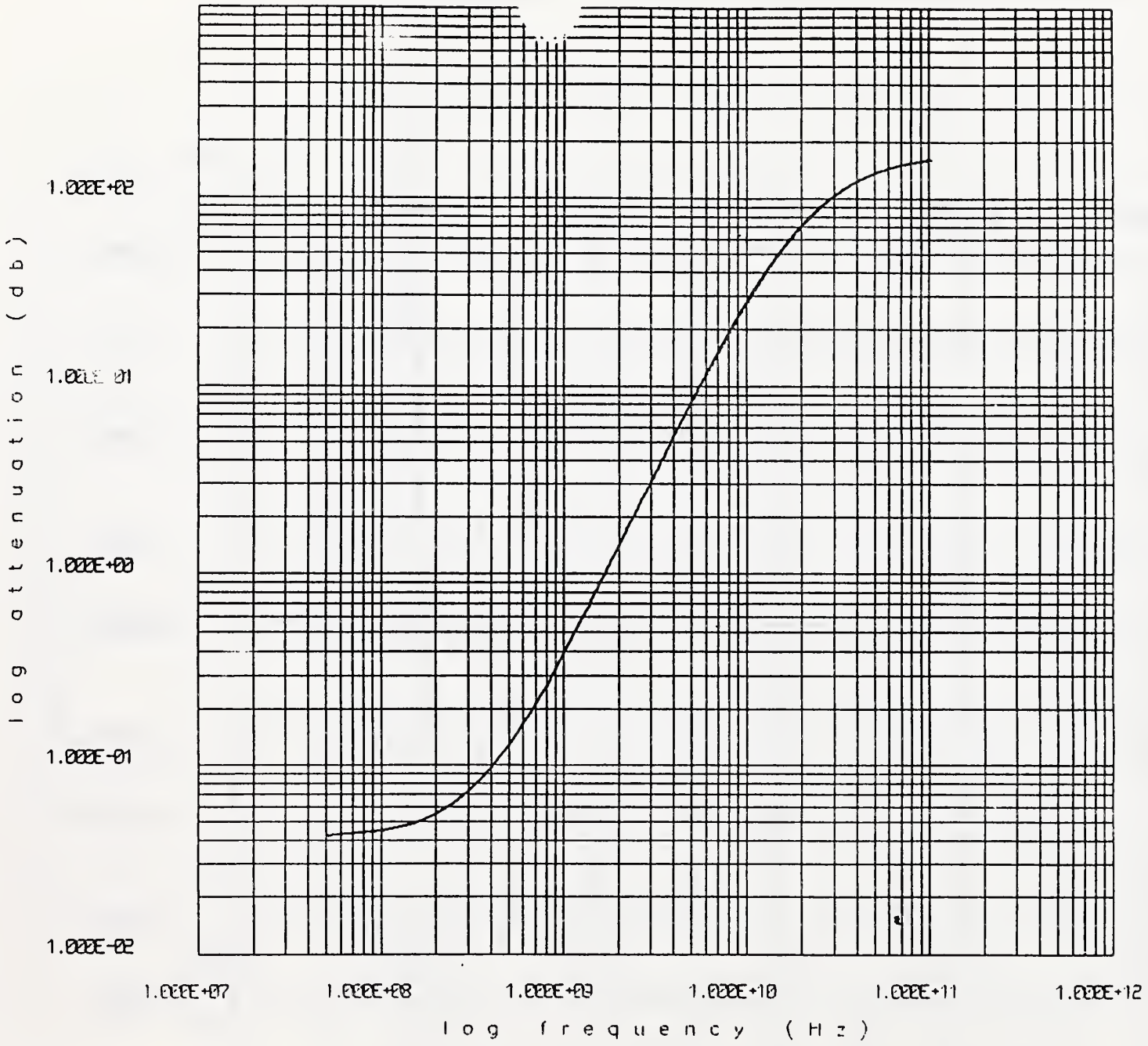

FIGURE 8

s 2 1 m 3 7 l n 2 . 5 0

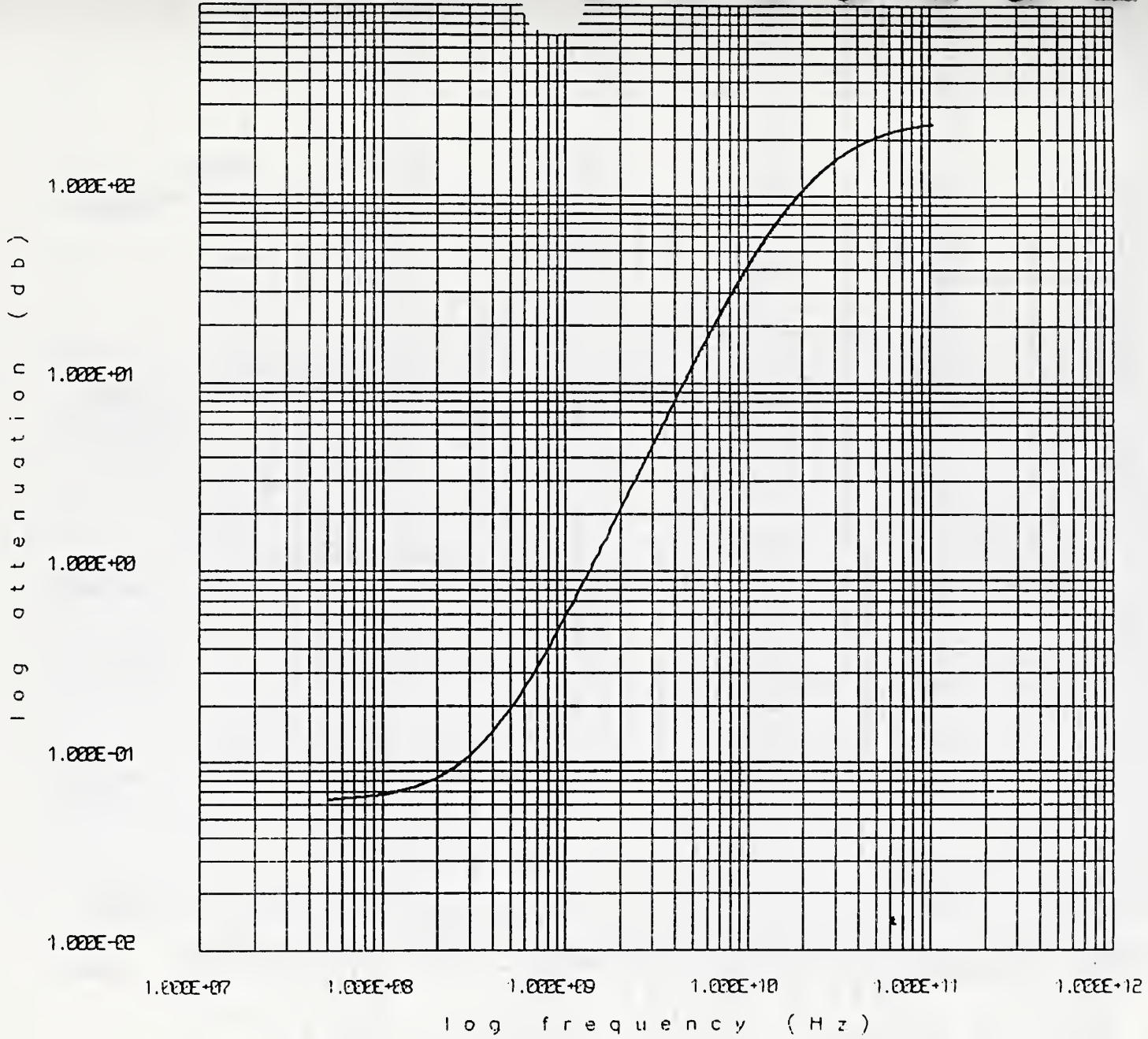
1.000E+02
1.000E+01
1.000E+00
1.000E-01
1.000E-02
log attenuation (db)
1.000E+07
1.000E+08
1.000E+09
1.000E+10
1.000E+11
1.000E+12
log frequency (Hz)
s21m37ln3.75

FIGURE 9

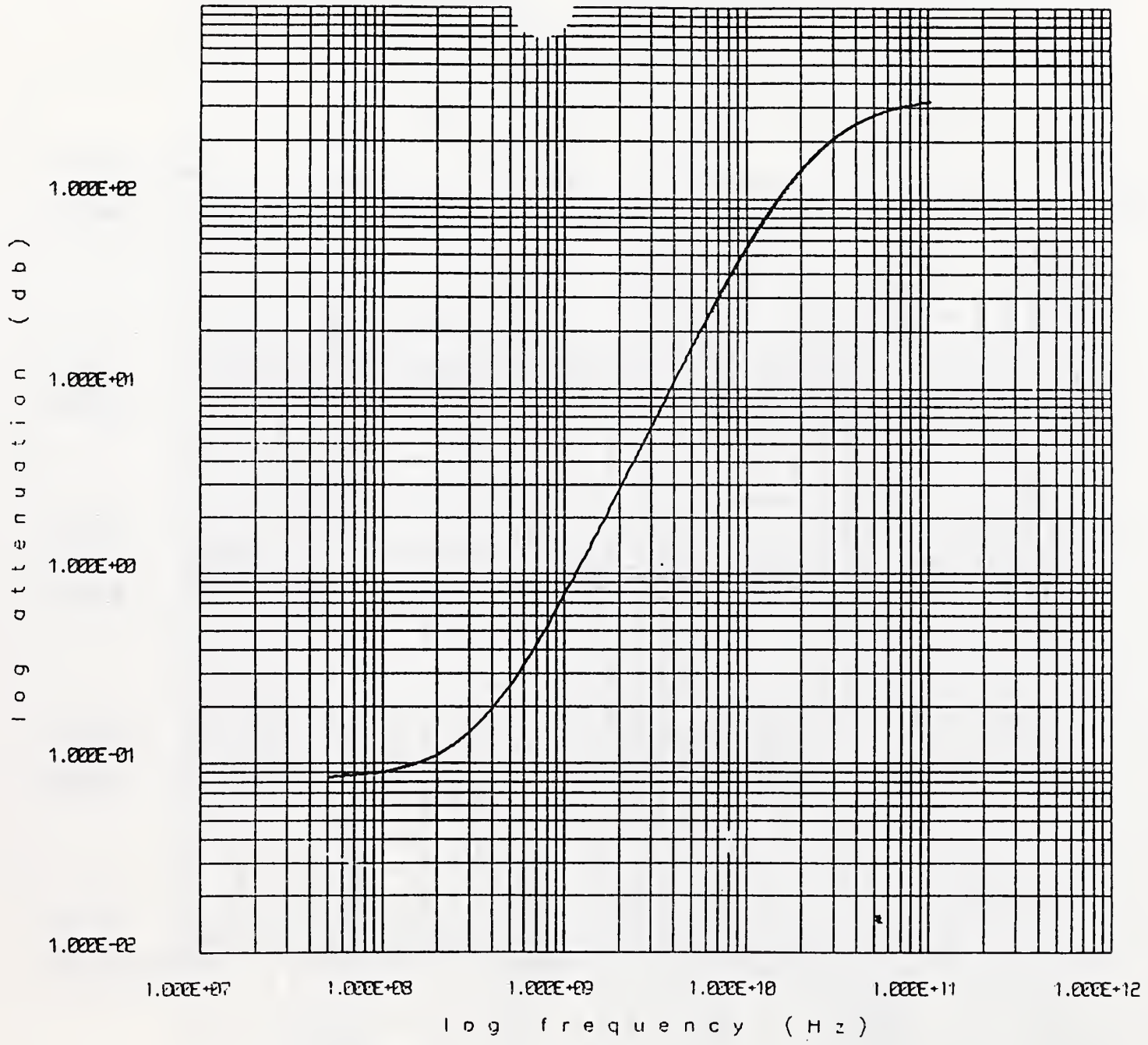

s 2 1 m 3 7 l n 5 . 0 0

FIGURE 10

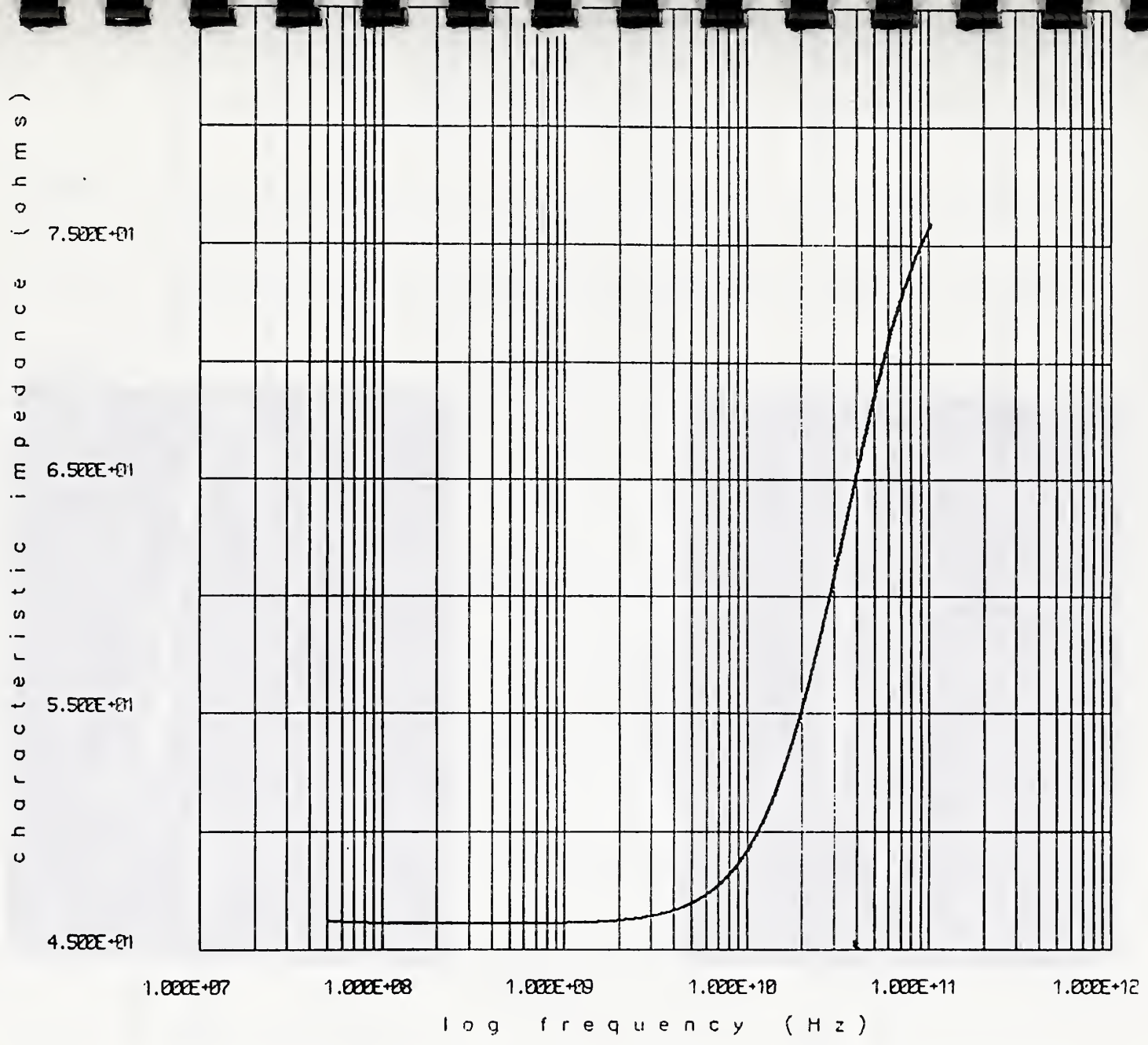
characteristic impedance (ohms)
7.500E+01
6.500E+01
5.500E+01
4.500E+01
1.000E+07
1.000E+08
1.000E+09
1.000E+10
1.000E+11
1.000E+12
log frequency (Hz)
zom37ln5.00

FIGURE 11

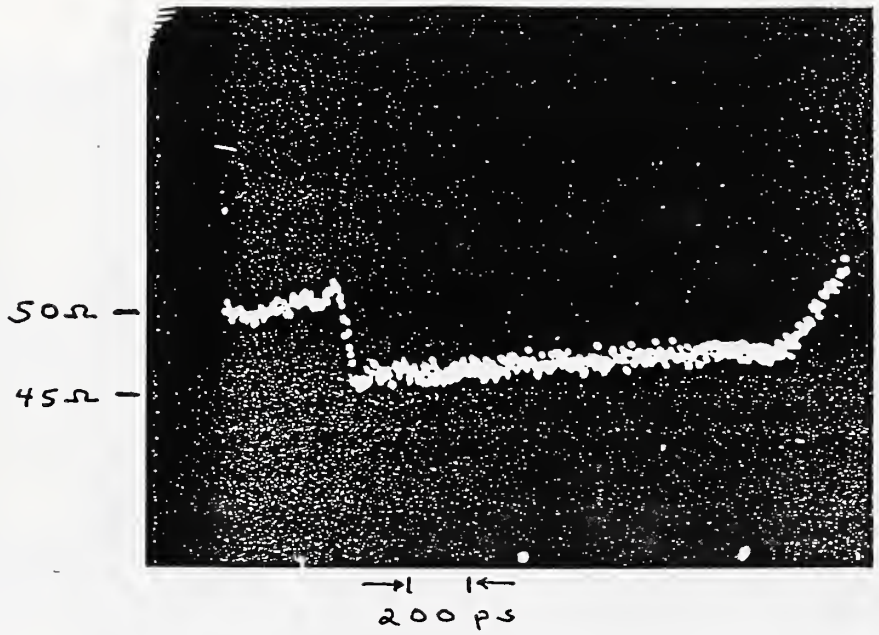

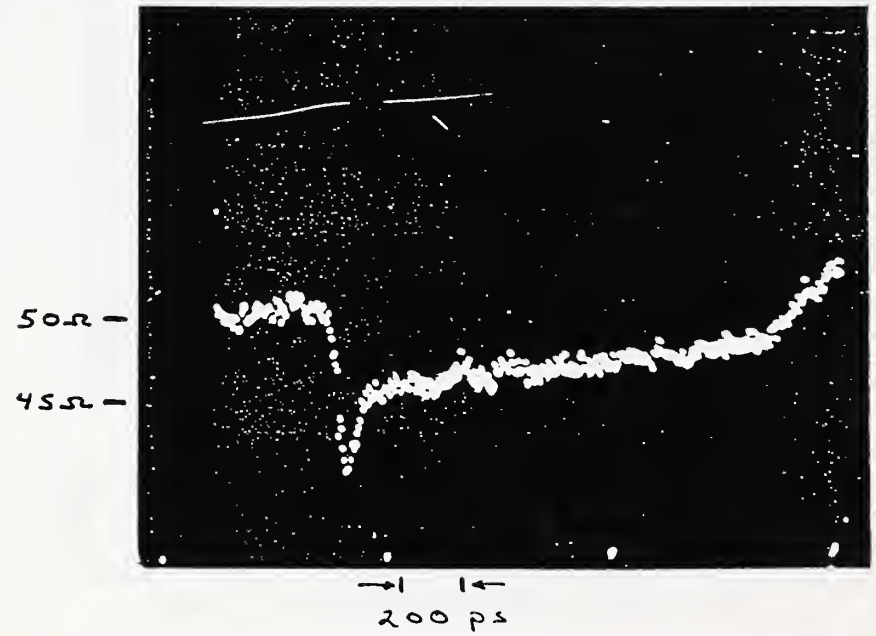

FIGURE 12

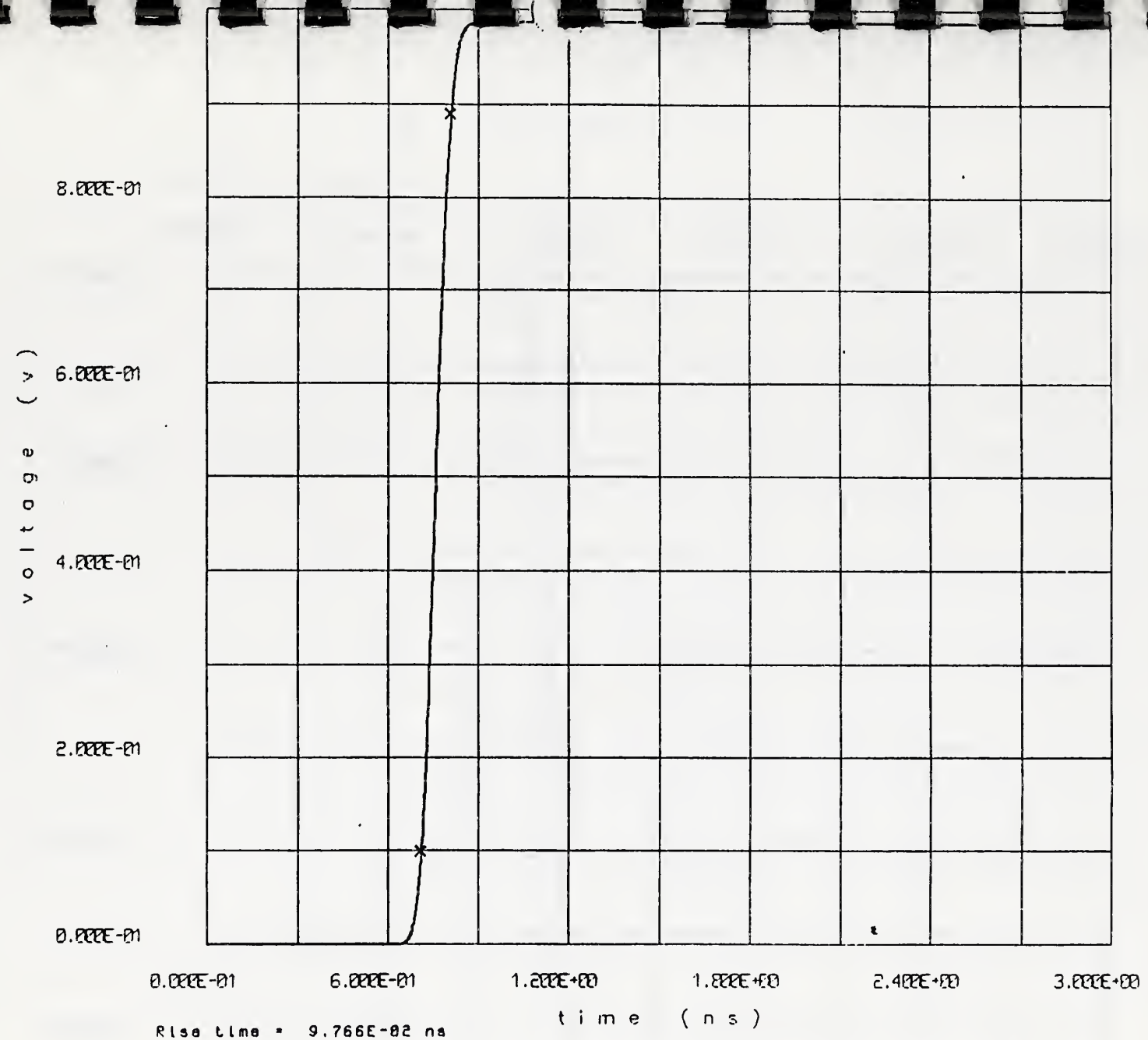
8.000E-01
6.000E-01
4.000E-01
2.000E-01
0.000E-01
voltage (v)
0.000E-01
6.000E-01
1.200E+00
1.800E+00
2.400E+00
3.000E+00
time (ns)
Rise time = 9.766E-02 ns
step100.62

FIGURE 13

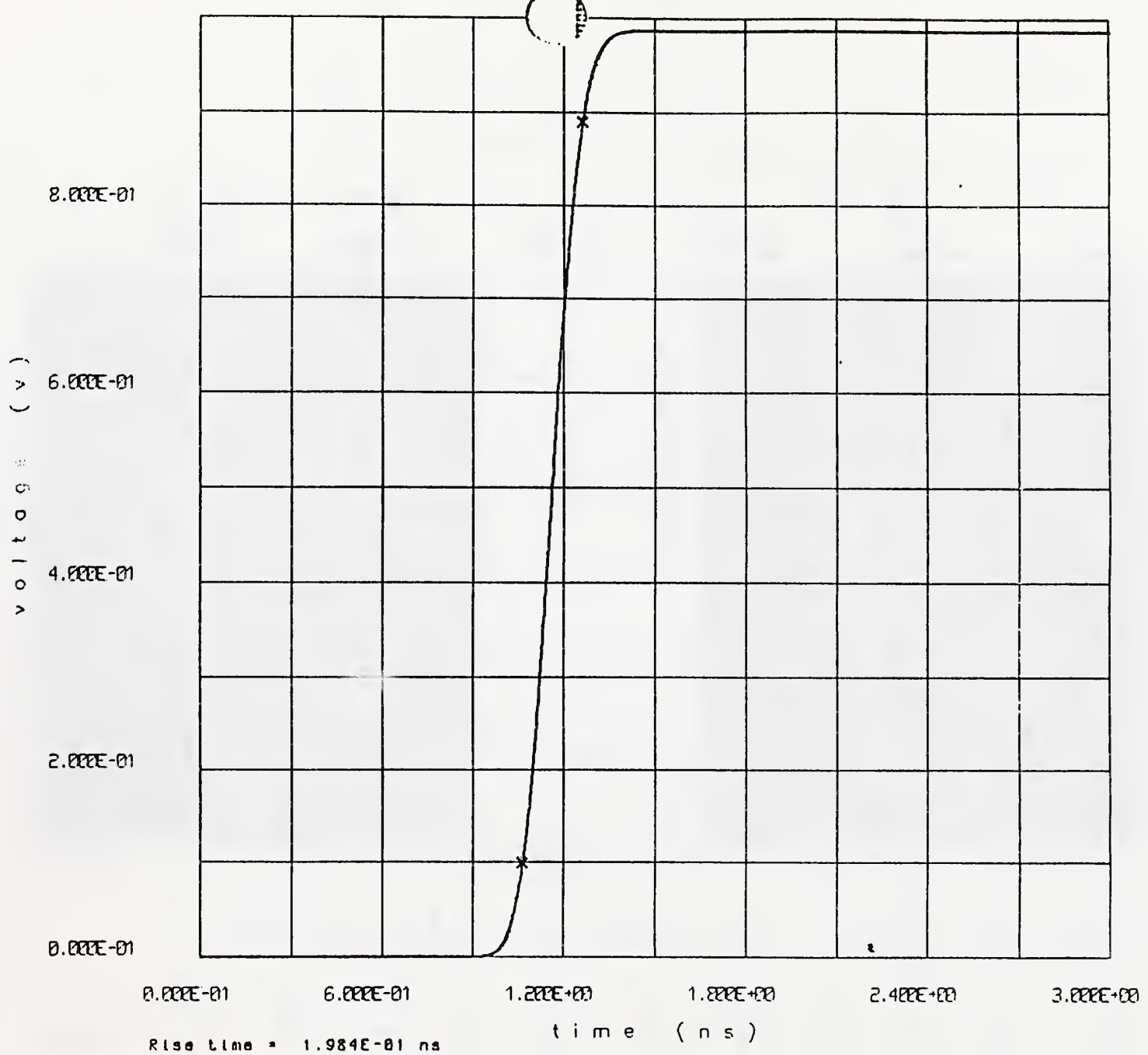

FIGURE 14

step200.62

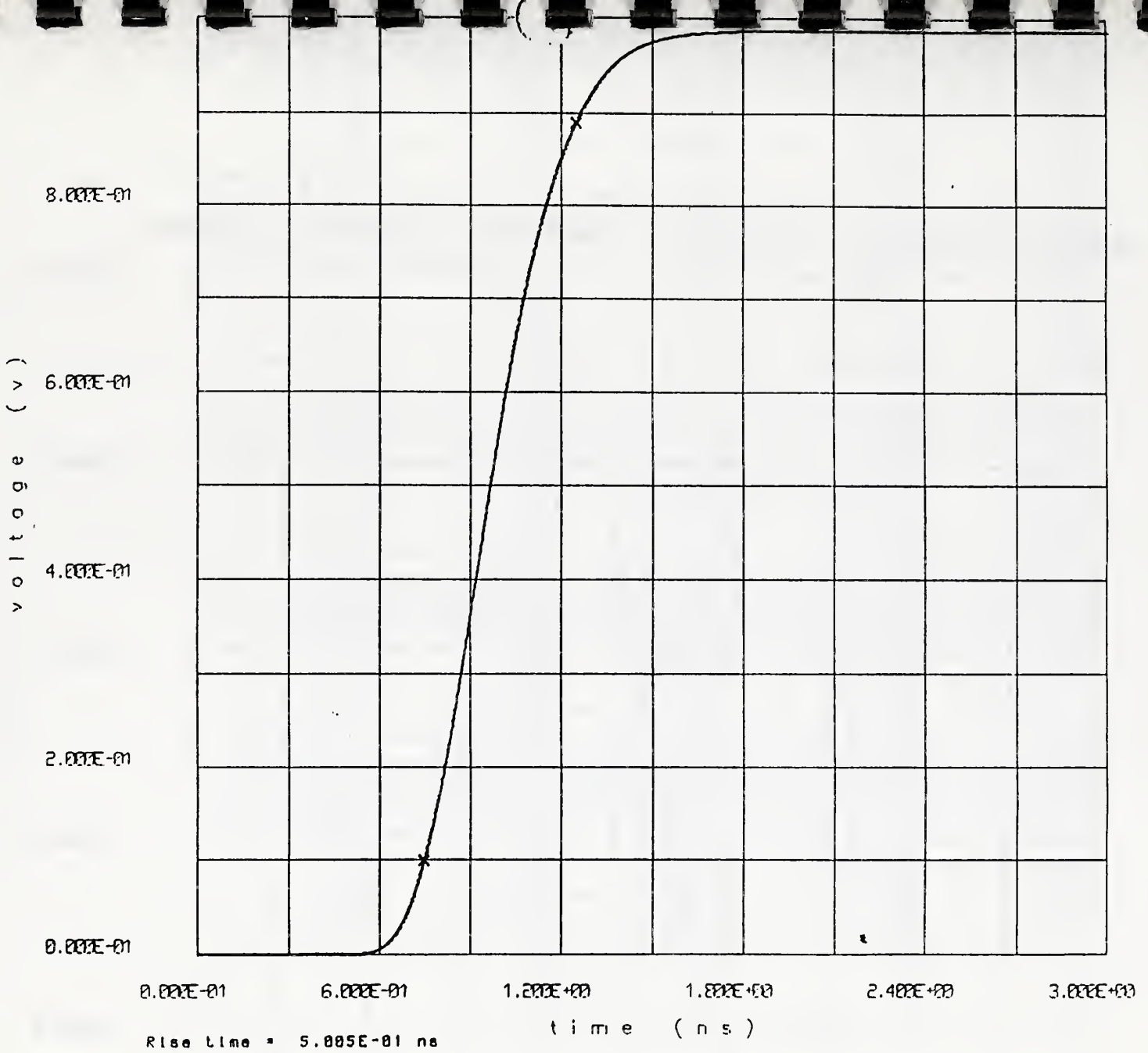

FIGURE 15

step500.62

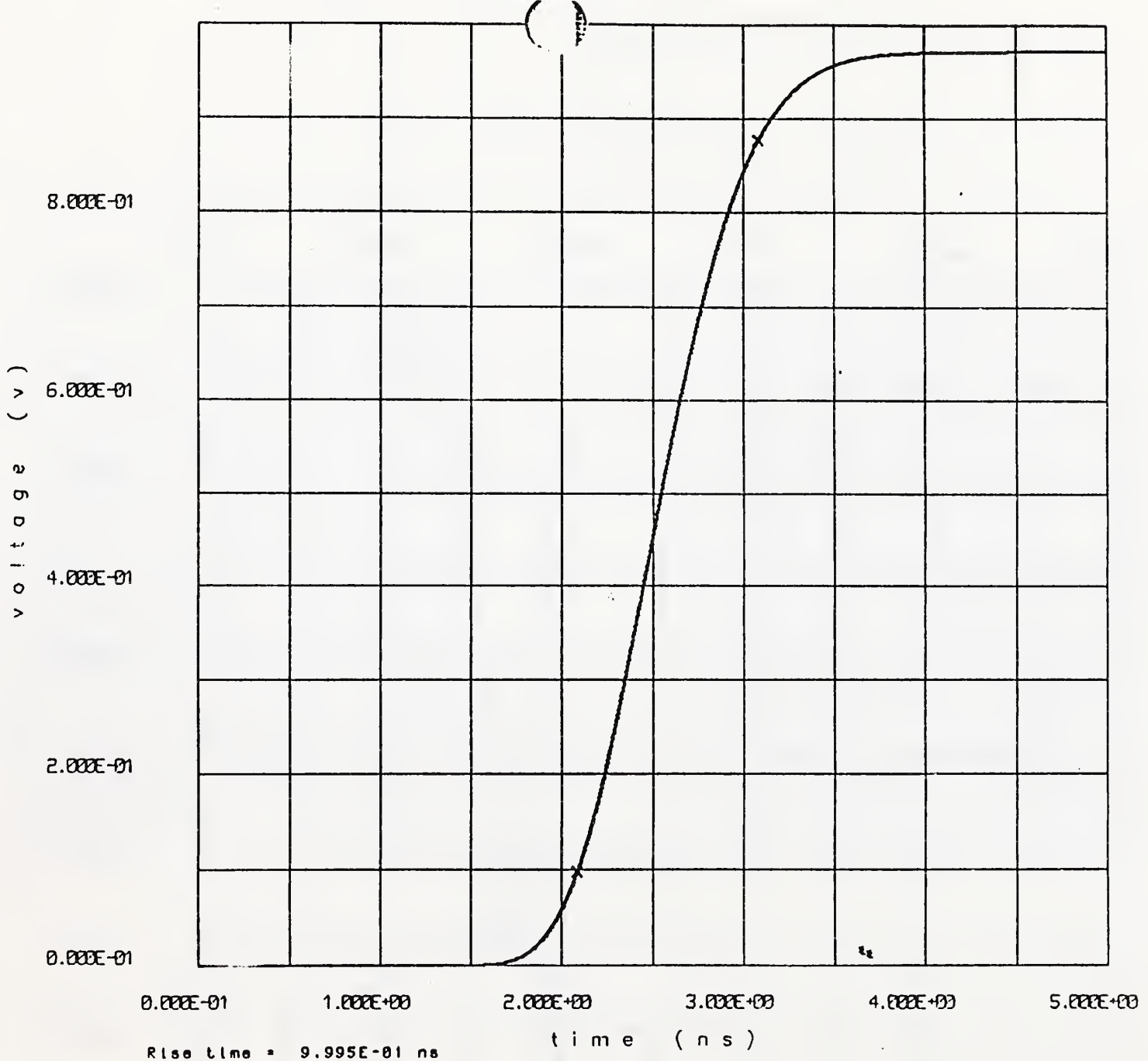
8.000E-01
6.000E-01
4.000E-01
2.000E-01
0.000E-01
voltage (v)
0.000E-01
1.000E+00
2.000E+00
3.000E+00
4.000E+00
5.000E+00
time (ns)
Rise time = 9.995E-01 ns
step1000.62

FIGURE 16

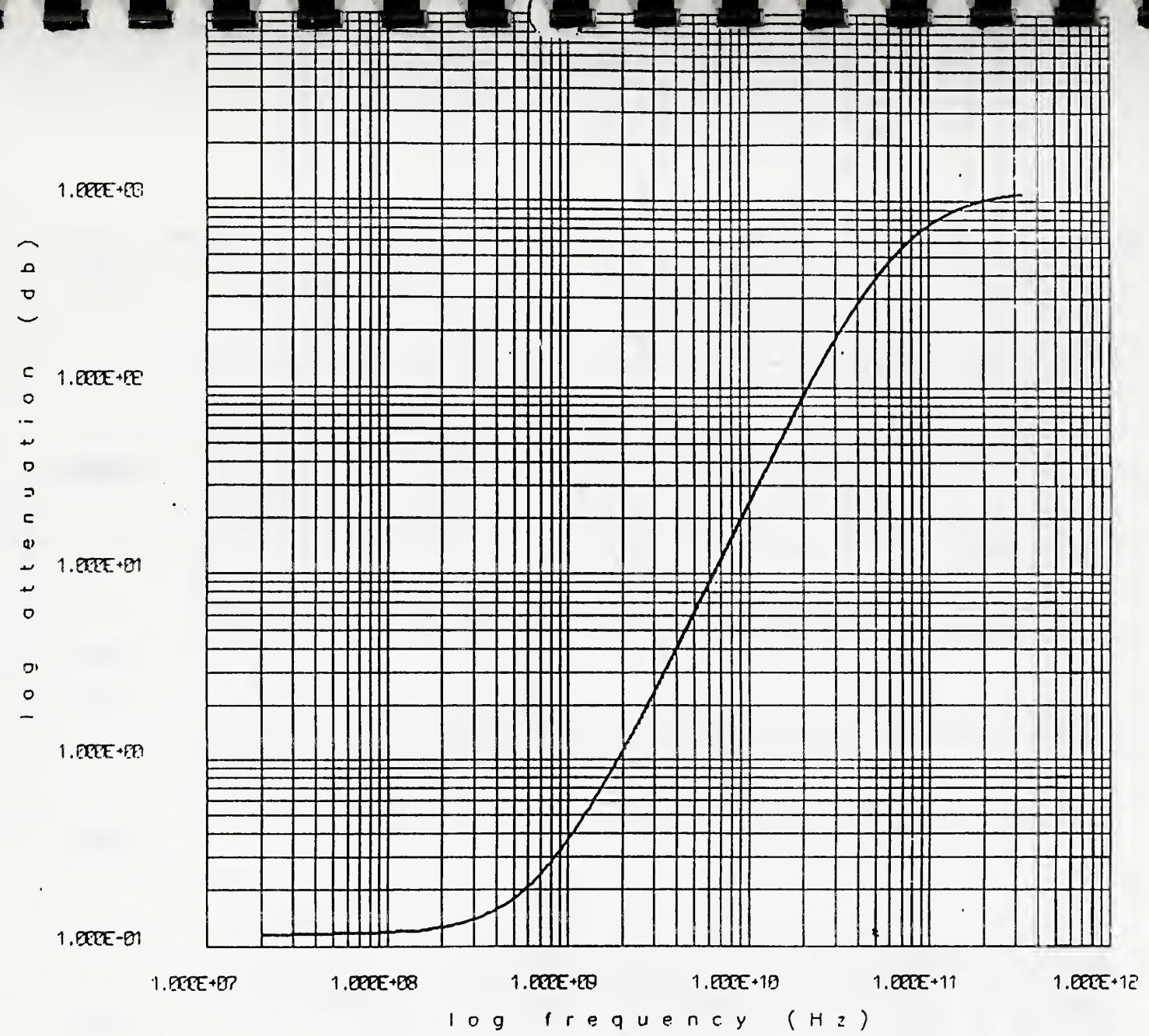
1.0000E+03
1.0000E+02
1.0000E+01
1.0000E+00
1.0000E-01
log attenuation (db)
1.0000E+07
1.0000E+08
1.0000E+09
1.0000E+10
1.0000E+11
1.0000E+12
log frequency (Hz)
s21m100.62

FIGURE 17

s21m2000.62
log frequency (Hz)
1.0000E+07
1.0000E+08
1.0000E+09
1.0000E+10
1.0000E+11
1.0000E+12
log attenuation (db)
1.0000E+03
1.0000E+02
1.0000E+01
1.0000E+00
1.0000E-01

FIGURE 18

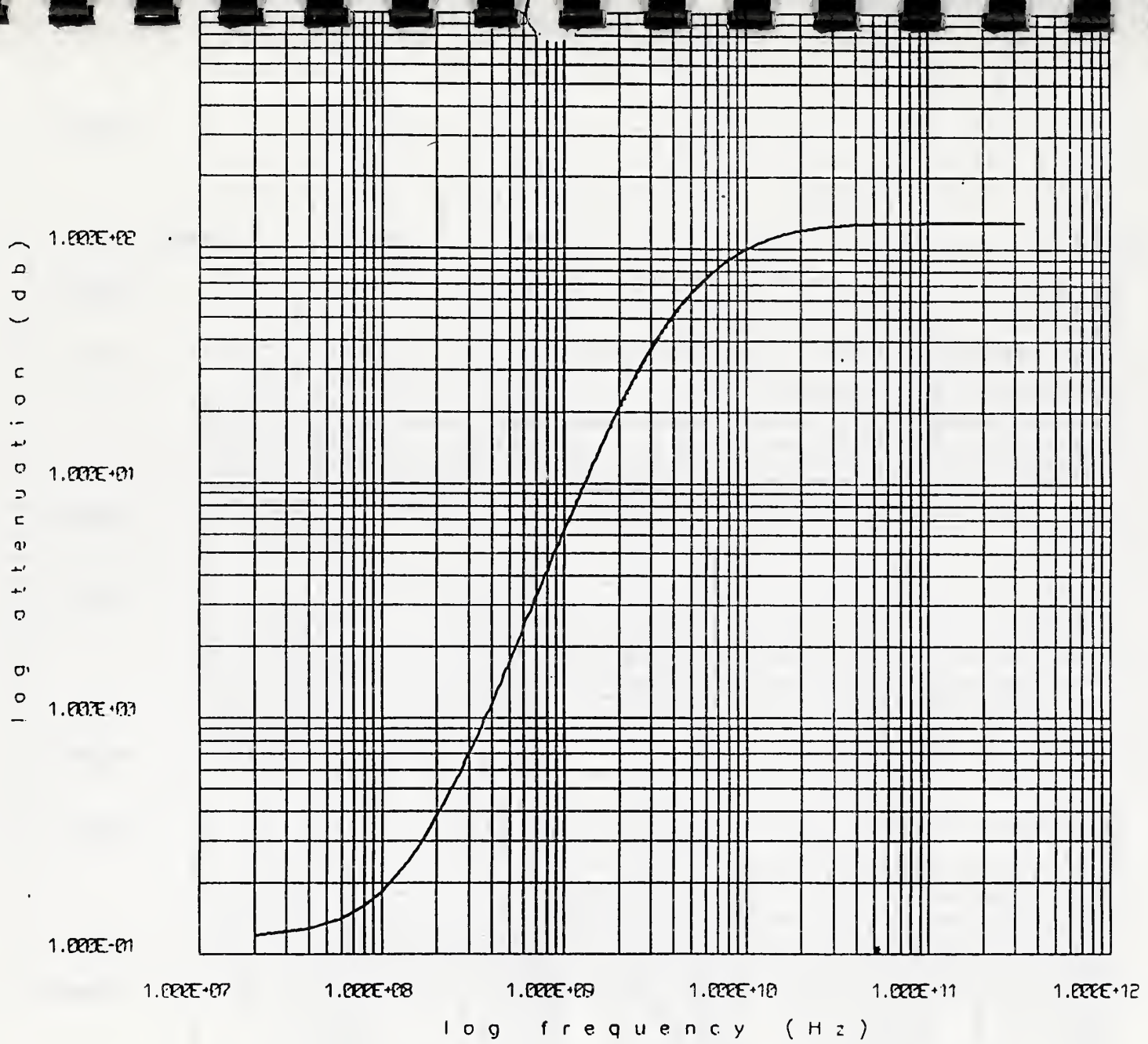
log attenuation (db)
1.000E+02
1.000E+01
1.000E+00
1.000E-01
1.000E+07
1.000E+08
1.000E+09
1.000E+10
1.000E+11
1.000E+12
log frequency (Hz)
s21m500.62

Figure 19

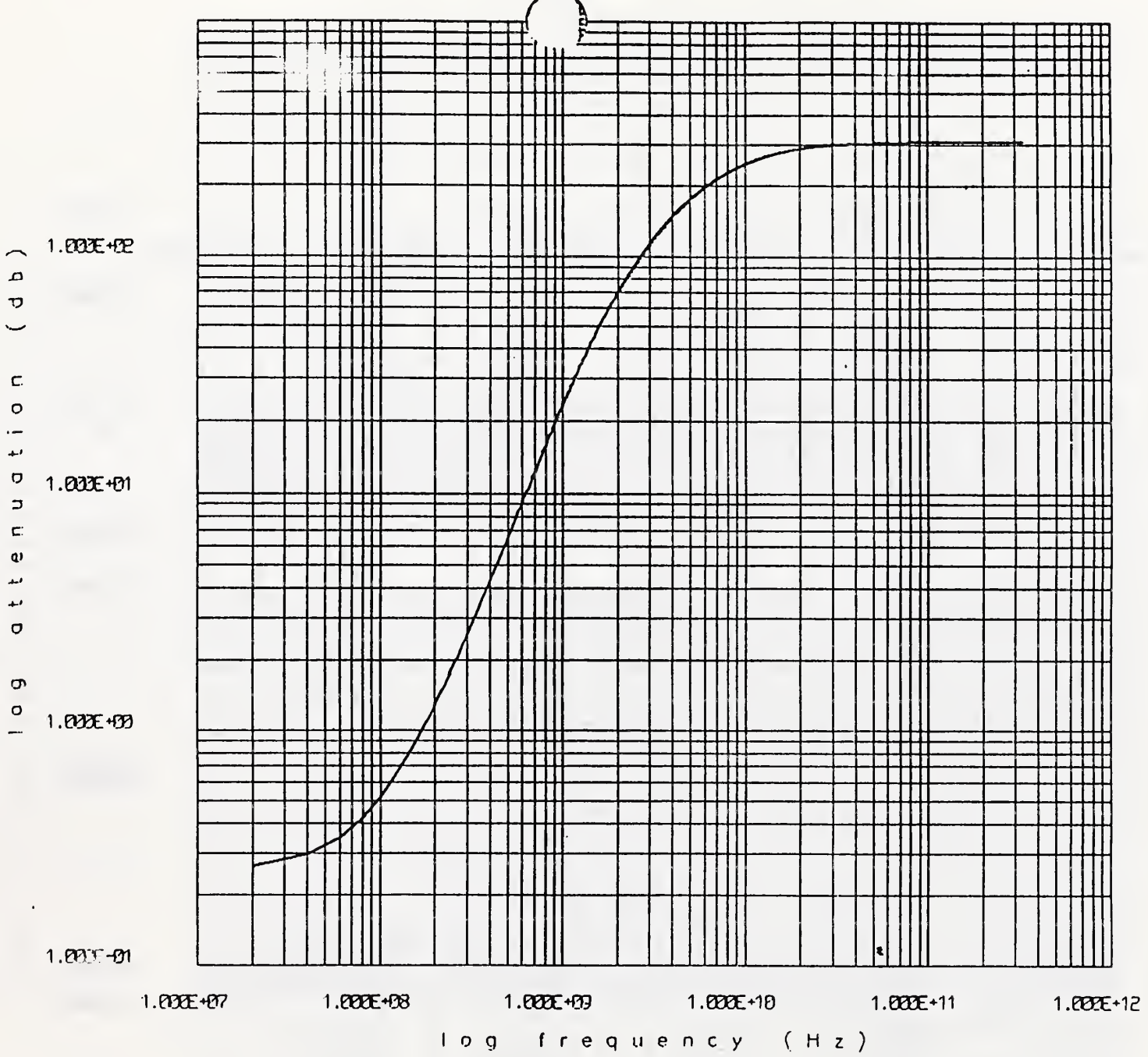

s21m1000.62

FIGURE 20

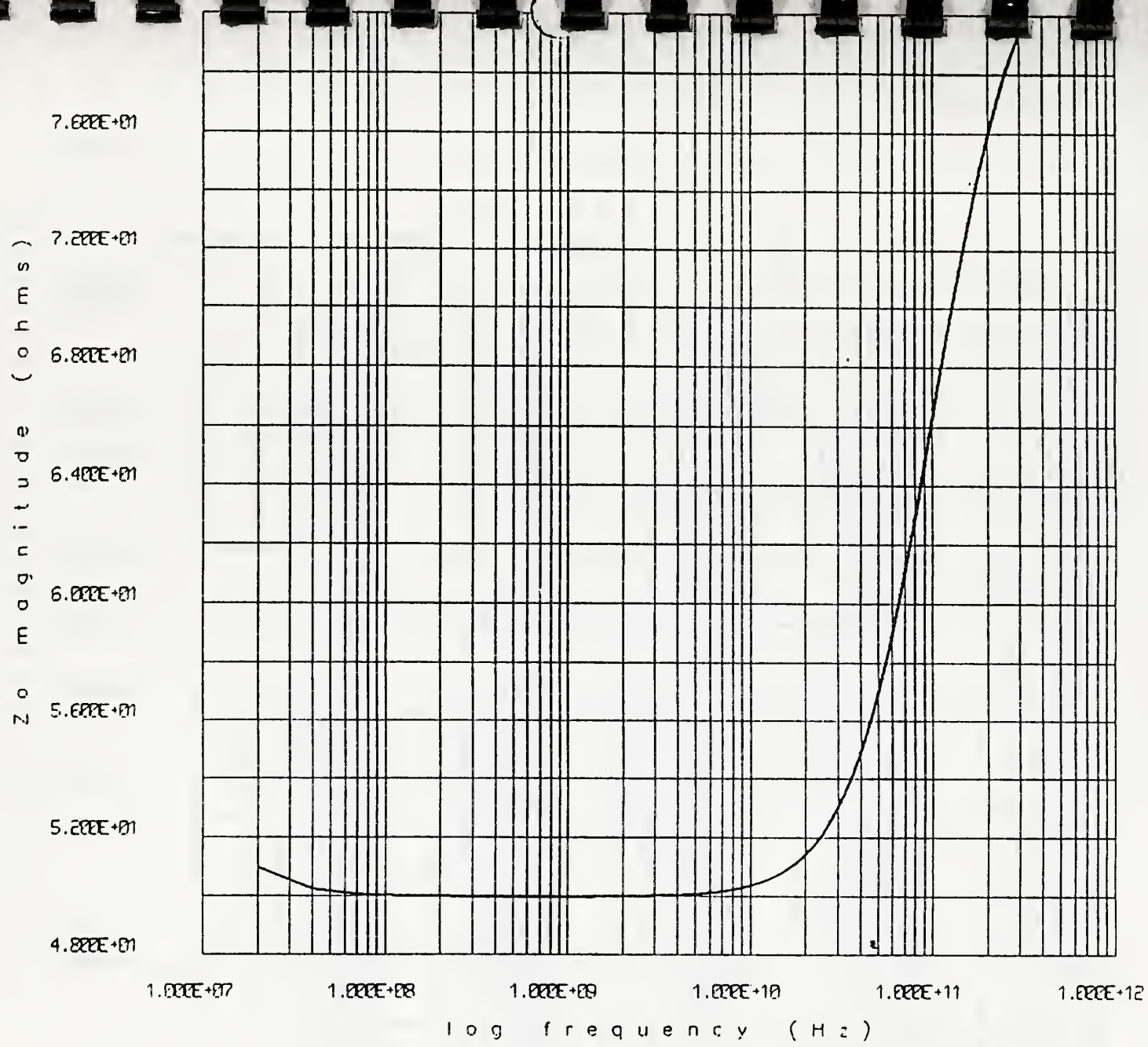
7.0000E+01
7.2000E+01
6.8000E+01
6.4000E+01
6.0000E+01
5.6000E+01
5.2000E+01
4.8000E+01
Zo magnitude (ohms)
1.0000E+07
1.0000E+08
1.0000E+09
1.0000E+10
1.0000E+11
1.0000E+12
log frequency (Hz)
zom100.62

FIGURE 21

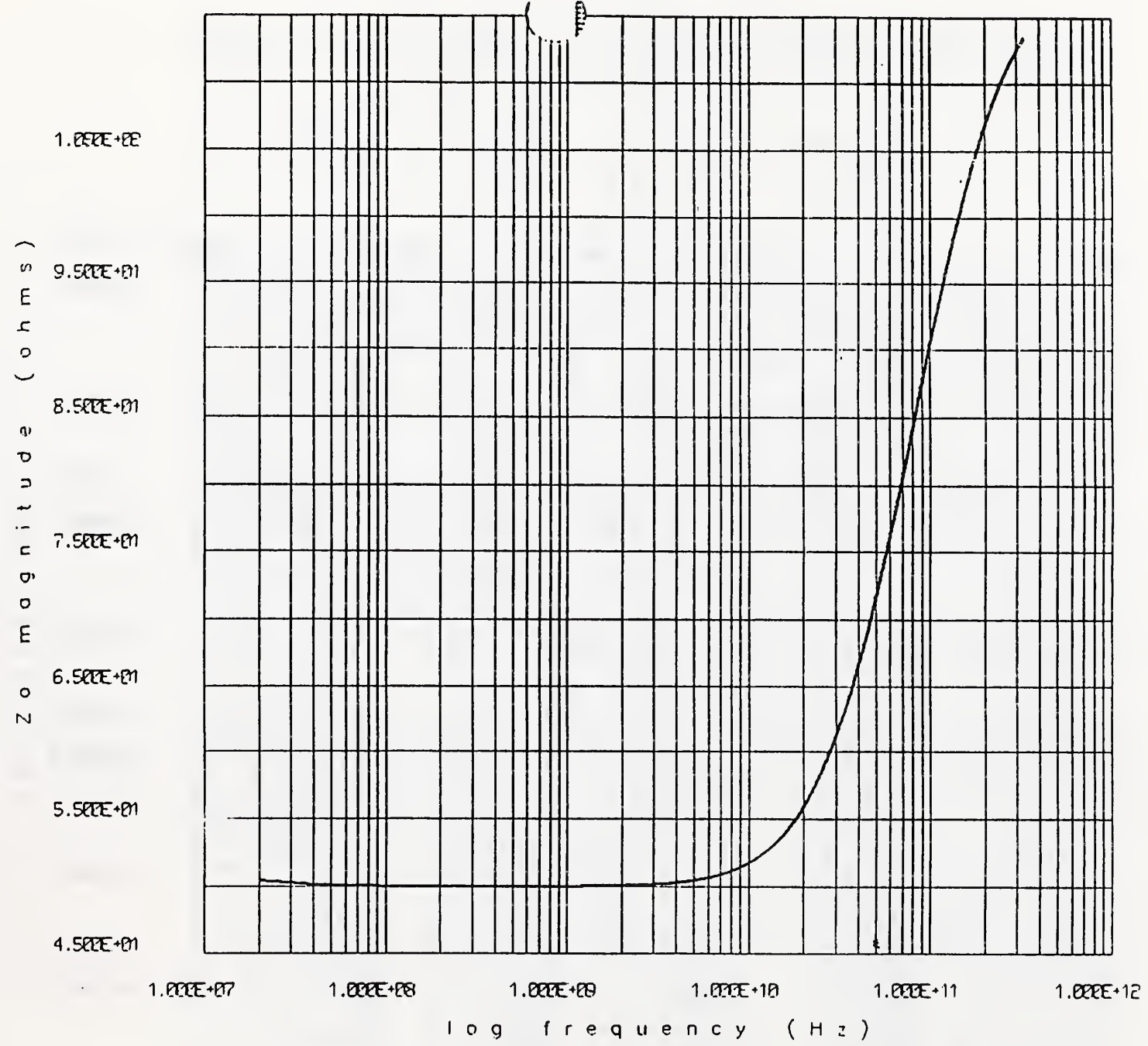
1.0000E+02
9.5000E+01
8.5000E+01
7.5000E+01
6.5000E+01
5.5000E+01
4.5000E+01
Zo magnitude (ohms)
1.0000E+07
1.0000E+08
1.0000E+09
1.0000E+10
1.0000E+11
1.0000E+12
log frequency (Hz)
zom200.62

FIGURE 22

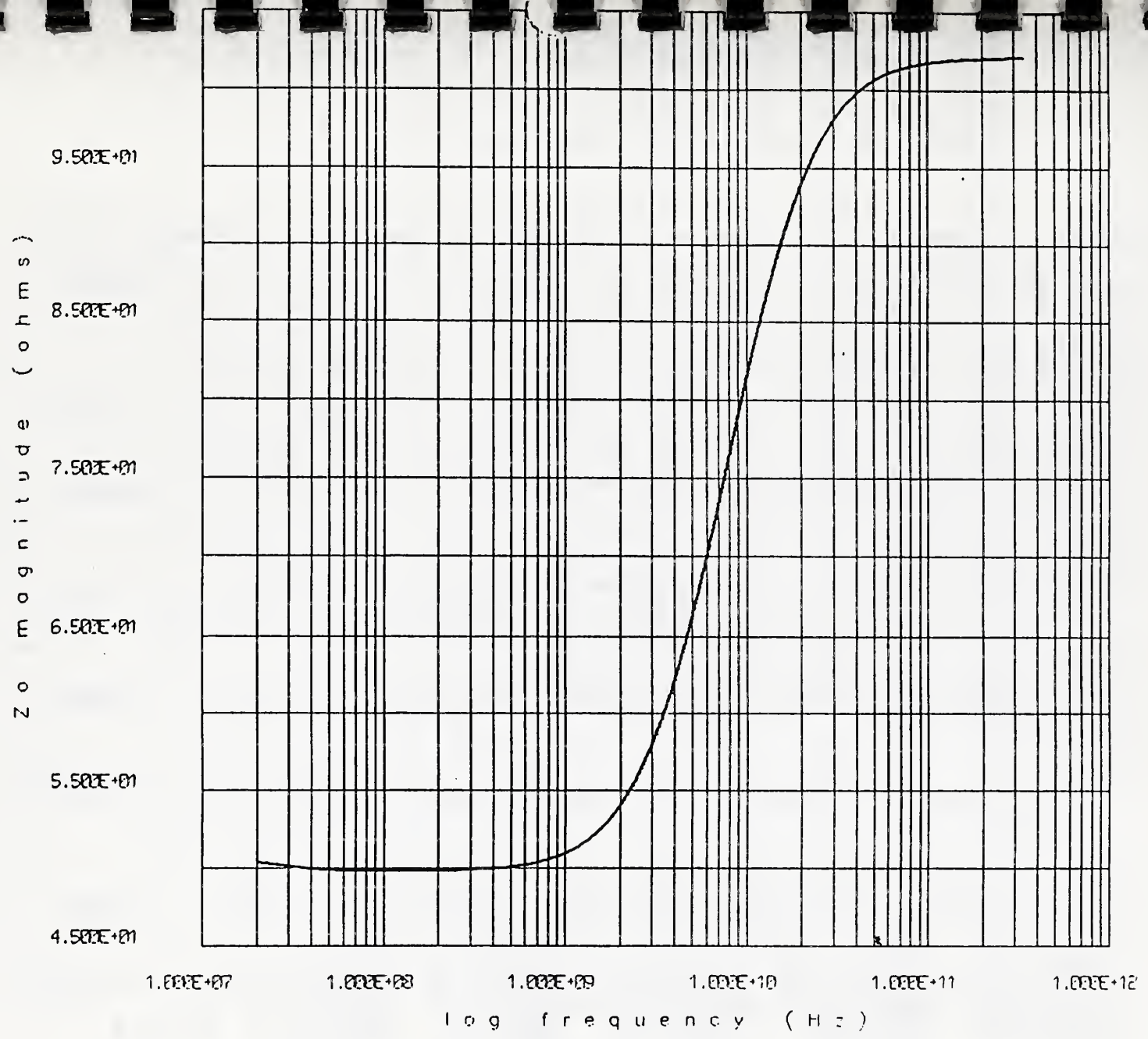
9.500E+01
8.500E+01
7.500E+01
6.500E+01
5.500E+01
4.500E+01
Zo magnitude (ohms)
1.000E+07
1.000E+08
1.000E+09
1.000E+10
1.000E+11
1.000E+12
log frequency (Hz)
zom500.62

FIGURE 23

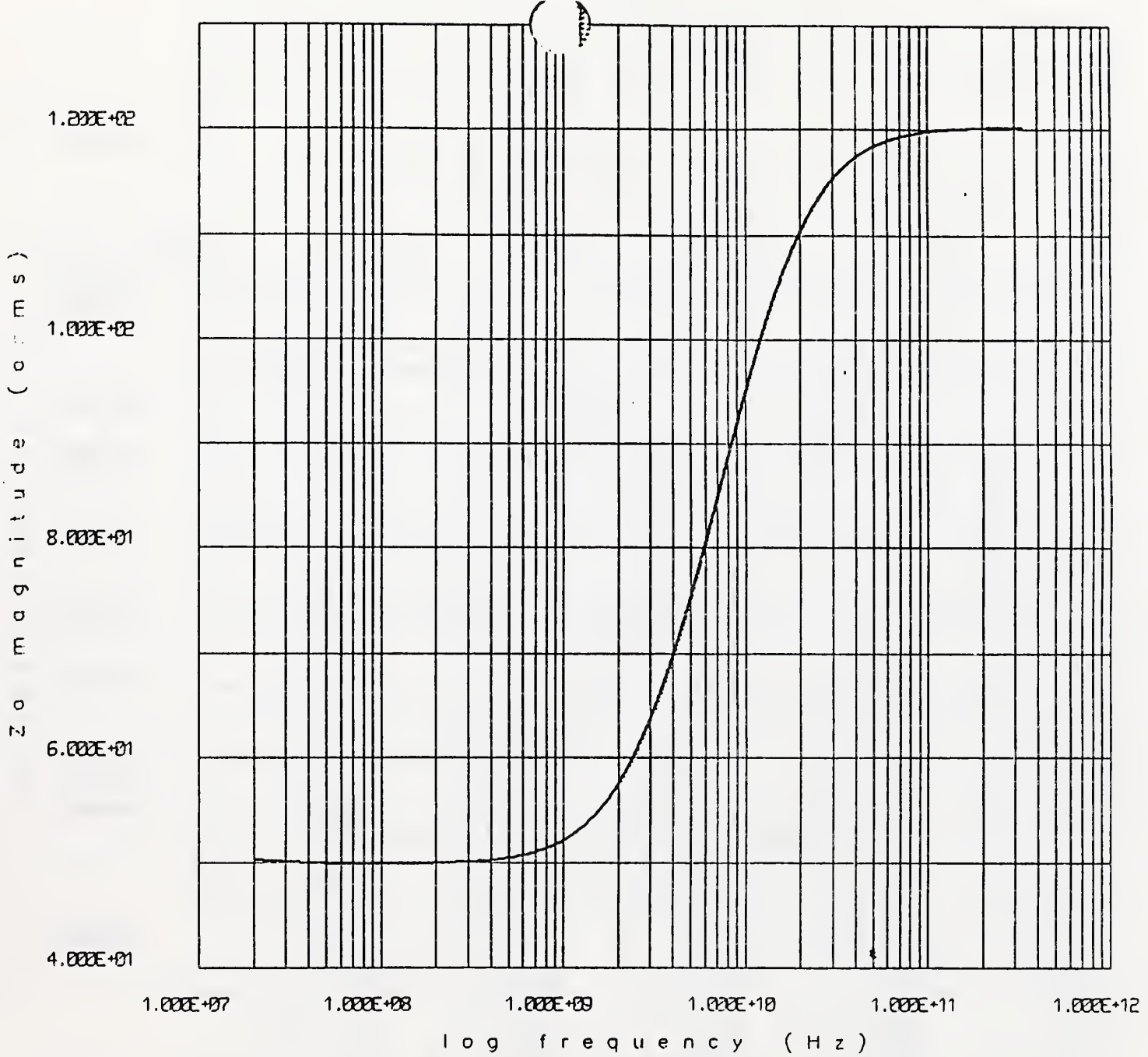
1.200E+02
1.000E+02
8.000E+01
6.000E+01
4.000E+01
Zo magnitude (ohms)
1.000E+07
1.000E+08
1.000E+09
1.000E+10
1.000E+11
1.000E+12
log frequency (Hz)
zom1000.62

FIGURE 24

FIGURE 25

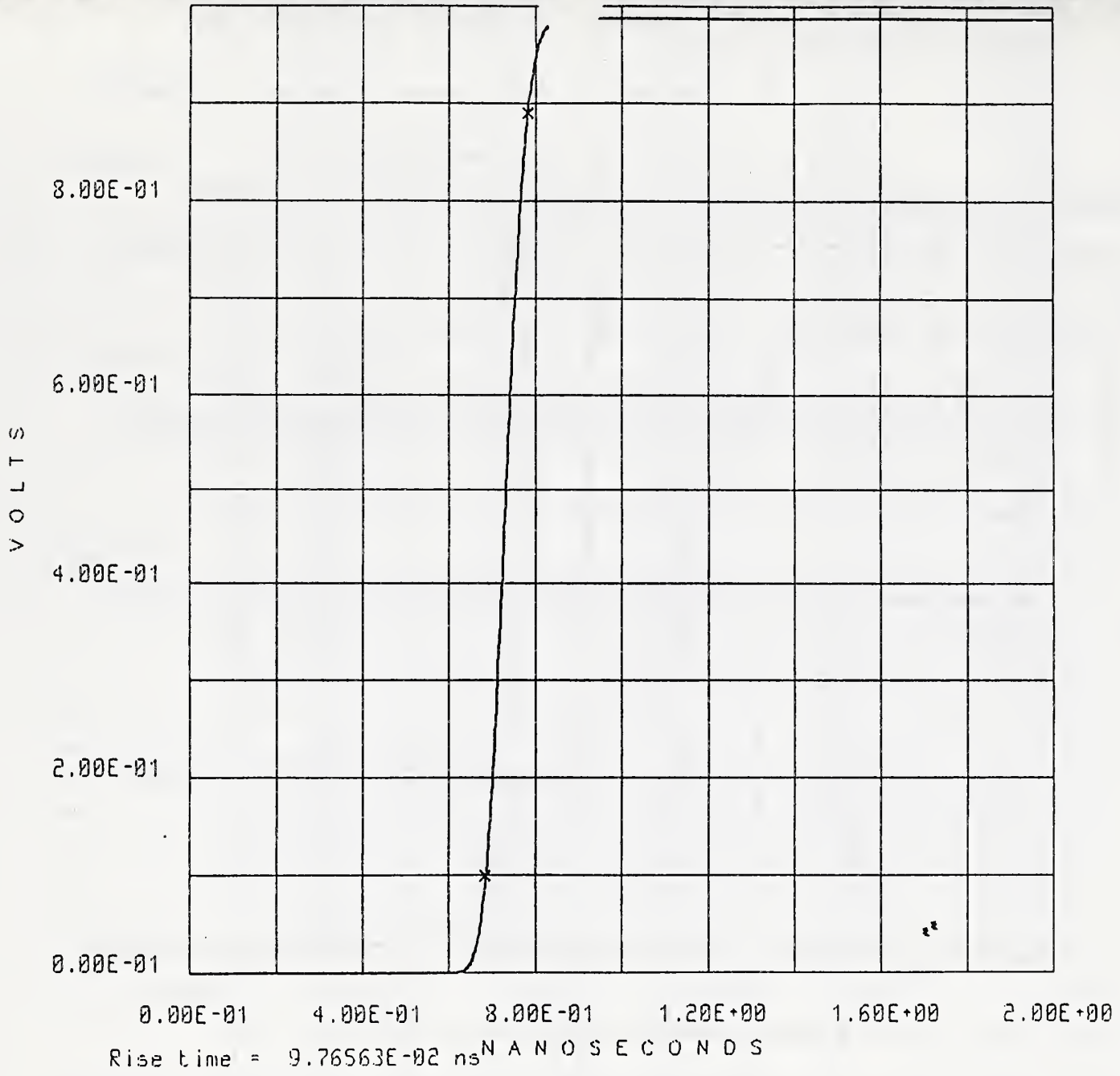

Rise time = 9.76563E-02 ns

COMMENT: 100 PS FILTER U(T) 2/17/89 WLG

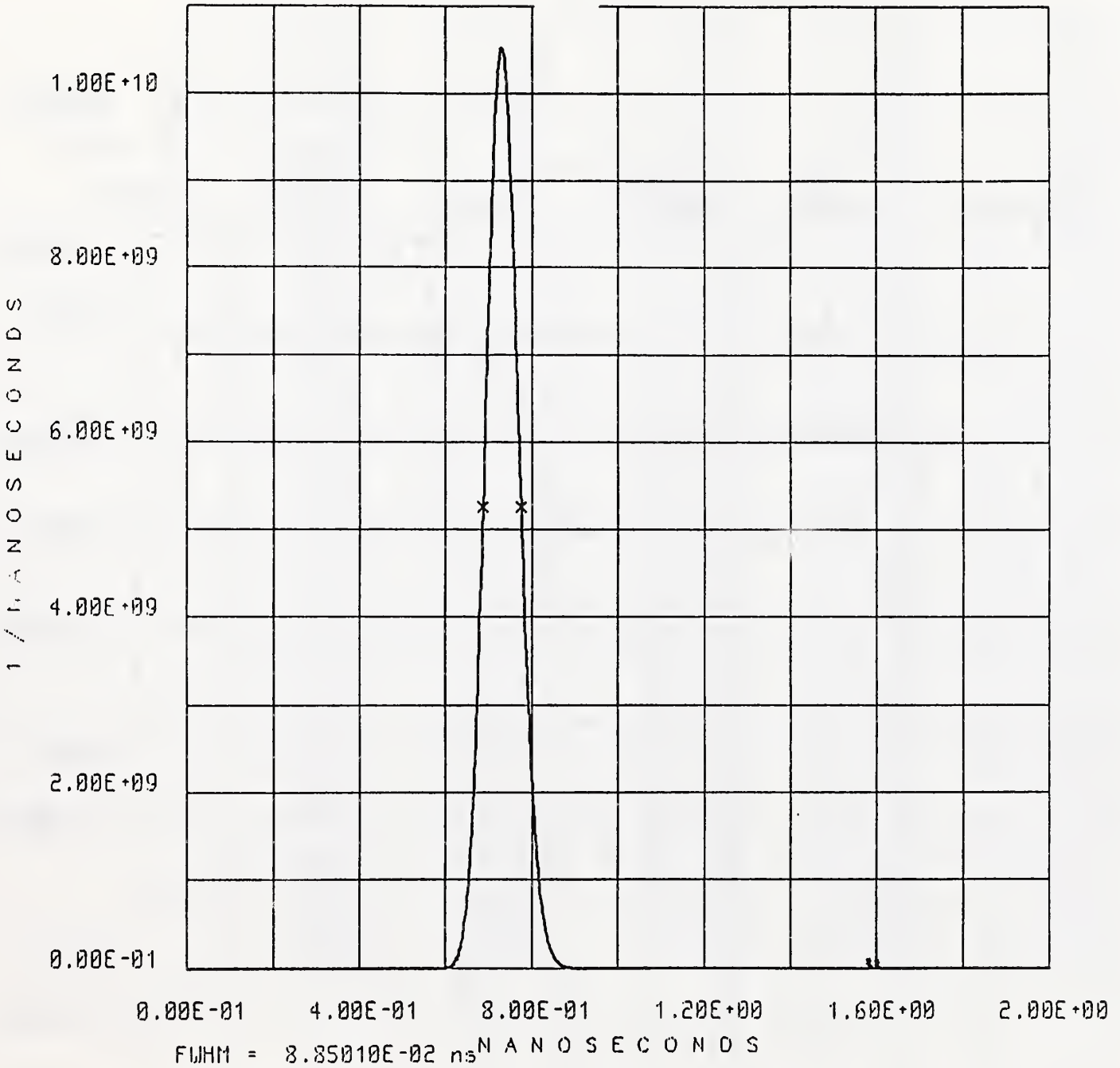
1.00E+10
8.00E+09
6.00E+09
4.00E+09
2.00E+09
0.00E-01
1/NANOSECONDS
0.00E-01
4.00E-01
8.00E-01
1.20E+00
1.60E+00
2.00E+00
FWHM = 8.85010E-02 ns
NANOSECONDS
COMMENT: 100 PS FILTER H(T) 2/17/89 WLG

FIGURE 26

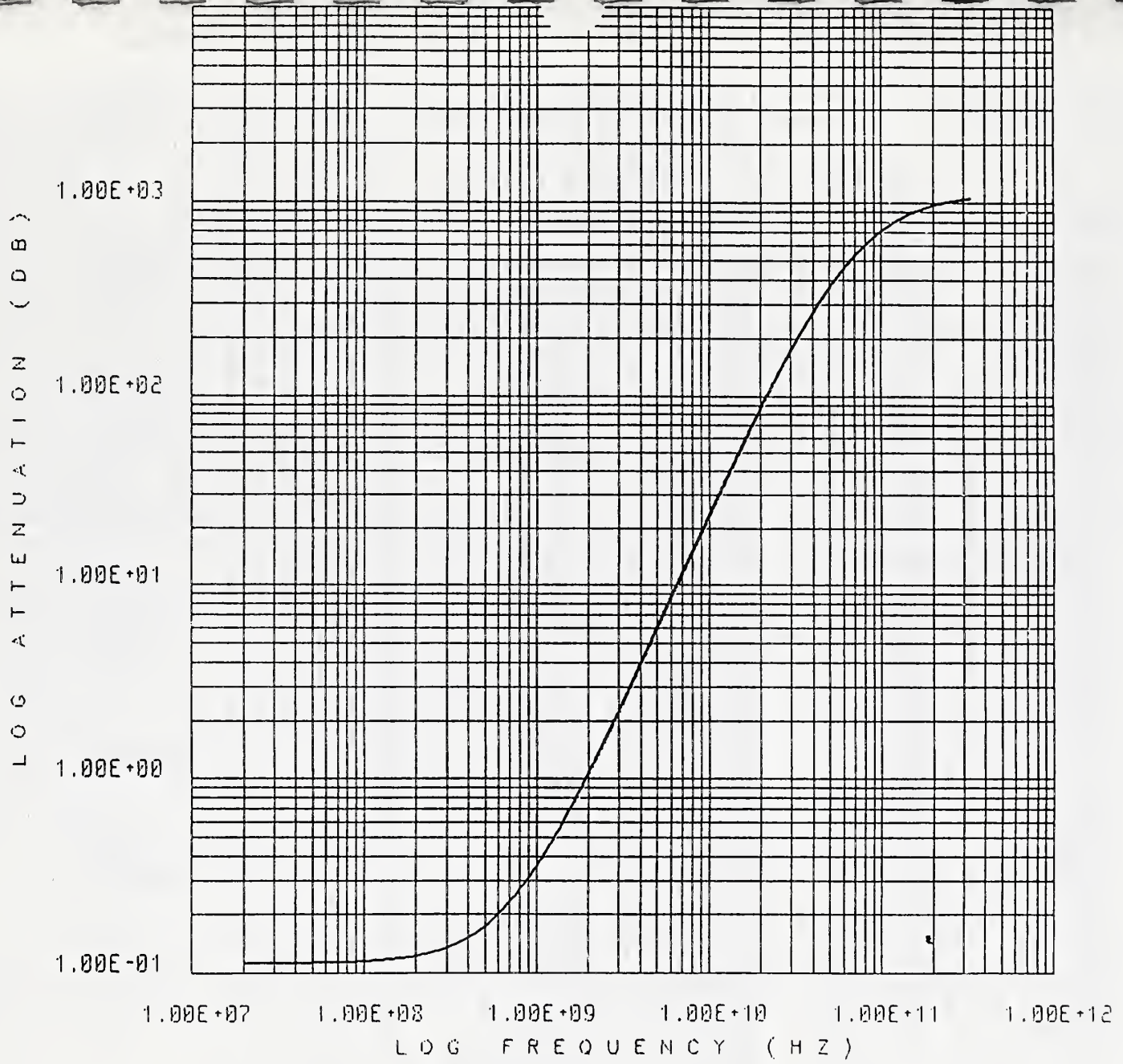

COMMENT: 100 PS FILTER S21(F) MAGNITUDE 2/17/89 WLG

Figure 27

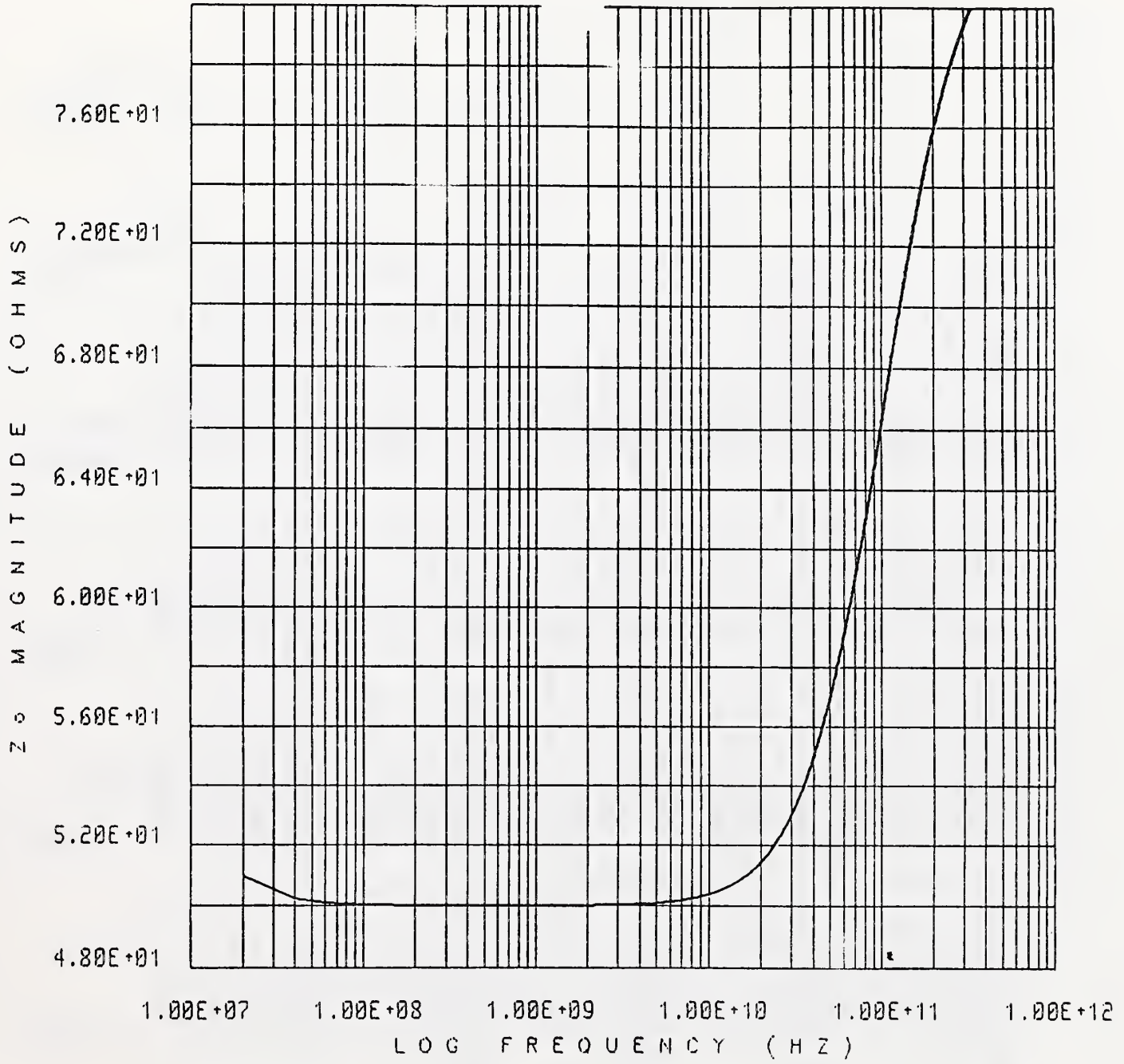

COMMENT: 100 PS FILTER Zo(F) MAGNITUDE 2/17/89 WLG

FIGURE 28

3" SILICON WAFER DRAWING FOR 100 PS FILTER

(POLISHED SIDE UP — SCALE = 2:1)

(WAFER THICKNESS ≈ 245 μm, σ ≈ 100 S/m)

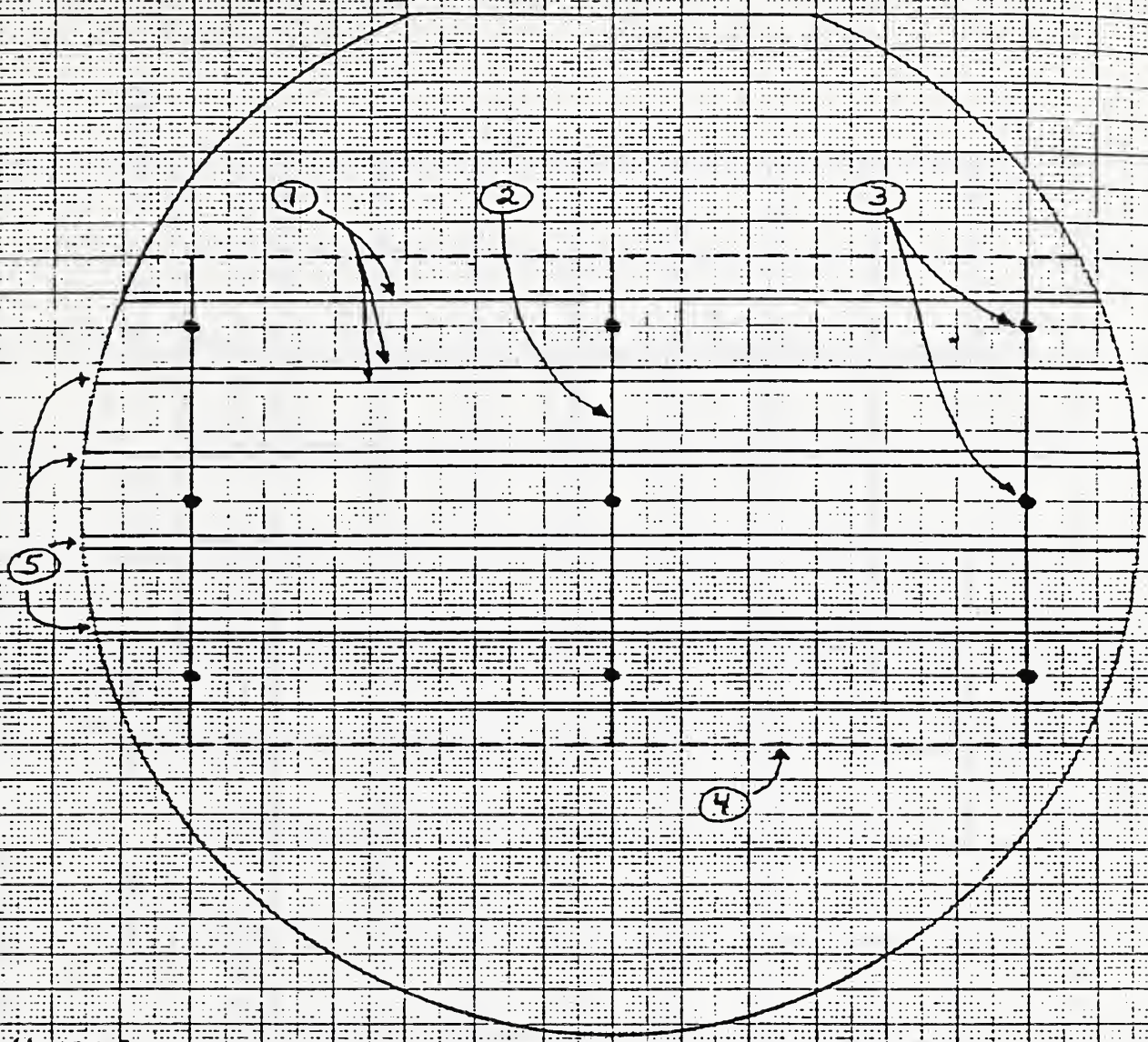

NOTES

(1) EVENTUAL CUT LINES FOR MICROSTRIP LINES (10 EA.)

(2) MEAS. PATHS FOR SiO_2 THICKNESS MEAS. (3 EA.)

(3) MEAS. POINTS FOR Si SUBSTRATE THICKNESS AND CONDUCTIVITY MEAS. (9 EA.)

(4) BOUNDARY LINES FOR REMOVAL OF SiO_2 COATING (2 EA.)

(5) 1 mm GAPS FOR REMOVAL OF SiO_2 COATING (4 EA.)

N.I.S.T. 4/3/89 WZA

FIGURE 29

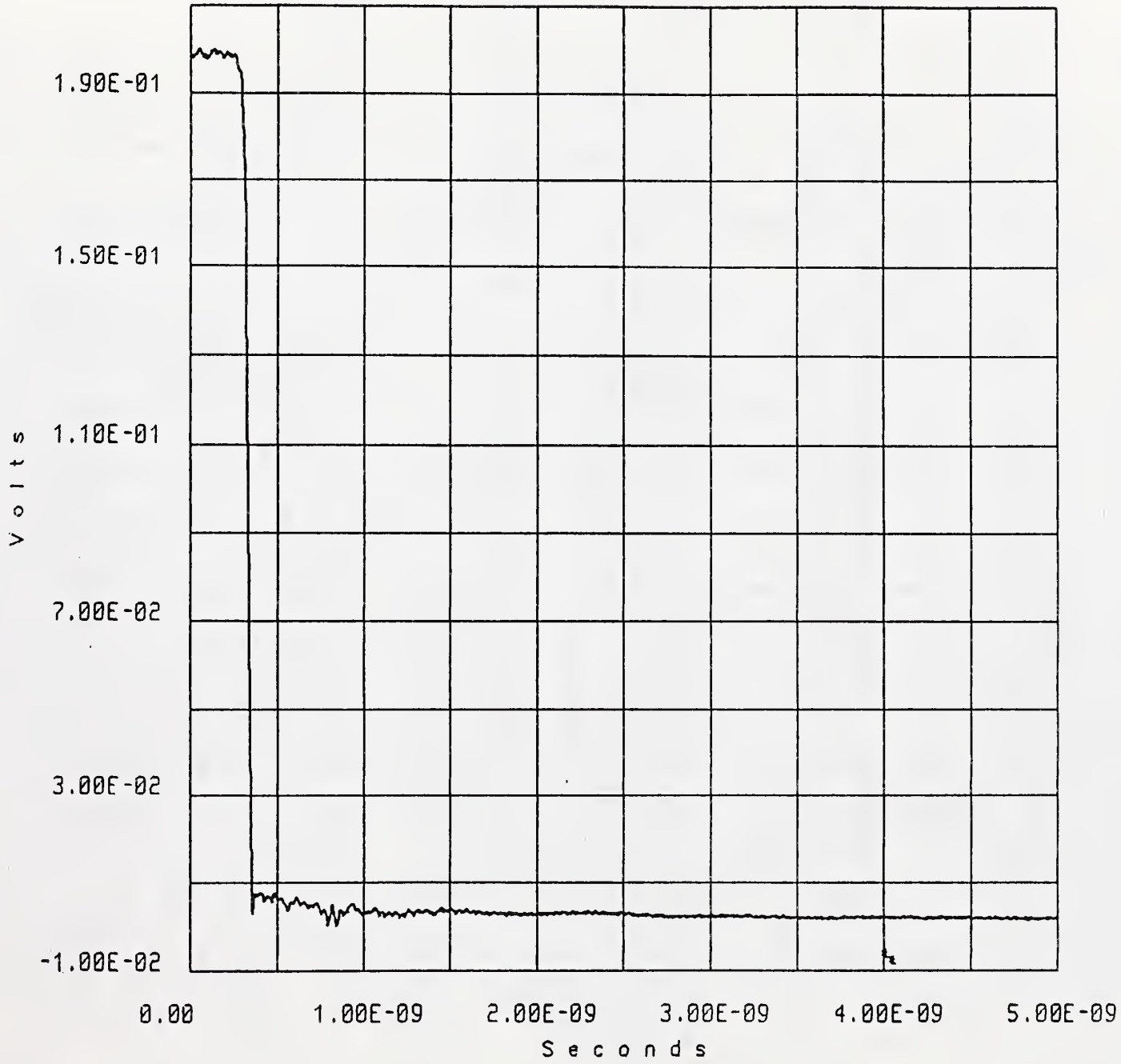
1.90E-01
1.50E-01
1.10E-01
7.00E-02
3.00E-02
-1.00E-02
Volts
0.00
1.00E-09
2.00E-09
3.00E-09
4.00E-09
5.00E-09
Seconds
COMMENT: refl from short ckt at Chan #1 5/3/91 wlg

FIGURE 30

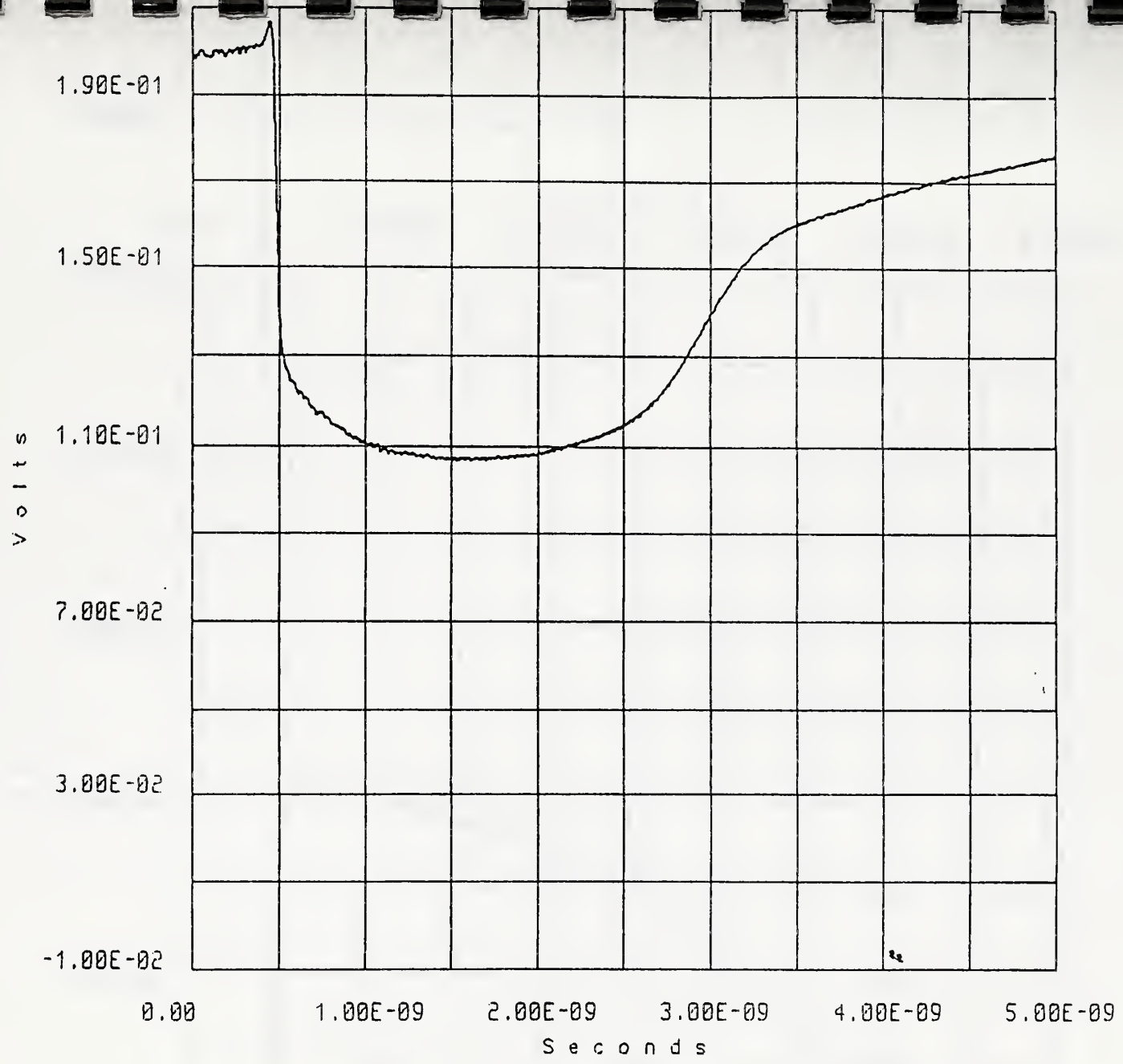

COMMENT: refl from line #2 5/3/91 wlg

FIGURE 31

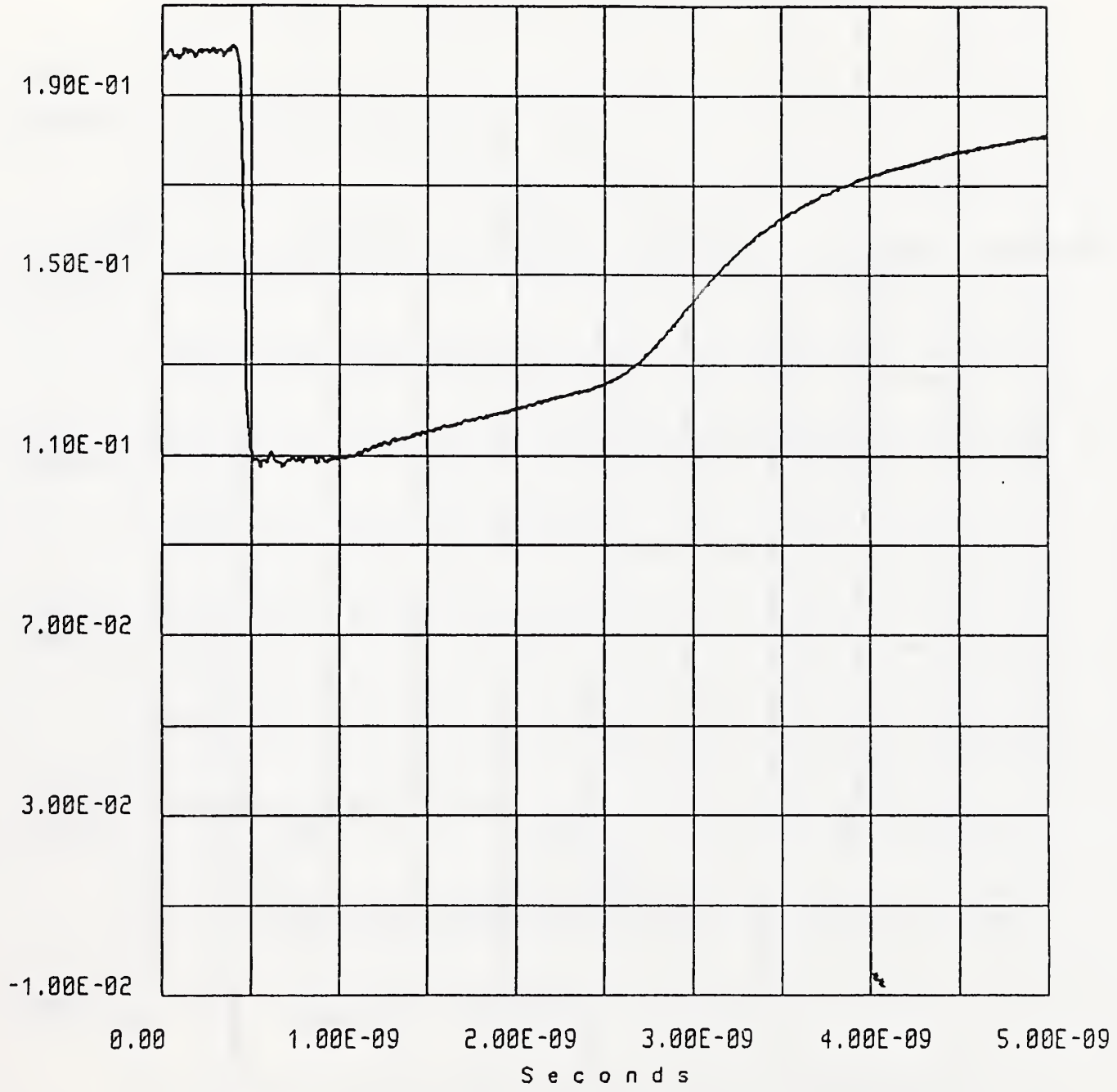

COMMENT: refl from line #3 5/4/91 wlg

FIGURE 32

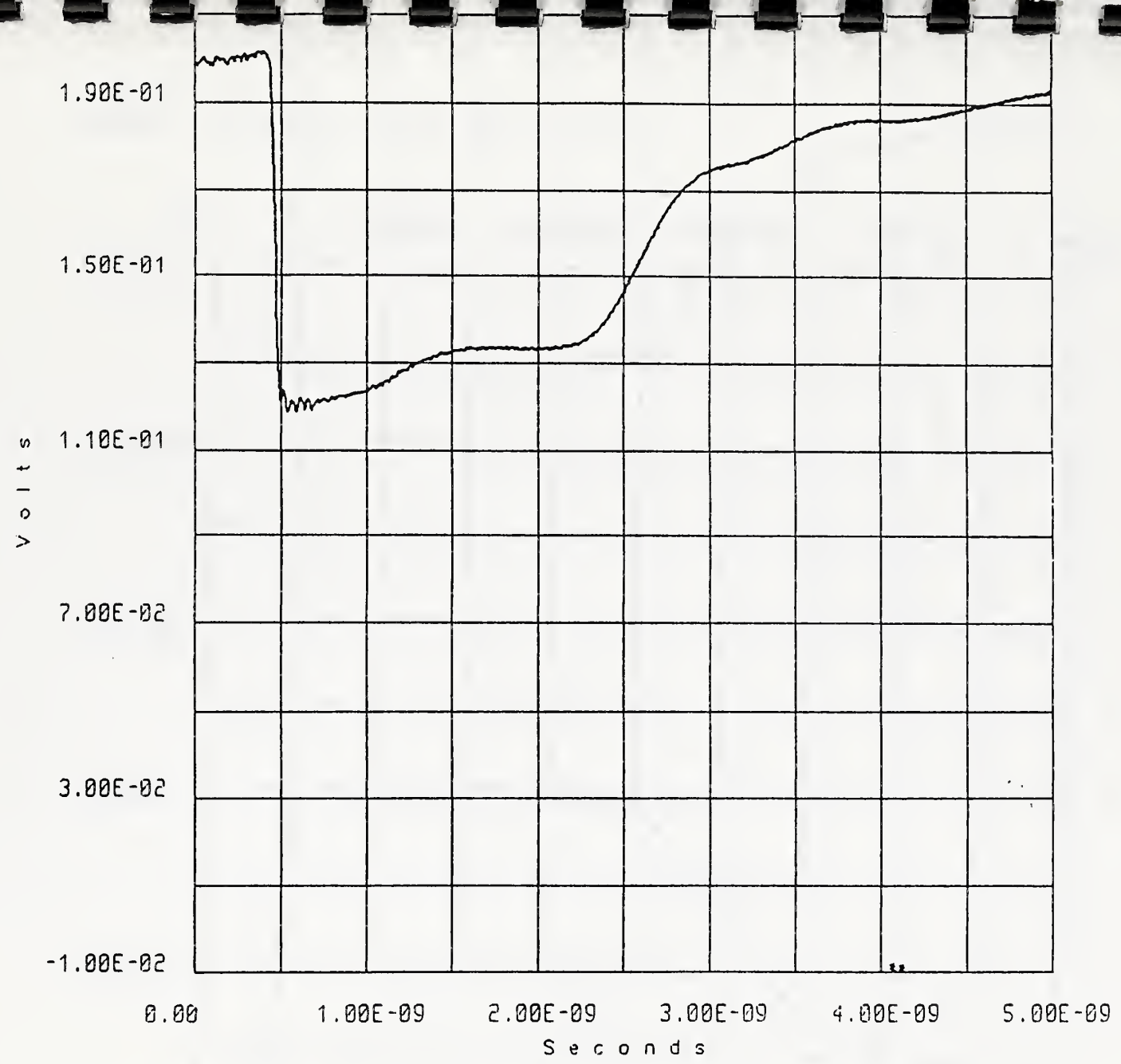
1.90E-01
1.50E-01
1.10E-01
7.00E-02
3.00E-02
-1.00E-02
Volts
0.00
1.00E-09
2.00E-09
3.00E-09
4.00E-09
5.00E-09
Seconds
COMMENT: refl from line #4 5/4/91 wlg

FIGURE 33

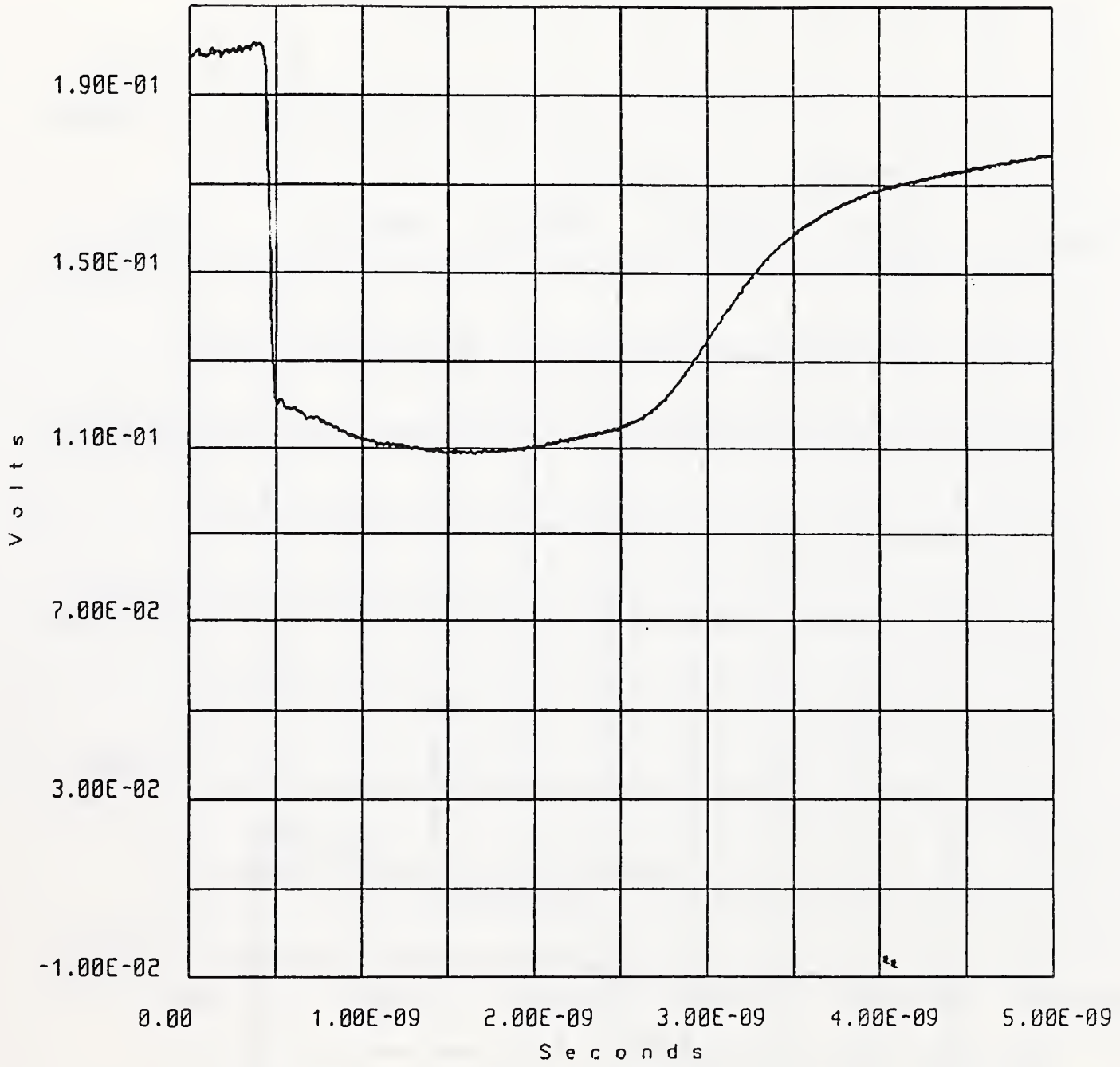
1.90E-01
1.50E-01
1.10E-01
7.00E-02
3.00E-02
-1.00E-02
Volts
0.00
1.00E-09
2.00E-09
3.00E-09
4.00E-09
5.00E-09
Seconds
COMMENT: refl from line #6 5/4/91 wlg

FIGURE 34

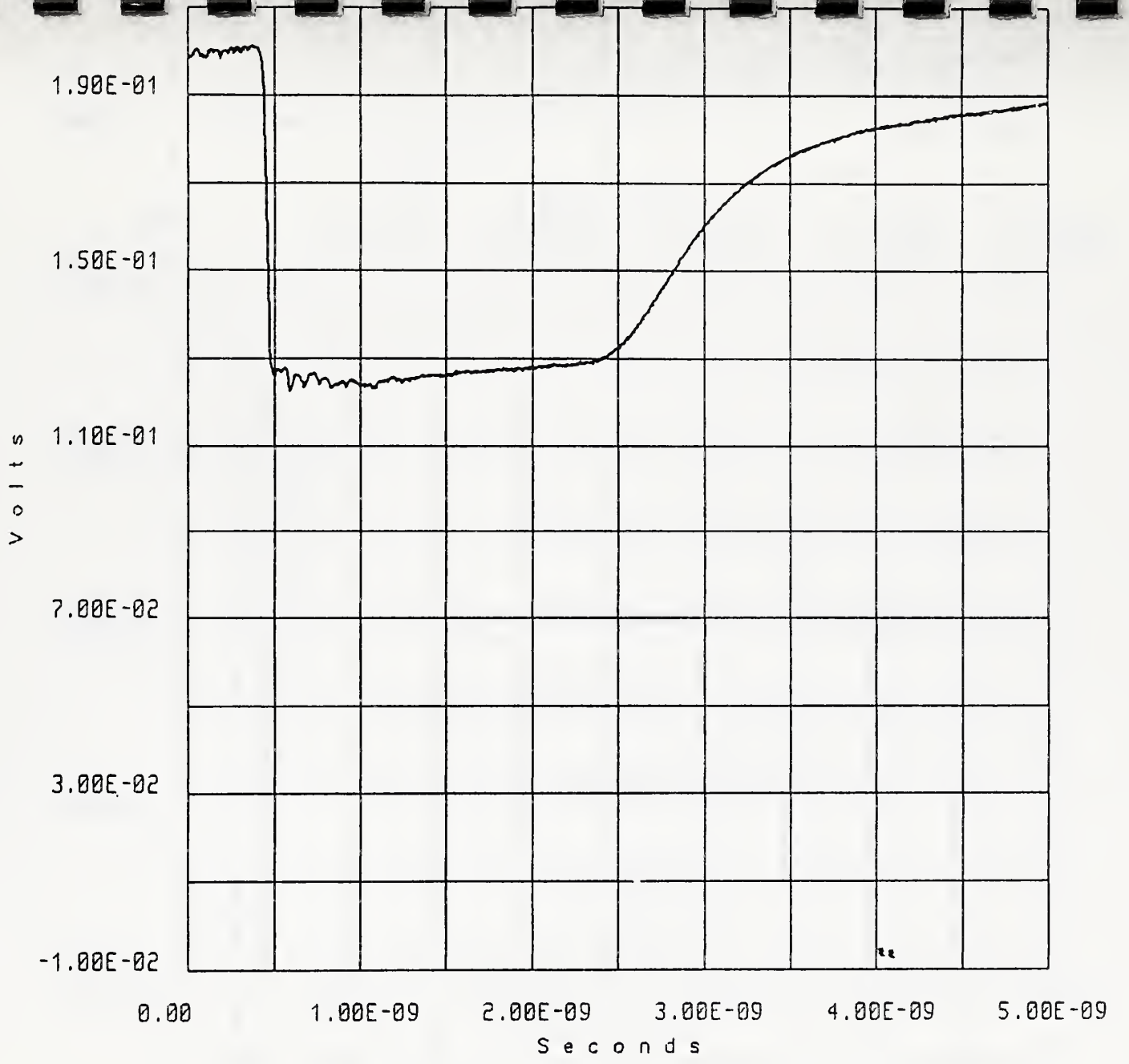

COMMENT: refl from line #7 5/3/91 wlg

FIGURE 35

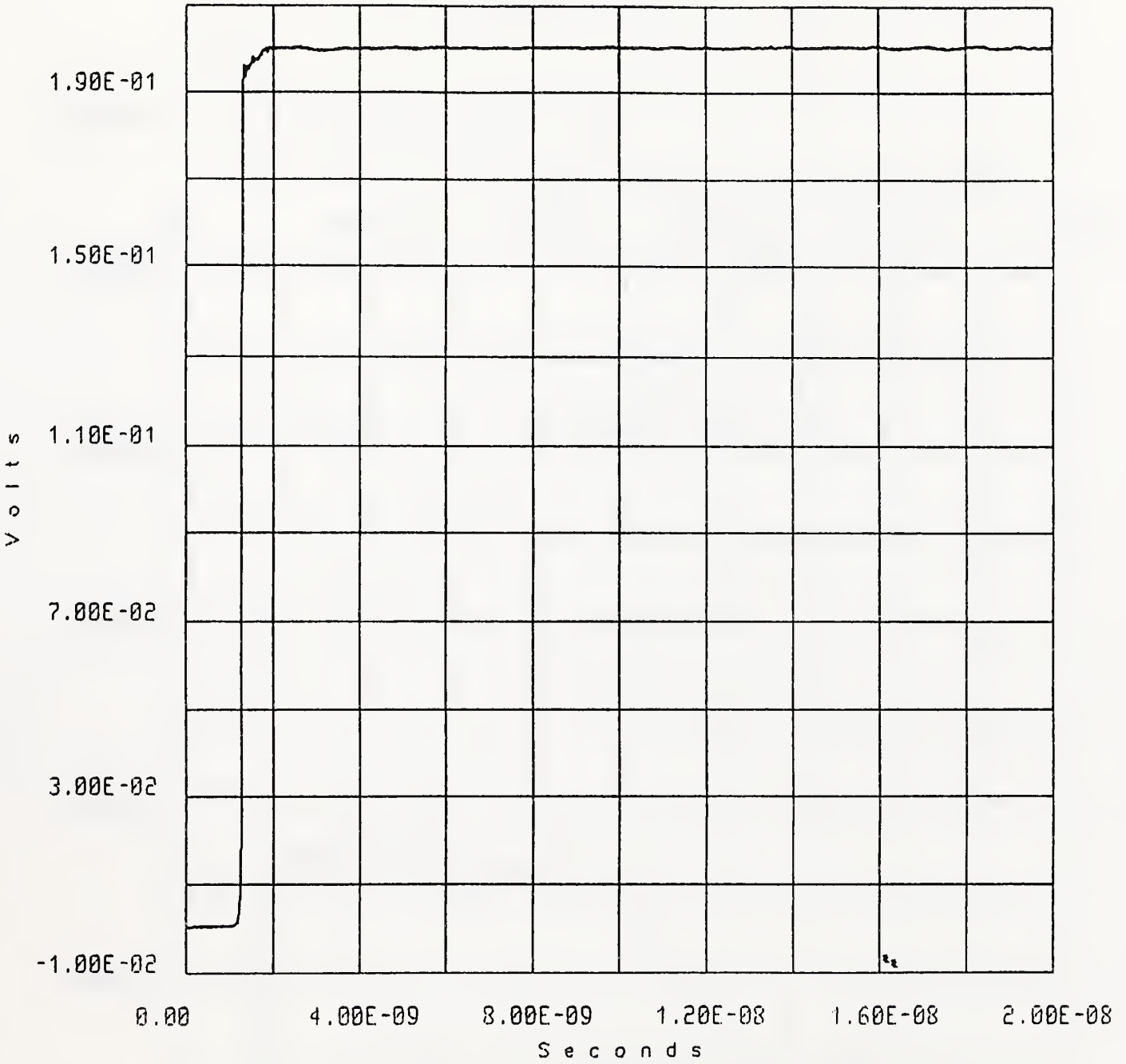

COMMENT: trans reference from Chan #1, Meas'd on Chan #4 5/3/91 wlg

FIGURE 36

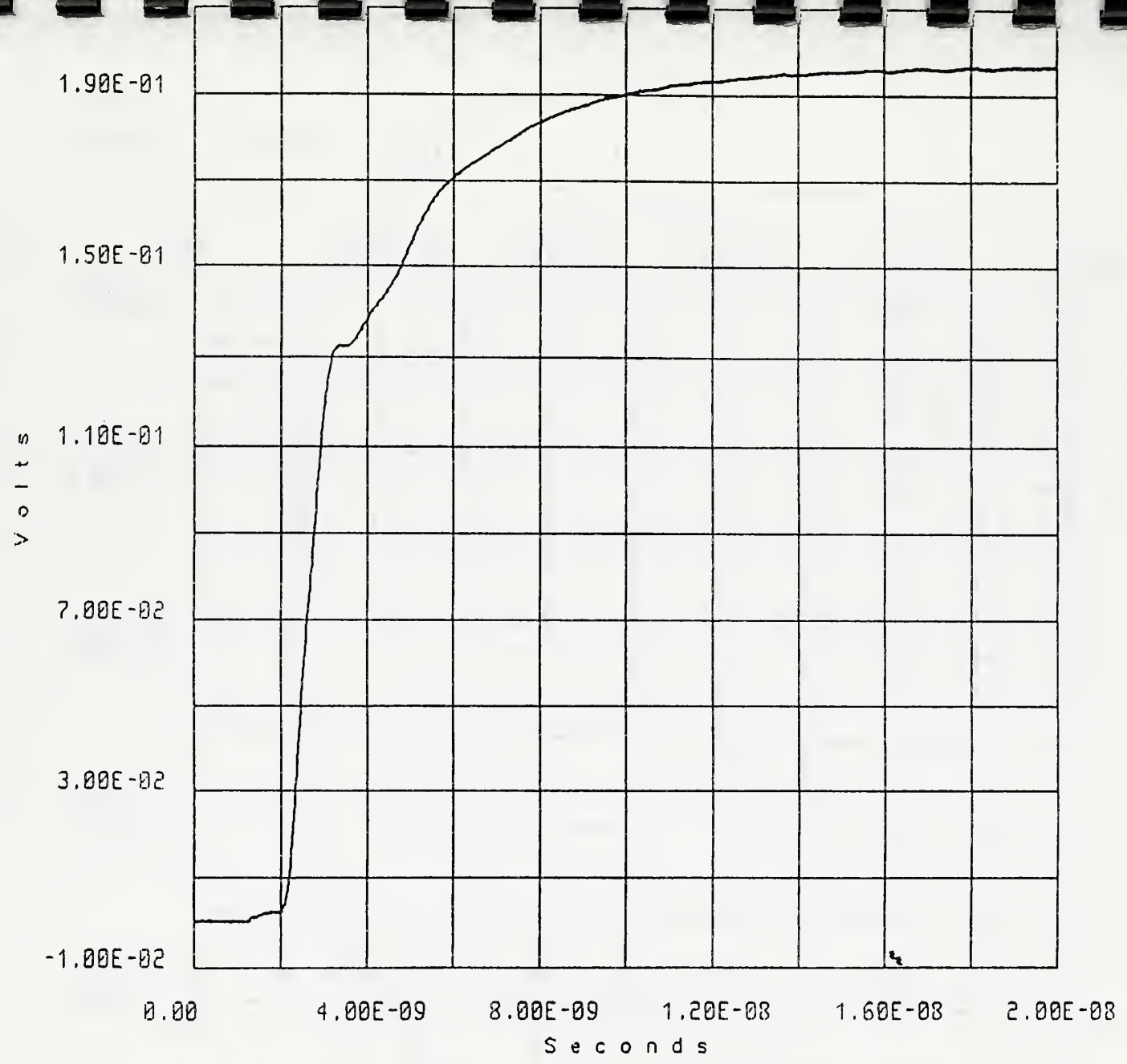

COMMENT: trans thru line #2 5/3/91 wlg

FIGURE 37

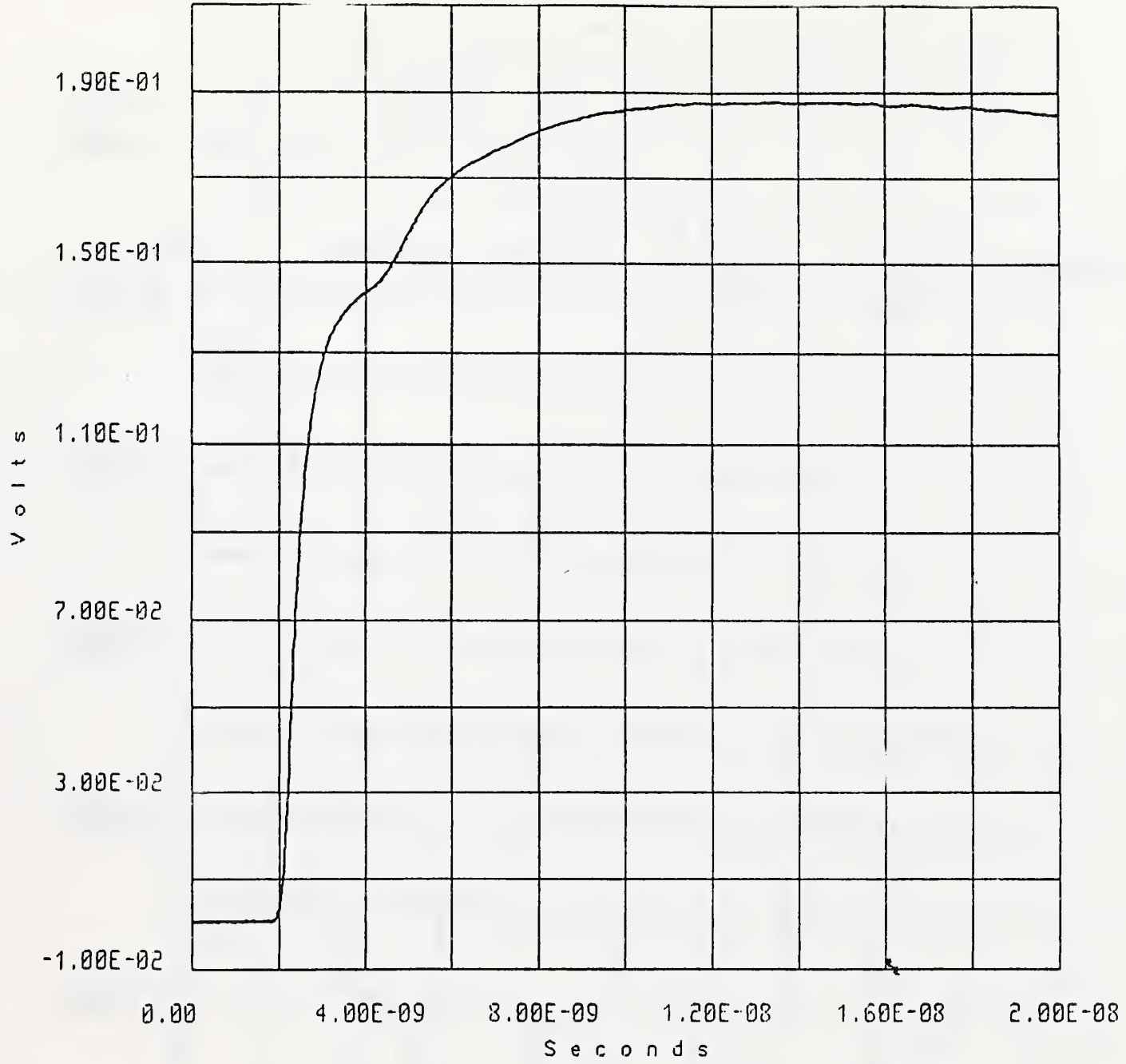

COMMENT: trans thru line #3 5/4/91 wlg

FIGURE 38

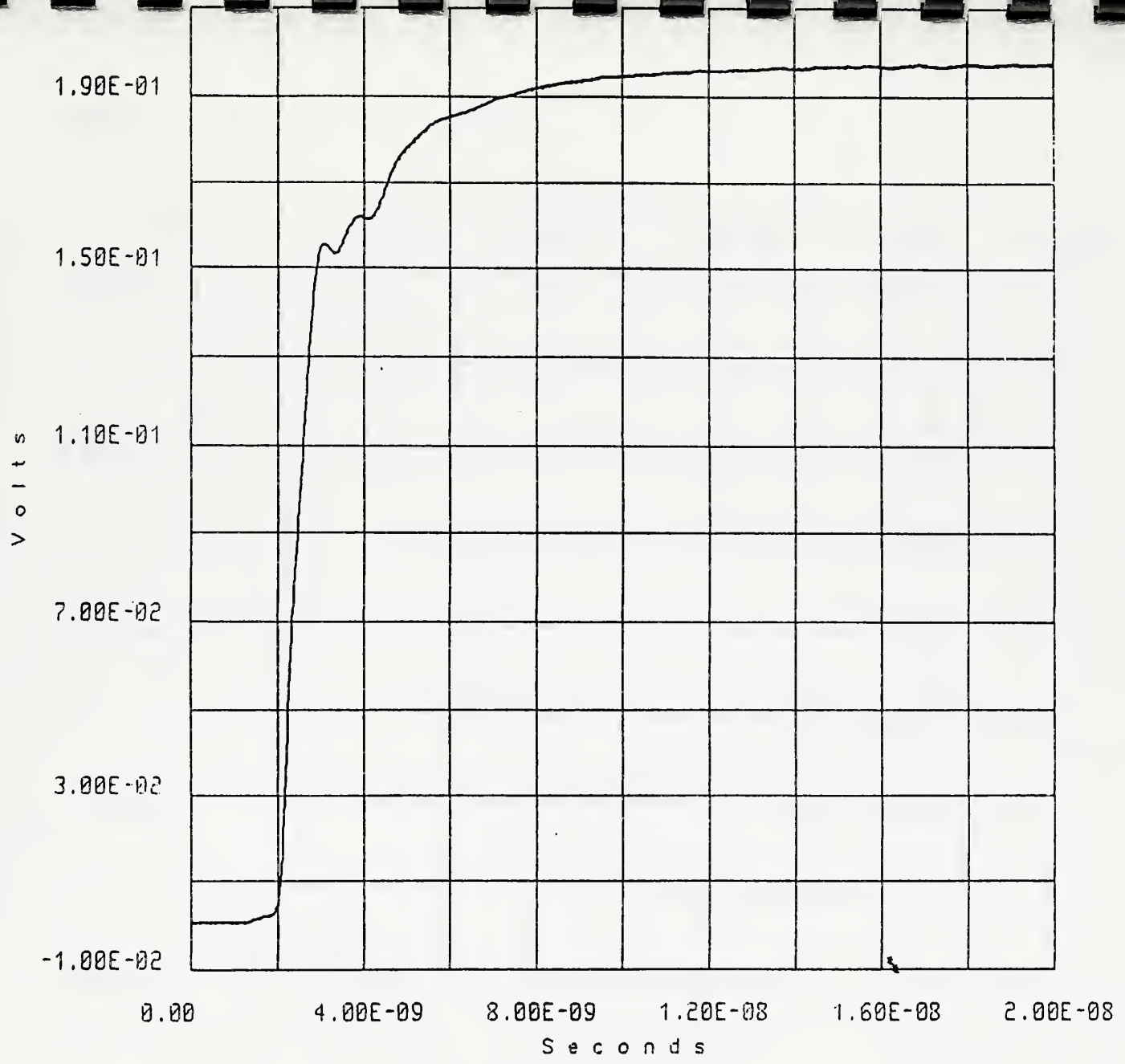

COMMENT: trans thru line #4 5/4/91 wlg

FIGURE 39

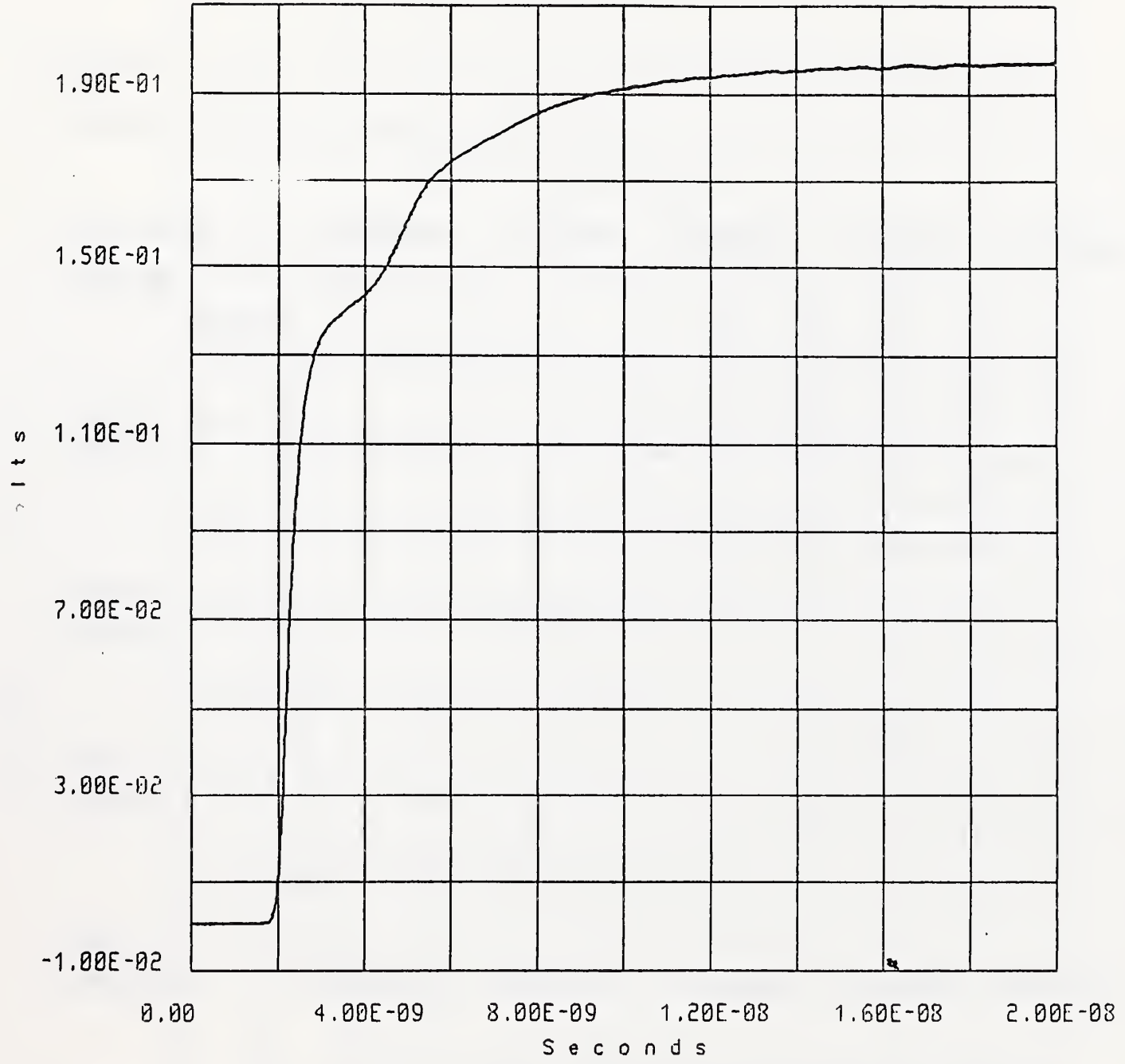

COMMENT: trans thru line #6 5/4/91 wlg

FIGURE 40

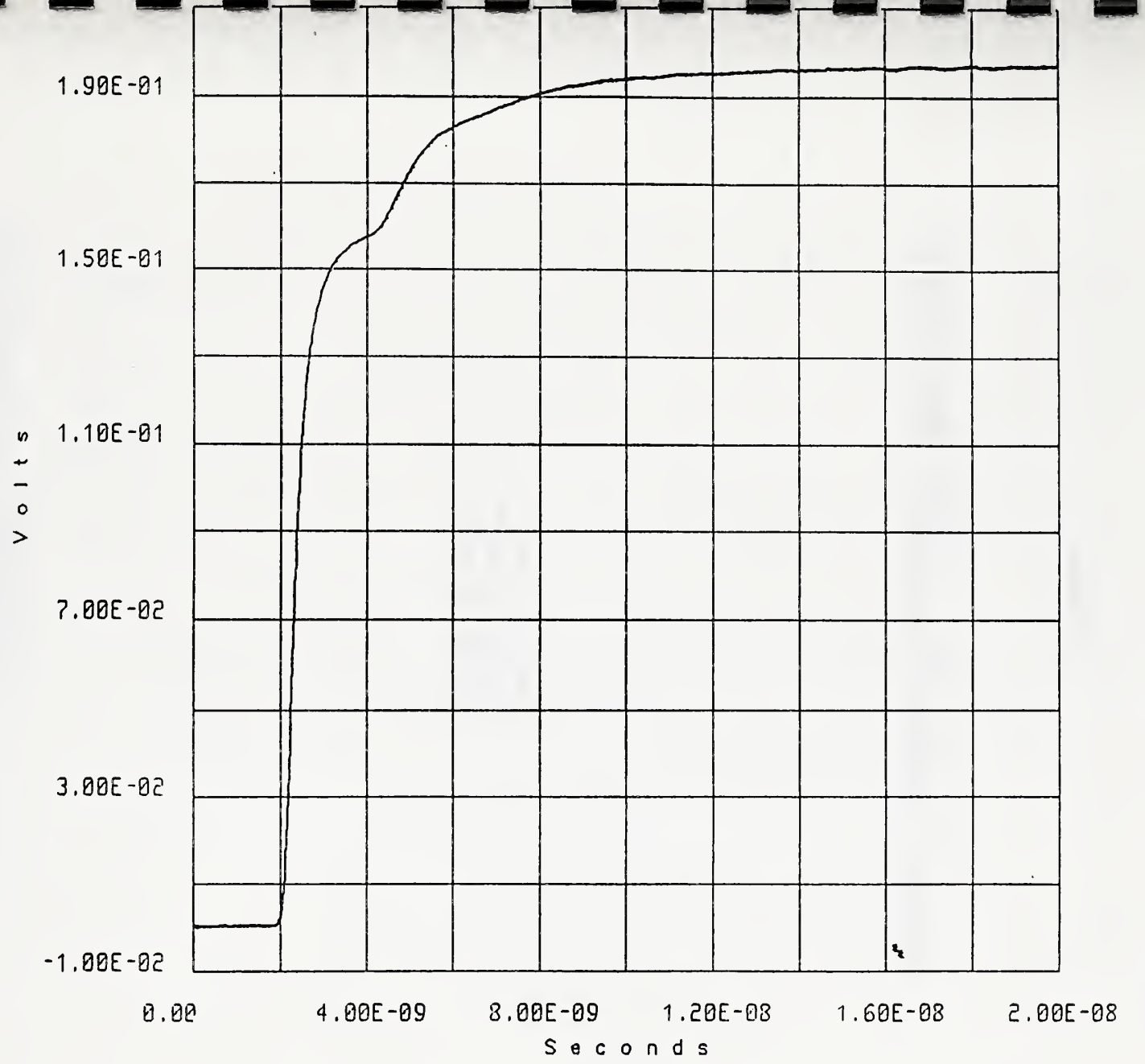

COMMENT: trans thru line #7 5/3/91 wlg

FIGURE 41

Appendix A

A Solid-State Reference Waveform Standard

Robert A. Lawton
Norris S. Nahman
Jeffrey M. Bigelow

Reprinted from
IEEE TRANSACTIONS ON INSTRUMENTATION AND MEASUREMENT
Vol. IM-33, No. 3, September 1984

A Solid-State Reference Waveform Standard

ROBERT A. LAWTON, SENIOR MEMBER, IEEE, NORRIS S. NAHMAN, FELLOW, IEEE, AND JEFFREY M. BIGELOW

Abstract—A solid-state reference waveform filter has been developed which uses the Maxwell-Wagner capacitor effect. This filter is realized in a stripline configuration with a lossy dielectric consisting of a thick (5-μm) layer of SiO_2 on Si. The equivalent circuit of this filter is equivalent to that for previously developed filters which used a lossy liquid dielectric. A preliminary design has been completed and a filter fabricated for which the design characteristic impedance, 38 Ω, and transition duration (rise time), 300 ps, agree with measured values to within 2 and 17 percent, respectively. The temperature dependence of the filter transition duration has been estimated from the temperature dependence of the filter conductance to be about 1 percent/°C.

INTRODUCTION

A TIME waveform history of various phenomena may now be acquired with much greater precision and convenience than ever before. This is due in large part to the inexpensive and convenient signal handling capability of microprocessors.

The question remains as to what degree this precision represents the truth. To help resolve such questions the National Bureau of Standards (NBS) has been charged with the responsibilities to 1) develop accurate measurement standards with which other measurements can be compared, and 2) encourage the use of standard measurement procedures.

Some of the basic standards developed by NBS include the second for time measurement, the meter for length measurement, and the volt for potential difference measurement. Standards which are derived from these basic quantities are now being developed for use in recording the time history of electrical waveforms. Two basic approaches have been used. The first method models the distortion caused by some measurement system and then removes it mathematically (deconvolves) to obtain an estimate of the true waveform [1]. The second method models the output waveform of a waveform generator whose output is applied to the measurement system; the measurement system's response is then compared to the predicted available waveform of the generator [2]. The generator with the modeled output is called a reference waveform generator.

A reference waveform generator can be used to evaluate an oscilloscope or waveform recorder by determining how closely the display resembles the "available waveform" of the reference generator for a load impedance equal to the measurement system's nominal input impedance.

The reference waveform is modified by the system transfer function $H(s)$ and the relation between $Z_{11}(s)$ and $Z_g(s)$ to produce the displayed waveform $e_d(t)$ as shown in Fig. 1. The

Manuscript received April 16, 1984.

The authors are with the National Bureau of Standards, Boulder, CO 80303.

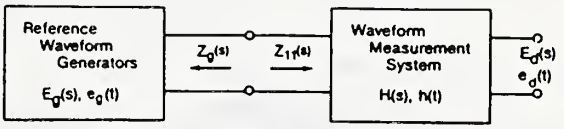

Fig. 1. Schematic diagram of the waveform measurement input/output parameters.

specific nature of $H(s)$ may be derived by stable deconvolution techniques [1] using the measured $e_d(t)$, the reference waveform $z_g(s)$, together with a frequency-domain or time-domain measurement of $Z_{11}(s)$.

One of the more popular waveforms used in testing waveform recording devices is a steplike waveform (which makes a transition from an initial level to a final one) since it provides a more complete system characterization than some other commonly used waveforms. The time it takes for a steplike waveform to go from 10 percent of the transition to 90 percent is called the transition duration or rise time. (Note this parameter has meaning only when dealing with steplike waveforms.) Over the years NBS has developed a set of transition duration standards which consist of lossy filters excited by fast step generators (tunnel diodes).

In the nanosecond and picosecond regions of the time domain, reflectionless (constant impedance) filters for waveform shaping cannot be built using discrete circuit elements. Distributed circuit elements must be used to avoid reflections and their effects on impedance and the resultant transmitted waveforms [2] The present waveshaping filters employed by NBS in the NBS reference waveform generators [2]-[4] use distributed elements comprised of polarliquid filled coaxial transmission lines approximately 24 cm in length. The resultant waveshaping is due to the Debye relaxation phenomena in the dilute polar solutions which serve as the dielectrics in the coaxial transmission lines. The present set of filters provide three steplike resultant waveforms having 50-, 100-, and 200-ps transition-durations.

The simple geometry makes it possible to develop an accurate model of the filter transient response. In addition, the waveform generator output is independent of the input excitation if the input excitation has a much shorter transition duration than that of the filter step response. The case where the input excitation is not fast enough is discussed elsewhere [5]. With the simple geometry and a fast input step one can produce a modeled reference waveform generator.

These filters have the additional attribute that the transition duration can be varied simply by varying the filter length while maintaining a constant characteristic impedance. However they are limited in their use as a portable transfer standard and are intended for use only as laboratory standards. In

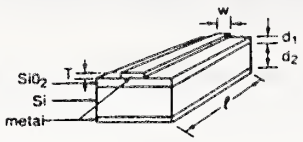

Fig. 2. Microstripline configuration used for reference waveform generator.

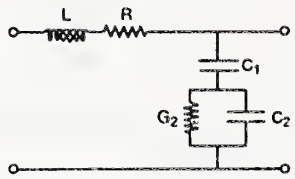

Fig. 3. Maxwell–Wagner capacitor microstripline filter equivalent circuit.

addition they are not well suited for transition durations longer than about 1 ns.

To extend the transition-duration range into the 1–10-ns range using the present liquid dielectric design would require unwieldy (long) transmission lines and/or higher concentrations of polar solute molecules in the dielectric solution. Higher solute concentrations are limited by second-order polarization effects which are not mathematically represented by the Debye (dilute solution) equations; consequently, such concentrations would not produce an *a priori* model based upon the well known and characterizable Debye model parameters.

To cover this extended range a new waveshaping filter has been developed which contains solid dielectric layers in a microstrip transmission line structure [6]. The filter size is much smaller than the liquid dielectric filters and can be fabricated as an integrated semiconductor circuit making it a very suitable candidate for portable standards covering the extended ranges, and also for improving the present standards in the tens to hundreds of picoseconds region. This new filter uses the Maxwell–Wagner two-layer dielectric capacitor concept [7] and is shown schematically in Fig. 2.

Theory

The equivalent circuit for the Maxwell–Wagner Capacitor stripline filter, assuming planar skin effect, is given in Fig. 3 and is similar to that for the liquid dielectric lines. In the layered dielectric, subscript 1 refers to the silicon dioxide dielectric and subscript 2 refers to the silicon dielectric. The characteristic impedance $Z_0(j\omega)$ is given by

$$Z_0(j\omega) = \sqrt{Z(j\omega)/Y(j\omega)} \tag{1}$$

where $Z(j\omega)$ is the distributed series impedance per unit length and $Y(j\omega)$ is the distributed shunt admittance per unit length. The propagation constant $\gamma(j\omega)$ is given by

$$\gamma(j\omega) = \alpha(\omega) + j\beta(\omega) = \sqrt{Z(j\omega)Y(j\omega)}\,. \tag{2}$$

Since $\alpha(\omega)$ is the real part of the propagation constant, it will determine the filter dispersion while the imaginary part $\beta(\omega)$ will determine the phase shift or time delay. Let us

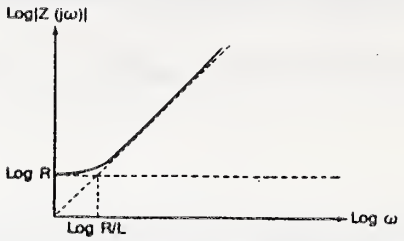

Fig. 4. Dependence of $Z(j\omega)$ on frequency.

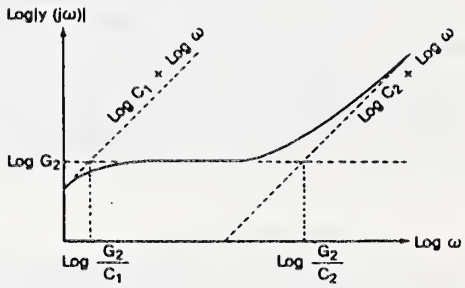

Fig. 5. Dependence of $Y(j\omega)$ on frequency.

now consider the behavior of $Z(j\omega)$ versus frequency. At zero frequency, $Z_0(0) = R$. At high frequency the resistance R is negligible and $Z(j\omega)$ is given by $j\omega L$ with the resulting functional form for $Z(j\omega)$ shown in Fig. 4.

Similarly, at very low frequencies, $Y(j\omega) = j\omega C_1$ and at very high frequencies it is equal to $j\omega C_\infty$, where C_∞ is the capacitance at infinite frequency and is given by $C_\infty = C_1C_2/(C_1 + C_2)$. The result is the functional form given in Fig. 5 for the case of $C_1 \gg C_2$. In this case $C_\infty \approx C_2$.

In Fig. 4, the resistance of the transmission line R may be safely neglected in the frequency range of $\omega > 10(R/L)$. Similarly C_2 can be ignored for $\omega < 0.1\ G_2/C_2$ in Fig. 5.

Now the effective values of the line parameters found by Hasegawa [8] for the stripline of Fig. 2 are

$$\begin{aligned} L &= \mu_0(d_1 + d_2)^+/w \\ C_1 &= \epsilon_0\epsilon^+_{SiO_2}w/d_1^+ \\ C_2 &= \epsilon_0\epsilon^+_{Si}w/d_2^+ \\ G_2 &= \sigma_2^+w/d_2^+. \end{aligned} \tag{3}$$

The symbols μ_0 and ϵ_0 in the above expressions represent the permeability and permittivity, respectively, of free space. In addition

$$\begin{aligned} d_i^+/w &= (1/2\pi)\ln\left[8(d_i/w) + (4d_i/w)^{-1}\right] \quad \text{for } d_i/w > 1. \\ &= \left[(w/d_i + 2.42 - 0.44\,(d_i/w) + (1 - d_i/w)^6\right]^{-1} \end{aligned} \tag{4}$$

for $d_i/w < 1$ where d_i^+ can be either d_1^+, d_2^+ or $(d_1 + d_2)^+$

$$\epsilon_i^+ = (\epsilon_i + 1)/2 + (\epsilon_i - 1)/[2(1 + 10d_i/w)^{1/2}]$$

where ϵ_i^+ can be either ϵ_{SiO_2} or ϵ_{Si}.
Finally,

$$\sigma_2^+ = (\sigma_2/2)[1 + (1 + 10d_2/w)^{-1/2}]$$

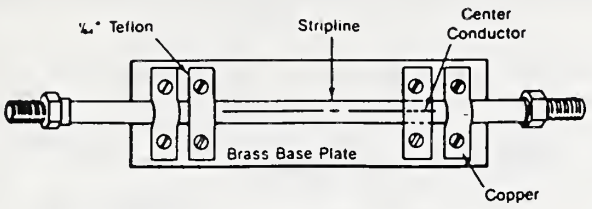

Fig. 6. Filter with coaxial lines for connectors.

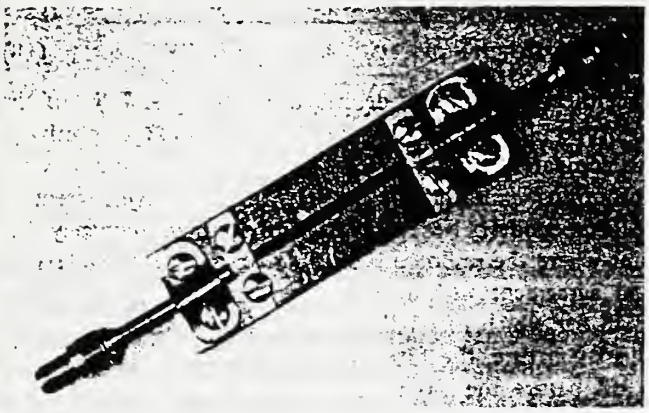

Fig. 7. Coaxial to microstrip mount arrangement used for reference waveform generator.

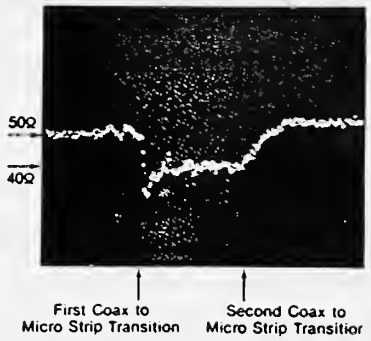

Fig. 8. TDR trace of microstripline filter.

and

$$R = 1/(\sigma_{Al} w T) \tag{5}$$

where σ_2 and σ_{Al} represent the conductivity of the silicon and the aluminum metallization, respectively. By substituting equations (4) and (5) in (3) one can calculate L, C_1, C_2, and G_2.

Filter Design

A prototype microstrip filter has been realized by growing a thick (5.5-μm) layer of silicon dioxide on a 5-Ω·cm, 300-μm-thick silicon wafer. A 7-μm-thick film of aluminum was then evaporated on both sides of the resulting wafer and several 70-μm-wide lines were then etched on one side forming the strip of the microstripline. These strips were then separated with a diamond saw, mounted on brass plates and connected to coaxial lines as shown in Figs. 6 and 7. A time-domain reflectometer (TDR) picture of the microstrip and transitions is given in Fig. 8 and a photograph of the output reference

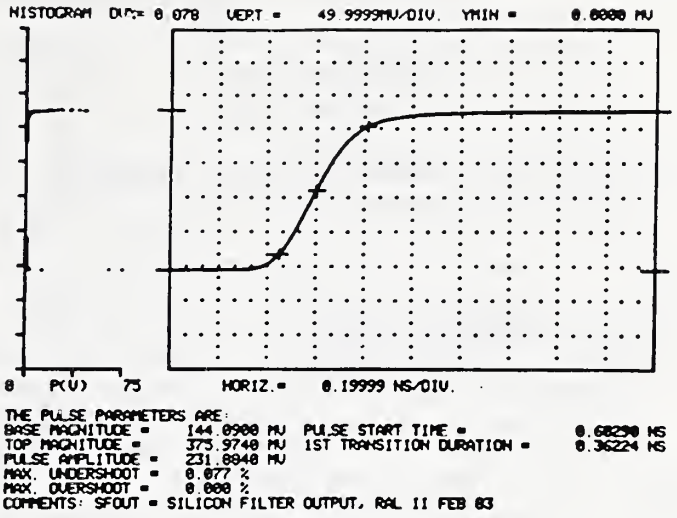

Fig. 9. Filter output reference waveform.

waveform as measured on the NBS automatic pulse-measurement system (APMS) [9] is given in Fig. 9.

For our prototype filter

$$\begin{aligned} T &= 7\ \mu\text{m} \\ W &= 70\ \mu\text{m} \\ l &= 4.6\ \text{cm} \\ d_1 &= 5.5\ \mu\text{m} \\ d_2 &= 300\ \mu\text{m} \\ \epsilon_{SiO_2} &= 4 \\ \epsilon_{Si} &= 12 \\ \sigma_{Si} &= 31\ \text{S/m} \\ \sigma_{Al} &= 3.7 \times 10^7\ \text{S/m}. \end{aligned} \tag{6}$$

From these parameters we calculate

$$\begin{aligned} L &= 7.14 \times 10^{-7}\ \text{H/m} \\ C_1 &= 504\ \text{pF/m} \\ C_2 &= 115\ \text{pF/m} \\ G_2 &= 31.7\ \text{S/m} \\ R &= 55.2\ \Omega\text{/m} \end{aligned} \tag{7}$$

which in turn are used to determine that R can be neglected for frequencies $(\omega/[2\pi])$ above 200 MHz and C_2 can be neglected below 2 GHz. Therefore, in the frequency region from 200 MHz to 2 GHz, we have the equivalent circuits shown in Fig. 10 for which

$$\begin{aligned} Z_0(j\omega) &= \sqrt{j\omega L\,[1/G_2 + 1/j\omega C_1]} \\ &= R_0\sqrt{1 + j\omega C_1/G_2} \quad \text{where } R_0 = \sqrt{L/C_1}. \end{aligned} \tag{8}$$

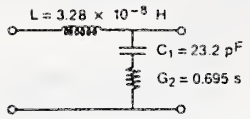

Fig. 10. Equivalent circuit of microstripline filter in frequency range of 200 MHz to 2 GHz.

Similarly,

$$\gamma(j\omega) = \sqrt{j\omega L/[1/G_2 + 1/j\omega C_1]}$$
$$= j\omega\sqrt{LC_1}\,/\,\sqrt{1 + j\omega C_1/G_2}$$
$$\approx j\omega\sqrt{LC_1}\,[1 - j\omega C_1/2G_2] \quad (9)$$

since $\omega \ll G_2/C_1$. Therefore, with (2) in (9)

$$\alpha(\omega) = C_1\sqrt{LC_1}(1/2G_2)\omega^2 \quad (10)$$

and the electromagnetic energy will be attenuated along the transmission line according to $e^{-\alpha(\omega)l}$ or $e^{-(\omega/\omega_0)^2 l}$ where $\omega_0 = \sqrt{2G_2/(C_1\sqrt{LC_1})}$. Note that this is a Gaussian function and as such has some special properties as an antialiasing waveform filter since an antialiasing filter that has a Gaussian rolloff characteristic can be designed with a cutoff frequency much closer to the Nyquist frequency than most other filters. Consider, for example, an antialiasing filter that will reduce the error due to the folded spectrum to less than one half of a least significant bit ($\frac{1}{2}$ LSB) for a 1024-point sampled waveform in a 5-ns time window. For a simple RC filter, the cutoff frequency can be no greater than 3 MHz while for a Gaussian filter the cutoff frequency is 18 GHz.

To calculate the filter transition duration, consider the Gaussian filter voltage transfer function with arbitrary parameters D and a

$$H(j\omega) = e^{-j\omega D}\, e^{(j\omega/2a)^2} \quad (11)$$

as a function of frequency. The transform of this function in the time domain gives the filter impulse response

$$h(t) = (a/\sqrt{\pi})e^{-a^2(t-D)^2} \quad (12)$$

from which the step response is found to be

$$v_s(t) = \tfrac{1}{2}\,\mathrm{erf}\,[a(t - D)] + \tfrac{1}{2} \quad (13)$$

for which the first transition duration (10-90 percent) is

$$t_1 = 1.8/a. \quad (14)$$

For the filter being analyzed

$$H(j\omega) = e^{\gamma(j\omega)l}$$
$$= e^{-j\omega l\sqrt{LC_1}}\, e^{-C_1\sqrt{LC_1}/(2G_2)\omega^2 l}. \quad (15)$$

Therefore,

$$a = \sqrt{G_2/2lC_1\sqrt{LC_1}}. \quad (16)$$

Substituting the calculated values for L, C_1, and G_2 in (16), and (16) in (14) yields

$$t_1 = 300\ \text{ps} \quad (17)$$

which compares favorably with the measured transition duration of 362 ps.

Similarly, substituting the calculated values for L and C_1 in the equation for R_0 yields

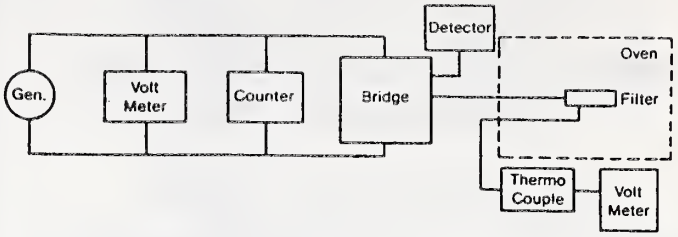

Fig. 11. Schematic of capacitance bridge measurement system.

$$R_0 = 38\ \Omega. \quad (18)$$

From the measurements described earlier, t_1 and R_0 of the prototype filter are found to be 362 ps and 40 Ω, respectively. This compares favorably with the modeled values and provides a promising confirmation of the theoretical development of the filter model. Note that the filter corner frequency, the point where the response is 3-dB down, occurs at 780 MHz in good agreement with a measurement of S_{21} made with the APMS for which the 3-dB point is at 800 MHz. Due to its Gaussian nature, the filter response will decay an additional 13 dB before the 2-GHz limit of our approximation region is reached and an additional 135 dB at the frequency where G_2 is comparable to ωC_1. Therefore, the approximation should yield good results.

Low-frequency measurements have also been made of L and C_1 from 10 kHz to 10 MHz which yield

$$lC_1 = 21.7\ \text{pF} \quad \text{or} \quad C_1 = 472\ \text{pF/m}$$
$$lL = 30\ \text{nH} \quad \text{or} \quad L = 6.5 \times 10^{-7}\ \text{H/m} \quad (19)$$

which compare favorably with the calculated values of 504 pF/m and 7.14×10^{-7} H/m.

Temperature Dependence

In order for this filter to be useful in producing precision reference waveforms, an accurate account must be made of any temperature dependence. According to (16), t_1 is the transition duration of the filter, the temperature dependence of the transition duration is primarily determined by the effect of temperature on the capacitance and conductance of the silicon layer (assuming negligible change of line length and line inductance with temperature).

To measure the capacitance and conductance as a function of temperature, a capacitance bridge was used, as shown in Fig. 11. An oven controlled the temperature and a thermocouple attached to the base plate of the filter measured the temperature. As resistance measurements were also necessary, a voltage source and a known resistance were put in series with the filter, as shown in Fig. 12, and the voltage across the filter was measured with four-digit accuracy. In the figure V_S and V_L are the reference and measured voltages from which the unknown resistance R_L can be calculated in terms of a reference resistor R_S with the formula

$$R_L = R_S V_L/(V_S - V_L). \quad (20)$$

Two mounts were used for the measurements. The first was the mount of Figs. 6 and 7 described earlier. The center conductor of each coaxial line makes direct contact with the aluminum. The second was a mount which used a modified SMA-to-stripline adapter, and is shown schematically in Fig. 13.

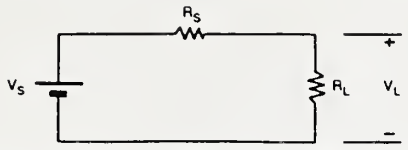

Fig. 12. Schematic of resistance measurement system.

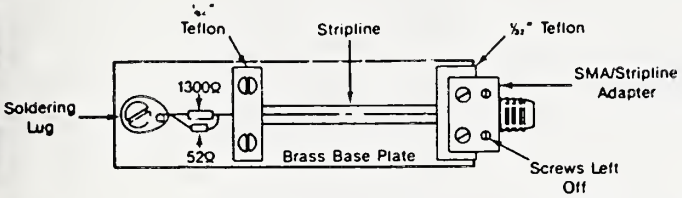

Fig. 13. Filter with coax to SMA adaptors for connectors.

The 1300- and 52-Ω resistors in parallel create the 50-Ω termination for the stripline.

In determining the dependence of conductance on temperature, it was necessary to measure the effect of temperature on the aluminum and contact resistance. To do this, the resistors on the filter of Fig. 13 were replaced with a short. The filter was placed in the oven and the resistance was measured using the circuit of Fig. 10 at temperatures near room temperature. The readings were taken at 20 V with a reference resistance of 577 Ω. With the short disconnected from the filter this same circuit was then used to measure the temperature dependence of the silicon conductance and capacitance. The bridge voltage was 10 V at 100 kHz.

To obtain small changes in temperature around room temperature, the oven blower only was turned on. After the oven reached the maximum desired temperature, the blower was turned off and, as the oven cavity cooled, a second set of measurements was taken. The later measurements took longer but allowed the temperature to stabilize before taking the thermocouple voltage reading. The results were all plotted against temperature over the measurement temperature range from 24 to 31°C. Since the results were basically linear, linear regression was used to get a best fit line for each measurement and the results were extrapolated to 20°C.

The coaxial line connector filter mount measurements gave a capacitance temperature coefficient of 0.01 percent/°C at 20°C and a conductance temperature coefficient of -1.1 percent/°C at 20°C. The corresponding results using the mount with the SMA adaptor were 0.0034 and -2.9 percent/°C, respectively. The measurement of the contact and aluminum resistance yielded a temperature coefficient of 0.34 percent/°C.

Even though the conductance temperature coefficient is different for the two mounts, the slopes of the lines are approximately equal. With the mount of Fig. 11, the conductances seen by the bridge are of the order of 0.04-μS range. For the second mount, the conductances are around 0.01 μS. Series resistance has the effect of increasing the observed shunt conductance. The coaxial lines can roll when connecting and disconnecting the connectors, weakening the contact and increasing the resistance with the result that the resistance is greater in the coaxial line filter mount. For this reason, the measurements of the filter on the mount with the coaxial lines were considered unrepresentative of the filter's characteristics and were disregarded, while the measurements made using the SMA connectors were used to determine the transition duration temperature dependence.

Because the temperature coefficient of the capacitance is less than 0.01 percent/°C and the temperature dependence of the aluminum and contact resistance is 0.34 percent/°C compared to 2.9 percent/°C for the conductance, the transition duration temperature dependence is primarily determined by the temperature dependence of the conductance.

Using the measured values of line length, inductance, capacitance, conductance and temperature dependence of conductance, the temperature dependence of the filter transition duration was estimated to be 1 percent/°C. This is approximately the same as the temperature coefficient of the liquid dielectric waveform filters [10].

Summary

A solid-state waveform filter with a lossy, two-layer dielectric has been constructed using silicon dioxide on silicon. A model has been developed and used to calculate the microstrip characteristic impedance and to generate a reference waveform. These modeled values have been compared with preliminary measured values using time domain reflectometry and the APMS, and have been found to agree to within about 2 percent for impedance and 17 percent for transition duration. In addition the temperature dependence of the filter transition duration has been estimated to be about 1 percent/°C.

Acknowledgment

The support of M. Shelton and L. Tarr of the U.S. Army Primary Standards Laboratory is hereby acknowledged. In addition the assistance of G. Carver and D. Novotny of the Semiconductor Materials & Processes Division of the National Bureau of Standards in fabricating the silicon striplines is also acknowledged.

References

[1] N. S. Nahman and M. E. Guillaume, "Deconvolution of time domain waveforms in the presence of noise," Nat. Bur. Stand. (U.S.) tech. note 1047, Oct. 1981.

[2] W. D. McCaa, Jr. and N. S. Nahman, "Generation of reference waveforms by uniform lossy transmission lines," *IEEE Trans. Instrum. Meas.*, vol. IM-19, no. 4, pp. 382-390, Nov. 1970.

[3] N. S. Nahman, R. M. Jickling, and D. R. Holt, "Reference waveform generation using Debye dielectric dispersion," Nat. Bur. Stand. (U.S.) NBSIR 73-304, Dec. 1972, 91 pp.

[4] R. P. Bagozi, "Pulse response of polar-liquid filled coaxial lines," M. S. thesis, Dept. of Elec. Eng., Univer. Colorado, Boulder, 1969.

[5] R. A. Lawton, "Photoconductive switches used for waveform generation at the National Bureau of Standards," in *Proc. SPIE 27th Ann. Tech. Symp.*, to be published.

[6] N. S. Nahman, "A silicon Debye line for reference pulse shaping," Nat. Bur. Stand. (U.S.) presented at E. M. Waveform Metrology Group Sem., Dec. 1980.

[7] A. R. Von Hippel, *Dielectrics and Waves*, New York: Wiley 1954, p. 228.

[8] H. Hasegawa, M. Furukawa, and Y. Hisayoshi, "Properties of microstrip line on Si-SiO_2 system," *IEEE Trans. Microwave Theory Tech.*, vol. MTT-19, no. 11, pp. 869-881, Nov. 1971.

[9] W. L. Gans, "Present capabilities of the NBS automatic pulse measurement system," *IEEE Trans. Instrum. Meas.*, vol. IM-25, no. 4, pp. 384-388, Dec. 1976.

[10] J. R. Andrews, "Pulse reference waveform standards development at NBS," in *Proc. ATE Sem./Exhibit*, PIV-13, Jan. 1981.

Appendix B

Two-Layer Dielectric Microstrip Line Structure: SiO_2 on Si and GaAs on Si: Modeling and Measurement

Robert A. Lawton
Wallace T. Anderson

Reprinted from
IEEE TRANSACTIONS ON MICROWAVE THEORY AND TECHNIQUES
Vol. 36, No. 4, April 1988

Two-Layer Dielectric Microstrip Line Structure: SiO_2 on Si and GaAs on Si: Modeling and Measurement

R. A. LAWTON, SENIOR MEMBER, IEEE, AND
WALLACE T. ANDERSON, MEMBER, IEEE

Abstract—Further development is reported of the modeling of the two-layer dielectric microstrip line structure by computing the scattering parameter S_{21} derived from the model and comparing the computed value with the measured value over the frequency range from 90 MHz to 18 GHz. The sensitivity of the phase of S_{21} and the magnitude of the characteristic impedance to various parameters of the equivalent circuit is

Manuscript received June 25, 1987; revised October 30, 1987.

R. A. Lawton was with the National Bureau of Standards, Boulder, CO. He is now with Boulder Research Associates, Boulder, CO 80303.

W. T. Anderson is with the Naval Research Laboratory, Washington, DC 20375.

IEEE Log Number 8719443.

also discussed. Examples are given of the measurement and modeling of the SiO_2 on silicon system to 18 GHz and the modeling of the GaAs on silicon system to 100 GHz.

I. Introduction

The two-layer dielectric microstrip line structure is a structure that has found use in a number of applications. Two examples are as follows: In [1] the two-layer structure is used to make a pulse waveform filter with useful characteristics, while in [2] one layer (a silicon layer) is used to provide a high-quality substrate for gallium arsenide devices.

To further amplify the application described in [2], the advantages of integrating GaAs devices on Si substrates include the possibilities of GaAs monolithic microwave integrated circuits (MMIC's) and/or GaAs digital IC's with Si VLSI, electro-optical GaAs devices with Si VLSI, GaAs power FET's on Si substrates for operation above 10 GHz making use of the higher thermal conductivity of Si, and allowing GaAs IC's to be fabricated on much larger diameter Si substrates (> 7.5 cm) than are now available for GaAs. Well-behaved GaAs MESFET's [4] and bipolar transistors [5] have been fabricated on GaAs molecular beam epitaxy (MBE) layers grown on Si. For low-loss applications, methods have been developed to grow high-resistivity GaAs layers on Si by low-temperature MBE (104 $\Omega \cdot$cm) [6] and by V-doped metal-organic chemical vapor deposition (MOCVD) (10^8 $\Omega \cdot$cm) [7].

Preliminary modeling of microstrip lines made from such structures has been described [1], [8]–[10]. Similar analyses have been developed for the increasingly important coplanar waveguide case [11]. In the previous work by Lawton *et al.* [1], the equivalent circuit relations developed by Hasegawa [8] were used to calculate an approximate relation for the microstrip line characteristic impedance and the transition duration of the microstrip line to a step input signal. This approximate relation was then compared with values determined experimentally. In this report, the complete equations for the characteristic impedance and propagation constant of the stripline are developed, including planar skin effect, and used in the calculations without the approximations of [1]. A measurement is then made of the S parameters of the stripline on an automatic network analyzer. In the process, an algorithm is used which transforms the data to the time domain and sets a time window which discards data due to the connectors, so that one is left with data due to the semiconductor stripline itself. The data are then transformed back to the frequency domain.

II. Theory

The structure of the two-layer dielectric transmission system is shown in Fig. 1. A more generalized form of the equivalent circuit will be used here than that of Hasegawa [8] and Lawton *et al.* [1]. This more general equivalent circuit will allow for loss in both dielectric layers and skin effect in the metallization. This equivalent circuit is shown in Fig. 2. Therefore the series impedance is given by

$$Z(j\omega) = j\omega L + R + k\sqrt{j\omega} \tag{1}$$

and the shunt admittance is given by

$$Y(j\omega) = \frac{1}{\frac{1}{G_1 + j\omega C_1} + \frac{1}{G_2 + j\omega C_2}} \tag{2}$$

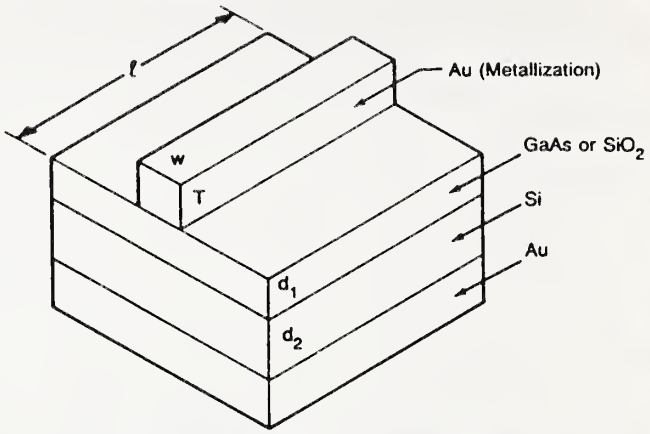

Fig. 1. Two-layer dielectric transmission system.

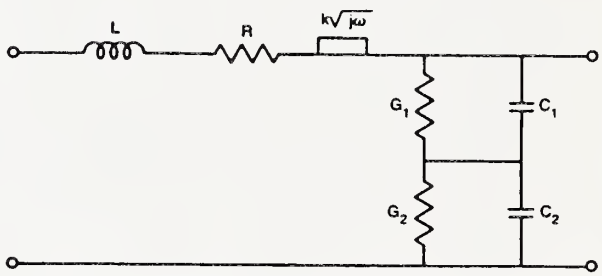

Fig. 2. Generalized two-layer dielectric equivalent circuit.

where

$$R = 1/(\sigma_{Au} wT)$$

$$L = \mu_0 (d_1 + d_2)^+ / w$$

$$C_1 = \epsilon_0 \epsilon_1^+ w/d_1^+$$

$$G_1 = \sigma_1^+ w/d_1^+$$

$$C_2 = \epsilon_0 \epsilon_2^+ w/d_2^+$$

$$G_2 = \sigma_2^+ w/d_2^+$$

ω = angular frequency.

The term $k\sqrt{j\omega}$ represents an impedance term due to planar skin effect. The terms μ and ϵ represent permeability and permittivity, respectively, with the subscripts denoting the medium (0 denotes free space). The other parameters are as defined in Fig. 1. The + superscript denotes effective values that take into account fringing and a mixed dielectric. The defining relations for these effective values are given in [1] and [3].

With the above parameters in (1) and (2), one can calculate the series impedance and shunt admittance elements. One can then substitute (1) and (2) into the expressions for the characteristic impedance:

$$Z_0(j\omega) = \sqrt{Z(j\omega)/Y(j\omega)} \tag{3}$$

and the propagation constant:

$$\gamma(j\omega) = \sqrt{Z(j\omega)Y(j\omega)}\,. \tag{4}$$

These are the parameters which are required to evaluate the behavior of the stripline with a microwave measurement system. However since most modern microwave measurements are made in terms of S parameters, it is desirable to make the further calculation

$$S_{21}(j\omega) = e^{-\gamma(j\omega)l}. \tag{5}$$

This expression is valid for the transmission between two reference planes on a uniform transmission line, which is the case in Fig. 1. The phase of S_{21} is given by the imaginary part of the exponent and the attenuation is given by $20\times\log_{10}|S_{21}|$.

III. Calculation for SiO_2 on Si

For ease of calculation and modeling, the complete calculations of Z_0 and the attenuation were performed on an electronic spreadsheet program which had integrated graphics. This integration made it very convenient to test a value for a parameter, compare the resulting calculation of the attenuation for example with the measured value, and then quickly try another value.

IV. Experimental Results

An automatic network analyzer was used to make measurements on a microstrip line structure consisting of silicon dioxide on silicon. The parameters of the structure were estimated before being measured using dimensional and conductivity measurements together with published values for the permittivity and permeability of both dielectric layers. This estimation process resulted in the following values:

$$\sigma_{Au} = 4.6\times10^7 \text{ S/m}$$
$$\epsilon_1 = 4.0$$
$$\epsilon_2 = 11.7$$
$$\sigma_2 = 34.5 \text{ S/m}$$
$$\sigma_1 = 0$$
$$d_1 = 15\ \mu\text{m}$$
$$d_2 = 300\ \mu\text{m}$$
$$w = 90\ \mu\text{m}$$
$$T = 7\ \mu\text{m}$$
$$l = 5.04 \text{ cm}.$$

The frequency range of the measurements was 90 MHz to 18 GHz and a windowing algorithm was used. This algorithm consisted of transforming the data to the time domain, deleting the data that corresponded to parts of the circuit not in the microstrip line itself, and retransforming back to the frequency domain. In other words only data in the time domain window that corresponded to the spatial location of the microstrip line were used. This had the effect of gating out all the reflections in the connectors to the microstrip line and in the transitions from coax to waveguide. The application of this windowing algorithm and the large number of data points (200) resulted in a smooth variation of the actual experimental data plotted in Fig. 3. The windowing algorithm also may have contributed some smoothing.

The various parameters in the model, L, C_1, C_2, G_2, and R, were adjusted, and it was found that the phase of S_{21} and the characteristic impedance were affected to first order only by L and C_1. Referring to the low-frequency approximate relations for Z_0 and $\beta(j\omega)$, the imaginary part of $\gamma(j\omega)$, in [1, eqs. (8) and (9)], we have

$$Z_0 \approx \sqrt{L/C_1} \tag{6}$$

$$\beta(j\omega) \approx \omega\sqrt{LC_1}\,. \tag{7}$$

The sensitivity experiment confirms that these relations are good approximations over much of the range of the measurements reported here. Therefore a measurement of the magnitudes of Z_0 and $\beta(j\omega)$ by curve fitting allows one to solve (6) and (7) to obtain a unique solution for L and C_1 within this approximation. Having determined these two parameters, it was then possible to determine R from the low-frequency attenuation and G_2 from the slope portion of the curve. The skin effect factor k was multiplied by a constant, less than 1, which was chosen to be such that the proper curvature in the knee of the curve was obtained. It was not possible to determine C_2 from the data since the high-frequency attenuation, where C_2 becomes important, exceeded the dynamic range of the measurement system. In this case, G_1 was taken to be zero since SiO_2 is a very low loss material. We see from Fig. 3 that the phase match is excellent except at the upper frequencies, where the system dynamic range is exceeded. Note that the attenuation match is also quite good.

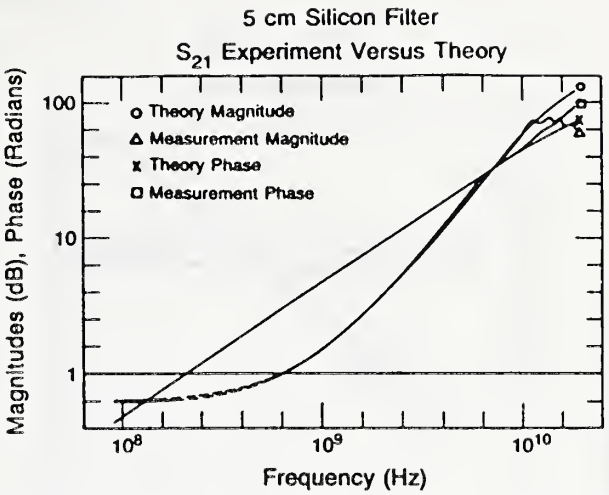

Fig. 3. Measured and modeled attenuation and phase of the microstrip line structure.

TABLE I
Comparison of Values of Parameters Obtained by Fitting Data to Values Obtained by Independent Measurements

Parameter	ANA Measurements	Impedance Measurements
L	711 nH/m	758 nH/m
C_1	306 pF/m	353 pF/m
Z_0	48.2 Ω	48 Ω

The results of the measurement and parameter fitting are given in Fig. 3. In this figure, the logarithm of the attenuation is plotted versus the logarithm of frequency. Since the attenuation is linearly proportional to the propagation constant γ, and γ is proportional to ω^2 in the midfrequency range, the plot should be linear with a slope of 2 in this range if the transfer function, S_{21}, of the microstrip line were Gaussian. In other words, this type of plot enables us to determine the frequency range over which the attenuation is Gaussian-like, which is an important property in network theory. Similarly, the logarithm of phase is plotted versus the logarithm of frequency.

The values of the equivalent circuit parameters obtained by fitting measured data to the model were

$$R = 130\ \Omega/\text{m}$$
$$L = 711 \text{ nH/m}$$
$$C_1 = 306 \text{ pF/m}$$
$$C_2 = 256 \text{ pF/m}$$
$$G_2 = 50 \text{ S/m}$$
$$G_1 = 0.$$

Two of these values together with the characteristic impedance

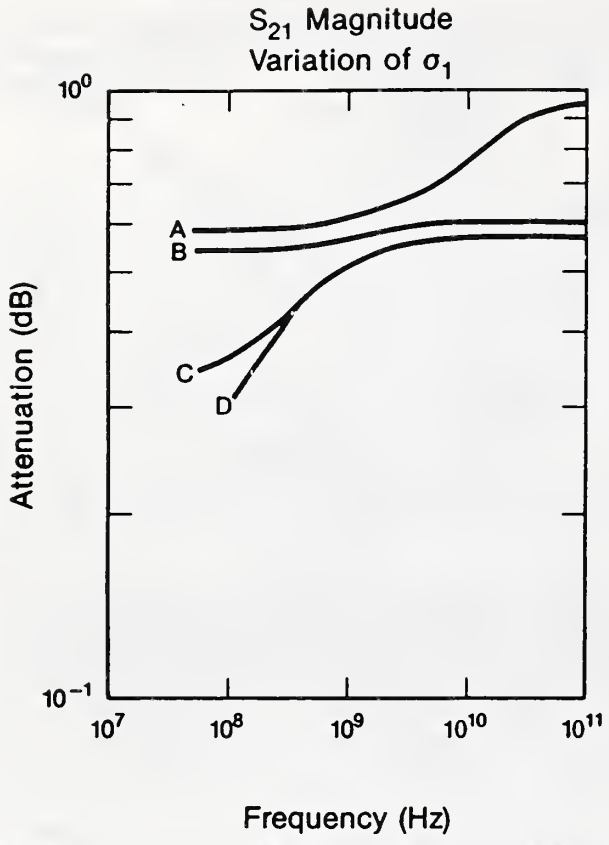

Fig. 4. Attenuation for GaAs on Si microstrip line 1 mm long with $d_1 = 4$ μm, $\sigma_2 = 1.4$ S/m (71 Ω·cm) and A) $\sigma_1 = 10$ S/m (10 Ω·cm), B) $\sigma_1 = 1$ S/m (100 Ω·cm), C) $\sigma_1 = 0.1$ S/m (1000 Ω·cm), and D) $\sigma_1 = 0.002$ S/m (5×10^4 Ω·cm).

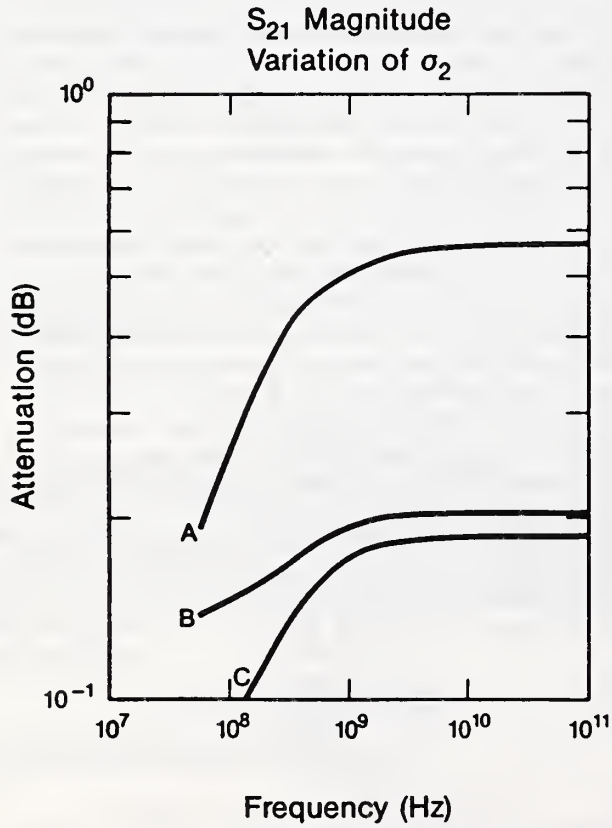

Fig. 5. Calculated attenuation for GaAs on Si microstrip line 1 mm long with $d_1 = 4$ μm, $\sigma_1 = 0.002$ S/m (5×10^4 Ω·cm) and A) $\sigma_2 = 1.4$ S/m (71 Ω·cm), B) $\sigma_2 = 0.1$ S/m (1000 Ω·cm), and C) $\sigma_2 = 0.01$ S/m (10 000 Ω·cm).

were then compared to values obtained by independent short- and open-circuit low-frequency impedance measurements. The result of this comparison is given in Table I.

The good agreement in the determination of Z_0 by the two methods is probably fortuitous since a large error in L can be compensated by a comparable error in C_1 because they occur as a ratio in the expression for Z_0. The discrepancy in the values for L and C_1 between the two methods could correspond to a potential discrepancy in the Z_0 values of 4 percent, which is reasonable for the preliminary measurements reported here.

V. Calculation for GaAs on Si

Having demonstrated the feasibility of determining the equivalent circuit parameters of microstrip lines from measurements, calculations were performed for the important two-layer dielectric case consisting of gallium arsenide on silicon. The purpose of this calculation was to see what range of attenuation to expect using typical dimensions that one might encounter in high-speed integrated circuits. To be consistent with typical materials that can be used for the technology appropriate to GaAs on Si, the following parameters were assumed for these calculations:

$$\sigma_{Au} = 1.5 \times 10^7 \text{ S/m } (6.67 \times 10^{-6}\ \Omega\cdot\text{cm})$$
$$\epsilon_2 = 11.5$$
$$\epsilon_1 = 12.5$$
$$\sigma_1 = 0.002 \text{ to } 10.0 \text{ S/m } (5 \times 10^4 \text{ to } 10\ \Omega\cdot\text{cm})$$
$$\sigma_2 = 0.01 \text{ to } 1.4 \text{ S/m } (10^4 \text{ to } 71\ \Omega\cdot\text{cm})$$
$$d_1 = 4\ \mu\text{m}$$
$$d_2 = 610\ \mu\text{m}$$
$$w = 10.7\ \mu\text{m}$$
$$T = 1\ \mu\text{m}$$
$$l = 1.0 \times 10^{-3}\ \text{m}.$$

The calculated attenuation is given in Fig. 4 for one value of σ_2 and four values of σ_1. Fig. 5 gives the attenuation for one value of σ_1 and three values of σ_2. Results are given to 100 GHz; however, above 20 GHz the simple low-frequency model will not give accurate results. Note that the conductivity of the gallium arsenide layer is not zero, as was the case for the silicon dioxide layer.

These curves illustrate the change in behavior of the attenuation versus frequency for various values of σ_1 and σ_2. The width w was chosen to obtain a characteristic impedance of about 50 Ω for $d_1 = 4$ μm and values of σ_2 greater than a few S/m (resistivity less than about 100 Ω·cm). Such values of σ_2 are required to achieve a constant characteristic impedance over a significant range of frequencies. Different values of T also were tried, but the only change was in the low-frequency attenuation, as expected.

These calculations were repeated for $d_1 = 1$ μm, with very little change in the attenuation characteristics. What changes did occur were at the higher frequencies and were not consistent in direction (increase or decrease).

VI. Conclusions

The above results demonstrate the capability to determine the model parameters from network analyzer measurements of structures important to microwave integrated circuits. We have determined that the microstrip line inductance and capacitance of the SiO_2 layer can be uniquely determined by fitting equivalent

circuit parameters to measured data in the frequency range from 90 MHz to 18 GHz. Having demonstrated that this procedure gives reasonable results for the SiO_2 on Si system, we have calculated the attenuation one might expect for GaAs on Si up to a frequency of 100 GHz when fabricating fast integrated circuit devices. However, according to the model used, in the worst case of a low-resistivity Si substrate with a low-resistivity GaAs layer, the loss is less than 1.0 dB/mm out to 100 GHz, which is acceptable for many device applications. Neglecting reflection effects, lower loss circuits could be fabricated using high-resistivity (10^4 $\Omega \cdot$cm) Si substrates with high resistivity (5×10^4 $\Omega \cdot$cm) GaAs layers, where the loss was found to be less than 0.2 dB/mm from 1 to 100 GHz.

References

[1] R. A. Lawton, N. S. Nahman, and J. M. Bigelow, "A solid state reference waveform standard," *IEEE Trans. Instrum. Meas.*, vol. IM-33, no. 3, pp. 201–205, Sept. 1984.

[2] J. P. Salerno, "Epitaxial growth of GaAs on silicon for integrated circuit applications," in *Proc. 1986 Producibility Millimeter Wave/Microwave Integrated Circuits Conf.* (Huntsville, AL), Nov. 4–5, 1986, p. 21.

[3] H. K. Choi, B. Y. Tsaur, G. M. Metze, G. W. Turner, and J. C. C. Fan, "GaAs MESFET's fabricated on monolithic GaAs Si substrates," *IEEE Electron Device Lett.*, vol. EDL-5, pp. 207–208, June 1984.

[4] H. Morkoc, C. K. Peng, T. Henderson, W. Kopp, R. Fischer, L. P. Erickson, M. D. Longerbone, and R. C. Youngman, "High-quality GaAs MESFET's grown on silicon substrates by molecular-beam epitaxy," *IEEE Electron Device Lett.*, vol. EDL-6, pp. 381–383, July 1985.

[5] R. Fischer, N. Chand, W. Kopp, H. Morkoc, L. P. Erickson, and R. Youngman, "GaAs bipolar transistors grown on (100) Si substrates by molecular beam epitaxy," *Appl. Phys. Lett.*, vol. 47, no. 4, pp. 397–399, Aug. 15, 1985.

[6] A. Christou, B. R. Wilkins, and W. F. Tseng, "Low-temperature epitaxial growth of GaAs on (100) silicon substrates," *Electron. Lett.*, vol. 21, no. 9, pp. 406–408, Apr. 25, 1985.

[7] T. Ishida, T. Nonaka, C. Yamagishi, Y. Kawarada, Y. Swano, M. Akiyama, and K. Kaminishi, "GaAs MESFET ring oscillator on Si substrate," *IEEE Trans. Electron Devices*, vol. ED-32, pp. 1037–1041, June 1985.

[8] H. Hasegawa, M. Furukawa, and Y. Hisayoshi, "Properties of microstrip line on Si–SiO_2 system," *IEEE Trans. Microwave Theory Tech.*, vol. MTT-19, pp. 869–881, Nov. 1971.

[9] V. M. Hietala, Y. R. Kwon, and K. S. Champlin, "Low-loss slow-wave propagation along a microstructure transmission line on a silicon surface," *Electron. Lett.*, vol. 22, no. 14, pp. 755–756, July 3, 1986.

[10] H. Hasegawa and S. Seki, "Analysis of interconnection delay on very high-speed LSI/VLSI chips using an MIS microstrip line model," *IEEE Trans. Electron Devices*, vol. ED-31, pp. 1954–1960, Dec. 1984.

[11] Y. Fukuoka, Y. Shih, and T. Itoh, "Analysis of slow-wave coplanar waveguide for monolithic integrated circuits," *IEEE Trans. Microwave Theory Tech.*, vol. MTT-31, pp. 567–573, July 1983.

0018-9480/88/0400-0789$01.00 ©1988 IEEE